The Bright SHARC Survey: The Cluster Catalog

Article (Published Version)

THE ASTROPHYSICAL JOURNAL SUPPLEMENT SERIES, 126:209–269, 2000 February

THE BRIGHT SHARC SURVEY: THE CLUSTER CATALOG[1]

A. K. ROMER[2] AND R. C. NICHOL[3,4]
Department of Physics, Carnegie Mellon University, 5000 Forbes Avenue, Pittsburgh, PA 15213; romer@cmu.edu, nichol@cmu.edu
B. P. HOLDEN[2,3]
Department of Astronomy and Astrophysics, University of Chicago, 5640 South Ellis Avenue, Chicago, IL 60637; holden@oddjob.uchicago.edu
M. P. ULMER AND R. A. PILDIS
Department of Physics and Astronomy, Northwestern University, 2131 North Sheridan Road, Evanston, IL 60207; ulmer@ossenu.astro.nwu.edu
A. J. MERRELLI[2]
Department of Physics, Carnegie Mellon University, 5000. Forbes Avenue, Pittsburgh, PA 15213; merrelli@andrew.cmu.edu
C. ADAMI[4]
Department of Physics and Astronomy, Northwestern University, 2131 North Sheridan Road, Evanston, IL 60207; adami@lilith.astro.nwu.edu; and Laboratoire d Astronomie Spatiale, Traverse du Siphon, 13012 Marseille, France
D. J. BURKE[3] AND C. A. COLLINS[3]
Astrophysics Research Institute, Liverpool John Moores University, Twelve Quays House, Egerton Wharf, Birkenhead, L41 1LD, UK; djb@astro.livjm.ac.uk, cac@astro.livjm.ac.uk
A. J. METEVIER
UCO/Lick Observatory, University of California, Santa Cruz, CA 95064; anne@ucolick.org
R. G. KRON
Department of Astronomy and Astrophysics, University of Chicago, 5640 South Ellis Avenue, Chicago, IL 60637; rich@oddjob.uchicago.edu
AND
K. COMMONS[2]
Department of Physics and Astronomy, Northwestern University, 2131 North Sheridan Road, Evanston, IL 60207; commons@lilith.astro.nwu.edu
Received 1999 April 12; accepted 1999 August 23

ABSTRACT

We present the Bright SHARC (Serendipitous High-Redshift Archival *ROSAT* Cluster) Survey, which is an objective search for serendipitously detected extended X-ray sources in 460 deep *ROSAT* PSPC pointings. The Bright SHARC Survey covers an area of 178.6 deg^2 and has yielded 374 extended sources. We discuss the X-ray data reduction, the candidate selection and present results from our ongoing optical follow-up campaign. The optical follow-up concentrates on the brightest 94 of the 374 extended sources and is now 97% complete. We have identified 37 clusters of galaxies, for which we present redshifts and luminosities. The clusters span a redshift range of $0.0696 < z < 0.83$ and a luminosity range of $0.065 < L_X < 8.3 \times 10^{44}$ ergs s^{-1} [0.5–2.0 keV] (assuming $H_0 = 50$ km s^{-1} Mpc^{-1} and $q_0 = 0.5$). Twelve of the clusters have redshifts greater than $z = 0.3$, eight of which are at luminosities brighter than $L_X = 3 \times 10^{44}$ ergs s^{-1}. Seventeen of the 37 optically confirmed Bright SHARC clusters have not been listed in any previously published catalog. We also report the discovery of three candidate "fossil groups" of the kind proposed by Ponman et al.

Subject headings: catalogs — galaxies: clusters: general — galaxies: distances and redshifts — surveys — X-rays: galaxies

1. INTRODUCTION

Clusters of galaxies play a key role in constraining cosmological models. It has been shown (e.g., Oukbir & Blanchard 1992; Carlberg et al. 1997; Henry 1997; Sadat, Blanchard, & Oukbir 1998; Viana & Liddle 1999) that measurements of the cluster number density, and its evolution, play an important role in the derivation of the mean mass density of the universe, Ω_m. At present, there is a large dispersion in the values of Ω_m derived from measurements of the cluster number density; e.g., $\Omega_m = 0.2^{+0.3}_{-0.1}$ (Bahcall & Fan 1998), $\Omega_m = 0.4^{+0.3}_{-0.2}$ (Borgani et al. 1999), $\Omega_m = 0.5^{\pm 0.14}$ (Henry 1997), $\Omega_m = 0.85^{\pm 0.2}$ (Sadat et al. 1998), $\Omega_m = 0.96^{+0.36}_{-0.32}$ (Reichart et al. 1999).

To fully exploit clusters as cosmological tools one needs to have access to large, objectively selected, cluster catalogs that cover a wide redshift range. Most cluster catalogs constructed prior to 1990 had a very limited redshift range and were not constructed in an objective manner (e.g., Abell 1958; Abell, Corwin, & Olowin 1989). However, recent developments, such as CCD mosaic cameras, optical plate digitizers, and imaging X-ray satellites, have resulted in a growing number of high-quality cluster catalogs. These include optically selected cluster samples derived from digitized plate material, e.g., the EDCC (Lumsden et al. 1992) and the APM (Dalton et al. 1994), or from CCD imaging

[1] Based on data taken at the European Southern Observatory, Kitt Peak National Observatory, Cerro Tololo Inter-American Observatory, Canada-France-Hawaii, and Apache Point Observatory.
[2] Visiting Astronomer, Kitt Peak National Observatory. KPNO is operated by AURA, Inc., under contract to the National Science Foundation.
[3] Visiting Astronomer, European Southern Observatory.
[4] Visiting Astronomer, Canada-France-Hawaii Telescope.

surveys, e.g., the PDCS (Postman et al. 1996) and the ESO Imaging Survey (Lobo et al. 1998). X-ray selected cluster samples derived from imaging X-ray satellite data include those from the *Einstein* mission, e.g., the EMSS cluster sample (Gioia et al. 1990), and those from the *ROSAT* (Trümper 1993) mission.

The various *ROSAT* cluster catalogs divide into two categories; those based on *ROSAT* All-Sky Survey (RASS) data and those based on *ROSAT* pointing data. The former category includes the SRCS (Romer 1995), XBACS (Ebeling et al. 1996), BCS (Ebeling et al. 1998), REFLEX (Böhringer et al. 1998; De Grandi et al. al 1999a) and NEP (Gioia et al. 1999; Henry et al. 1997) surveys. Examples of surveys based on *ROSAT* pointing data are the SHARC (Collins et al. 1997); RIXOS (Castander et al. 1995); RDCS (Rosati et al. 1998); WARPS (Jones et al. 1998) and 160 deg^2 (Vikhlinin et al. 1998a) surveys. The *ROSAT* instrument of choice for cluster surveys has been the PSPC, which combines imaging capabilities with a large field of view (2° in diameter), low background contamination and some spectral resolution. The angular resolution of the *ROSAT* PSPC is better than that of *Einstein*, allowing one to take advantage of the extended nature of cluster emission to distinguish clusters from X-ray point sources, e.g., active galactic nuclei (AGNs) and quasars. Moreover, the enhanced sensitivity of *ROSAT* over *Einstein* means that *ROSAT* cluster surveys can reach fainter flux limits than the EMSS.

The RASS surveys have yielded several important insights into the clustering properties (Romer et al. 1994) and evolution (Ebeling et al. 1997; De Grandi et al. 1999b) of the $z < 0.3$ cluster population. At higher redshifts, the *ROSAT* pointing data surveys have shown that there is no evidence for evolution in the cluster population at luminosities fainter than $L_X = 5 \times 10^{44}$ ergs s^{-1} [0.5–2.0 keV] and redshifts less than $z \simeq 0.7$ (Nichol et al. 1997; Burke et al. 1997; Collins et al. 1997; Vikhlinin et al. 1998b; Rosati et al. 1998; Jones et al. 1998; Nichol et al. 1999). At brighter luminosities, the 160 deg^2 and Bright SHARC surveys, have provided evidence for negative evolution (Nichol et al. 1999; Vikhlinin et al. 1998b) similar to that seen in the EMSS cluster sample (Henry et al. 1992; Reichart et al. 1999).

The SHARC (Serendipitous High-Redshift Archival *ROSAT* Cluster) survey was designed to optimize studies of X-ray cluster evolution and combines two complementary surveys; a narrow area deep survey and a wide area shallow survey. The former, known as the Southern SHARC, has been described elsewhere (Collins et al. 1997; Burke et al. 1997). We introduce the latter survey, the Bright SHARC, here. Unlike the Southern SHARC, the philosophy of the Bright SHARC has been to achieve maximum areal coverage rather than maximum sensitivity. The Bright SHARC survey covers a total area of 178.6 deg^2 and has yielded a catalog of 37 clusters with fluxes $\geq 1.63 \times 10^{-13}$ ergs s^{-1} cm^{-2}. In contrast, the Southern SHARC survey covers only 17.7 deg^2 but has yielded a similar number of clusters (36) with fluxes $\geq 4.66 \times 10^{-14}$ ergs s^{-1} cm^{-2}.

We describe below the reduction of the 460 *ROSAT* PSPC pointings in the Bright SHARC survey (§ 2), our source detection methodology (§ 3) and the selection and optical follow-up of cluster candidates (§§ 4 and 5). In §§ 6 and 7 we present and discuss the Bright SHARC cluster catalog. Throughout this paper we use $H_0 = 50$ km s^{-1} Mpc^{-1} and $q_0 = 0.5$ and define f_{-13} and L_{44} to be the unabsorbed flux (observer frame) and luminosity (rest frame) in the [0.5–2.0 keV] energy band in units of 10^{-13} ergs s^{-1} cm^{-2} and 10^{44} ergs s^{-1}, respectively.

2. TRANSFER AND REDUCTION OF *ROSAT* PSPC POINTING DATA

The pointed PSPC data used in the construction of the Bright SHARC was obtained from the HEASARC *ROSAT* data archive using an automated FTP process over a period of two years starting in 1995 June. The criteria used to select data from the archive were (i) a listed exposure time greater than 10 ks and (ii) an absolute Galactic latitude greater than 20°. Based on these criteria, 638 PSPC pointings were transferred to local machines and then reduced using a pipeline processing based on the Extended Source Analysis Software (ESAS) package (Snowden et al. 1994).

An overview of our pipeline is as follows. First, the raw data were sorted into good and bad time intervals. Bad intervals were defined as those in which the background level was higher than 170 counts s^{-1}. Data obtained during bad intervals were discarded. The remaining data were binned, as a function of position, into seven different energy bands—which Snowden et al. (1994) define as R1 through R7—to produce seven 512 × 512 pixel maps with a pixel scale of 14.″947. The five highest energy bands, R3 through R7, were then co-added to produce a hard band [0.4–2.0 keV] count rate map for each pointing. Accompanying each count rate map was a count rate uncertainty map and a vignetting corrected exposure map.

For each of the 638 pointings reduced by the ESAS pipeline, the *ROSAT* pointing name (col. [1]), the J2000 position (cols. [2] and [3]), Galactic latitude in degrees (b, col. [4]), the exposure time in seconds (col. [5]) and pointing target (col. [6]) are listed in Tables 4 and 5 (see Appendix A and Appendix B). Table 4 lists the 460 pointings selected to form the Bright SHARC survey. Two points should be noted about these 460 pointings. First, 371 of the pointings, those with three character extensions e.g., "n00," "a01" etc., were processed after an important change was made to the Standard Analysis Software System (SASS). This change effected those pointings for which the total exposure time was broken up into more than one observation interval. After the change, each observation interval was analyzed separately, whereas before the change they were analyzed together. Of these 371 pointings, only 45 have more than one observing interval. For simplicity we decided to include only the longest observing interval in our analysis. Second, the Bright SHARC survey does not include the central 2.′5 radius region of PSPC (see § 4). This means that we were able to include several pointings in the survey which had intrinsically extended central targets, e.g., galaxies and clusters—as long as those targets did not extend beyond 2.′5. We discuss cases where Bright SHARC clusters are detected in pointings with cluster targets in Table 2 (see § 6) and § 7.2.

The 178 pointings listed in Table 5 (Appendix B) were not included in the Bright SHARC because either an extended X-ray (or optical) source covers most of the field of view, or the pointing is within less than 6° of the Magellanic clouds. Extended X-ray and optical objects include low-redshift Abell clusters and Galactic globular clusters. The pointings listed in Table 5 were removed after visual inspections of the reduced X-ray data and the Digitized Sky Survey. Despite its subjective nature, this procedure does not undermine the serendipitous nature of the SHARC survey, since it was

performed before the cluster candidate list was constructed. We have indicated in column [7] of Table 5 why each pointing was rejected from the survey.

3. SOURCE DETECTION

Our source detection algorithm was based on wavelet transforms (Slezak, Bijaoui, & Oukbir 1990). For our purposes, we required a detection algorithm that (i) was sensitive to both extended and pointlike sources, (ii) worked in crowded fields, and (iii) took into account a varying background level. Moreover, we wanted our method to be as simple as possible, so that we could define our selection function a posteriori using simulations. With these concerns in mind, we chose to convolve the PSPC count rate maps with a spherically symmetric, "Mexican-hat" wavelet. This wavelet, in one dimension, is given by

$$w(x) = \left(1 - \frac{x^2}{a^2}\right) e^{-x^2/2a^2}, \quad (1)$$

and is the second derivative of a Gaussian (Slezak et al. 1990) of width $\sigma = a$. The radially averaged point spread function of the *ROSAT* PSPC can be approximated to a Gaussian (Hasinger et al. 1992), so this wavelet is well suited to the detection of sources in PSPC images. An additional attraction of this wavelet is that it can be used to determine the extent of a source, since it has a width of $2 \times a$ at its zero-crossing points. A wavelet transform of a PSPC count rate map will, therefore, produce a wavelet coefficient map in which all the sources are bounded by a ring of zero values. The diameter of these zero-crossing rings provides a direct measure of the source's extent in wavelet space.

Ideally, a should be scaled logarithmically to provide statistically independent wavelet images over the whole range of real and k-space. For any given source, the wavelet coefficient will have a maximum when the value of a matches the sigma of the best-fit Gaussian. However, the use of multiple wavelets would make a posteriori simulations of the selection function very complex and CPU intensive. We therefore decided to use only one wavelet convolution ($a =$ 3 pixels or 45″) in our source detection pipeline. This particular wavelet was found, empirically, to be the best compromise between smaller wavelets, which tended to fragment extended sources, and larger wavelets, which tended to blend neighboring sources. The penalty for this simplification was the inclusion of some blended sources in our extended candidate list (§ 5) and underestimated cluster count rates (§ 6.1).

Sources were identified in the wavelet coefficient map by selecting pixels with coefficients above a given threshold. This threshold was set, empirically, to be 7 σ above the peak of the coefficient distribution. The thresholding technique only highlights the cores of each source, since that is where the wavelet coefficients are highest, so a "friends-of-friends" analysis was run to identify other associated pixels. This was done by growing the sources outward in the wavelet coefficient map until they reached the zero-crossing ring. Once the source boundaries were defined, best-fit centroids and ellipses were computed. A filling factor was also derived for each source. This was defined as ratio of the area within the fitted ellipse to the area within the zero-crossing boundary. For $f = 1$, the ellipse fits the source shape exactly, while $f \gg 1$ indicates the presence of blended sources (dumbbell shapes) or percolation runaways (filamentary shapes).

In total, 10,277 sources were detected in the 460 pointings. To keep track of all of these sources, and their boundaries, a mask file was generated for each pointing so that pixels associated with sources could be distinguished from those that were not. For each source, a 51×51 pixel box, with the source at its center, was extracted from the count rate map. An average background for the box was calculated using all pixels not flagged as belonging to sources. The count rate for the central source was then derived by subtracting this background (appropriately scaled) from the sum of the pixels enclosed by the source boundary. We used this method because it was easy to apply to the thousands of sources detected in the Bright SHARC Survey. (We will refer to the count rates derived in this manner as "wavelet count rates," or cr_W.) However, the method has the disadvantage of underestimating the true count rate if the source is extended beyond the wavelet boundary (in § 6.1 we describe an alternative method used to derive count rates for known clusters). An approximate signal-to-noise value for each source was also calculated using the count rate uncertainty maps produced by ESAS.

It should be noted that certain pixels, those which received less than half the exposure time of the central pixel in the count rate maps, were not included in the "friends-of-friends" analysis. Such pixels included those in the shadow of the PSPC window support structure and those at the edge of the field of view. These regions, which are noisier than those that were well exposed, were not used to define source centers, shapes, or wavelet count rates.

4. SELECTION OF CLUSTER CANDIDATES

The majority of X-ray sources can be considered pointlike in their spatial properties, e.g., stars and AGNs. In the minority are objects with complex and extended X-ray profiles, such as supernova remnants, galaxies, and clusters of galaxies. Of these, only clusters are large enough and bright enough to be detected as extended beyond $z \simeq 0.1$. Therefore, the strategy adopted by the SHARC has been to search for clusters only among those *ROSAT* sources that have a significant extent. This reduces the required optical follow-up significantly. The disadvantage of this approach, however, is that some clusters, e.g., those with compact surface brightness distributions, may be excluded from the survey.

Bright SHARC Cluster candidates were selected from the 10,277 sources found in the survey using the following six criteria: The source had to (i) have a signal-to-noise ratio greater than 8, (ii) its centroid had to fall within 90 pixels (22.4) of the pointing center, (iii) its centroid had to fall more than 10 pixels (2.5) from the pointing center, (iv) its filling factor had to be less than $f = 1.3$, (v) it had to be more than 3 σ extended, and (vi) it have to have a count rate higher than 0.01163 counts s^{-1}. The imposition of these criteria cut down the source list from 10,277 (total) to 3,334 (criterion [i]) to 1,706 (criterion [ii]) to 374 (criteria [iii]–[v]) to 94 (criterion [vi]). Criterion (i) was imposed because it has been shown (Wirth & Bershady 2000, in preparation) that extent measures can only be derived with confidence for sources meeting a minimum signal-to-noise threshold. Criterion (iii) was applied to avoid including the intended target of the pointing in the candidate list. Criterion (iv) was set empirically with the aim of reducing the number of blended sources and percolation runaways in the candidate list. The rationale for the other criteria is provided below.

The point spread function of the PSPC degrades significantly as one moves out from the center of the detector (Hasinger et al. 1992). It therefore becomes increasingly difficult to distinguish extended sources from point sources as the off-axis angle increases. To overcome this, we used all 3334 of the S/N > 8 sources in our survey to study statistically how source size varies as a function of position on the PSPC. The method used has been described previously (Nichol et al. 1997), but we include an overview here for completeness. Figure 1 shows the distribution of source size (as defined by the lengths of the major and minor axes of the best-fit ellipses) as a function of off-axis angle. After collecting these data into 10 pixel bins, we were able to determine how the mean and FWHM of the distribution varied with off-axis angle. (Beyond an off-axis angle of 90 pixels, the dispersion in source sizes became too large to define a reliable FWHM, hence the imposition of criterion [ii]). Under the assumption of a Gaussian distribution, the FWHM values were converted into sigma values and a 3 σ curve was determined by fitting a fourth-order polynomial to the [mean + 3 σ] values. A source was defined to be extended if it had a major and/or a minor axis more than 3 σ from the mean.

In total, 374 sources were found to meet criteria (i) through (v). These are listed in Table 6 (Appendix E) in right ascension order. Wavelet count rates (cr_W) are given for each source in units of 1×10^{-2} counts s^{-1} (col. [4]). We note that duplicate entries, e.g., RX J0056.5−2730—which was detected in two pointings, wp700528 and rp701223n00—have not been excised from this list. The fluxes for these 374 sources (assuming thermal spectra see § 6.2) range from $0.2 \lesssim f_{-13} \lesssim 40$. In the interests of completing the optical follow-up in a timely fashion, it was decided to concentrate only on the brightest of these 374. An arbitrary count rate cut ($cr_W > 0.01163$) was imposed to reduce the sample size to roughly 100 (criterion [vi]). At the redshift of the most distant cluster in the EMSS sample ($z = 0.81$), this count rate corresponds to a luminosity of $\simeq 3.9 L_{44}$, which is approximately equal to locally determined values of $L_\star$, e.g., $L_\star = 5.7 L_{44}$ (Ebeling et al. 1997), $L_\star = 3.8 L_{44}$ (De Grandi et al. 1999a).

The total areal coverage of the Bright SHARC survey is 178.6 deg^2. This value was determined by calculating the area available for candidate detection in each of the 460 pointings in the survey. This area includes all pixels at radii greater than 2.′5 and less than 22.′4, which (i) had exposure times more than half that of the central pixel and (ii) did not overlap pixels in a higher exposure pointing. (There were 21 pairs of pointings with some overlap between them.)

5. IDENTIFICATION OF EXTENDED SOURCES

We present the 94 unique[5] extended sources in the Bright SHARC survey in Table 1 and Appendix C. For each candidate, we provide the source name (col. [1]), its J2000 position (cols. [2] and [3]), the wavelet count rate [0.4–2.0 keV] (cr_W in units of 1×10^{-2} counts s^{-1} col. [4]), the pointing in which it was detected (col. [5]), the source type (col. [6]), and the method used to identify the source (col. [7]). Alternate source names and redshifts (where available) are listed in column (8). We note that Abell clusters (Abell 1958; Abell et al. 1989) are denoted by "A." Likewise for EMSS sources ("MS"; Stocke et al. 1991), 160 deg^2 clusters ("V"; Vikhlinin et al. 1998a, hereafter V98), Hickson groups ("HCG"; Hickson 1982), and Zwicky clusters ("Z"; Zwicky, Herzog, & Wild 1968). When an object is listed in more than one catalog, we have defaulted to the name given in the older catalog, e.g., for RX J0237.9 we have listed the Abell number (A3038), not the V98 number (V28).

In Appendix C, we present small (6.′6 × 6.′6) Digitized Sky Survey (DSS) images of each of the 94 extended sources listed in Table 1. The source outlines, as defined by our friends-of-friends analysis, are overlaid on these images. We note that the source centroids were defined in a weighted fashion and do not necessarily coincide with the geometric center of the source outline. No external astrometric solution was applied before making these DSS images, because the expected pointing offset is much smaller ($\lesssim 6''$) than the typical size of one of our extended sources.

In some cases it was possible to identify the source using the DSS images alone. For example, the X-ray emission from source RX J0324.6−5103 is clearly associated with a bright star (HD 21360). This source was flagged as extended because emission from the star was blended by the friends-

[5] Duplicate entries for RX J0237.9−5224 and RX J1211.2+3911 have been removed.

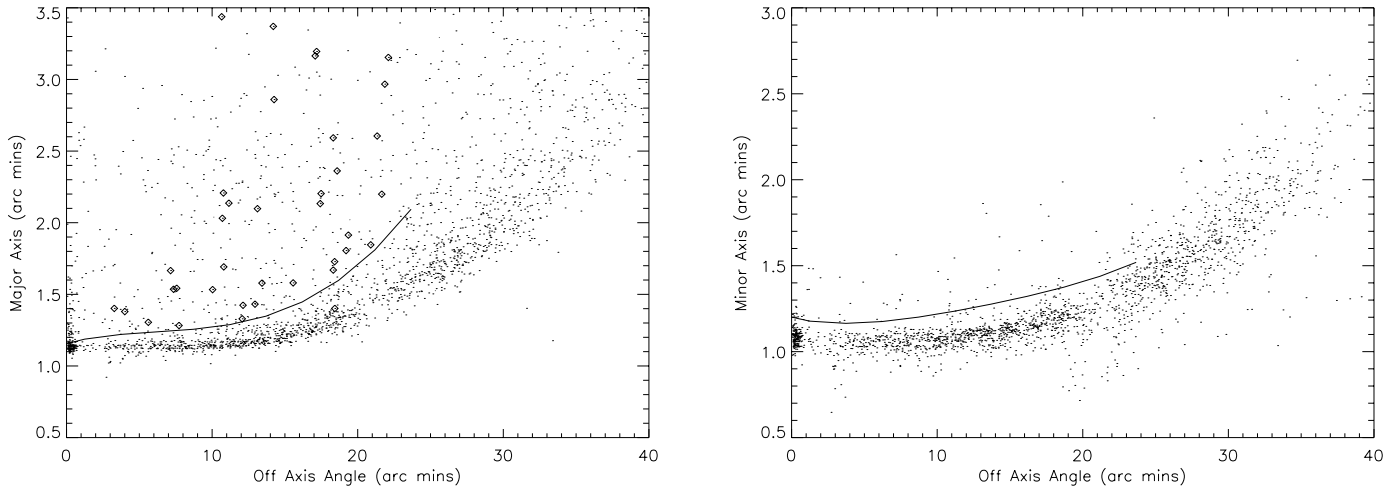

FIG. 1.—Distribution of major and minor axes for the 3334 S/N > 8 sources in the Bright SHARC survey as a function of off-axis angle. The solid lines correspond to the fitted 3 σ extent curves; any sources falling above these lines are classified as extended. For illustration purposes, we have plotted, as open diamonds, the points corresponding to the 37 Bright SHARC clusters on the major axis plot (the numerical values for these points can be found in Table 2).

TABLE 1

EXTENDED SOURCES IN THE BRIGHT SHARC SURVEY

Source (1)	R.A. (J2000) (2)	Decl. (J2000) (3)	cr_W (4)	Pointing (5)	ID (6)	ID Code (7)	Notes (8)	References (9)
RX J0031.0−3547.....	00 31 03.0	−35 47 21.8	1.26	wp800387n00	Blend	X S N C	AGN, $z = 0.25 + ?$	
RX J0031.9−3556.....	00 31 59.5	−35 56 12.1	1.19	wp800387n00	Blend	X S C	id pending	
RX J0058.0−2721.....	00 58 00.5	−27 21 29.3	1.18	rp701223n00	Blend	S N C	Mstar + ?	
RX J0117.6−2238.....	01 17 36.5	−22 38 13.5	1.25	rp100376n00	Cluster	S N C	A2894, $z = 0.207$	
RX J0124.8+0932.....	01 24 48.2	+09 32 30.8	1.92	rp700976	Galaxy	N	NGC 524, $cz = 2421$ km s^{-1}	1
RX J0152.7−1357.....	01 52 42.0	−13 57 52.9	1.71	rp600005n00	Cluster	S O C	$z = 0.83$	2
RX J0209.4−1008.....	02 09 24.2	−10 08 04.2	1.34	rp800114n00	Galaxy	N	NGC0835, $z = 0.0135$	3
RX J0209.9−1003.....	02 09 58.1	−10 03 19.2	1.47	rp800114n00	Blend	X S N C	QSO: MS0207.4, $z = 1.97 + ?$	4
RX J0217.4−1800.....	02 17 26.1	−18 00 05.7	1.38	rp900352n00	Blend	S C	AGN, $z = 0.345 + ?$	
RX J0221.1+1958.....	02 21 08.4	+19 58 25.9	1.54	wp900147	Cluster	S C	$z = 0.45$	
RX J0223.4−0852.....	02 23 28.1	−08 52 14.3	1.20	rp800016n00	Cluster	S O N C	$z = 0.163$	5
RX J0237.9−5224.....	02 37 59.1	−52 24 45.7	2.32	rp300201n00	Cluster	S O N C	A3038, $z = 0.133$	6
RX J0250.0+1908.....	02 50 02.9	+19 08 29.4	1.42	rp700920	Cluster	S C	$z = 0.12$	
RX J0256.5+0006.....	02 56 32.9	+00 06 11.6	3.61	rp701403n00	Cluster	S C	$z = 0.36$	
RX J0318.2−0301.....	03 18 17.3	−03 01 21.1	1.33	wp800555n00	Blend	X S C	Cluster, $z = 0.37$ + AGN, $z = 0.233$	
RX J0318.5−0302.....	03 18 33.3	−03 02 46.7	2.76	wp800555n00	Cluster	S C	$z = 0.37$	
RX J0321.9−5119.....	03 21 57.0	−51 19 33.1	6.18	wp800371n00	Cluster	N	A3120, $z = 0.0696$	7
RX J0324.6−5103.....	03 24 37.9	−51 03 52.1	1.32	wp800371n00	Blend	X D	Star:HD21360 + ?	
RX J0327.9+0233.....	03 27 54.3	+02 33 43.2	3.23	rp700099m01	Galaxy	N	UGC2748, $z = 0.0302$	8
RX J0337.5−2518.....	03 37 34.2	−25 18 01.5	2.13	wp300079	Blend	X C	id pending	
RX J0340.1−4458.....	03 40 09.0	−44 58 48.2	1.24	rp900495n00	Id pending	C		
RX J0359.1−5300.....	03 59 11.9	−53 00 56.2	1.51	rp800308	Blend	X D	2 stars	
RX J0414.0−1224.....	04 14 05.7	−12 24 24.9	2.50	rp900242n00	Blend	S N	AGN, $z = 0.572 + ?$	9
RX J0415.7−5535.....	04 15 45.4	−55 35 31.0	1.20	wp600623n00	Galaxy	N	NGC1549, $cz = 1197$ km s^{-1}	10
RX J0416.1−5546.....	04 16 10.3	−55 46 46.3	3.65	wp600623n00	Galaxy	N	NGC1553, $cz = 1080$ km s^{-1}	11
RX J0420.9+1444.....	04 20 58.7	+14 44 07.7	2.83	wp200441	Blend	S C	AGN + ?	
RX J0421.2+1340.....	04 21 16.8	+13 40 14.8	1.32	rp200776n00	Blend	X S C	star + ?	
RX J0426.1+1655.....	04 26 07.3	+16 55 12.1	1.79	rp201369n00	Cluster	S C	$z = 0.38$	
RX J0454.3−0239.....	04 54 19.6	−02 39 50.0	1.59	rp800229n00	Cluster	S C	$z = 0.26$	
RX J0514.2−4826.....	05 14 16.7	−48 26 53.4	1.58	wp800368n00	Blend	X S C	AGN, $z = 0.230 + ?$	
RX J0609.1−4854.....	06 09 06.5	−48 54 50.4	2.15	rp300111	Blend	D	star + ?	
RX J0849.1+3731.....	08 49 08.9	+37 31 47.9	1.29	rp700546n00	Cluster	S N C	A708, $z = 0.23$	
RX J0853.6+1349.....	08 53 41.1	+13 49 29.5	1.17	rp700887n00	Blend	X D N	Star + Galaxy:MS0850.8, $z = 0.194$	12
RX J0945.6−1434.....	09 45 40.4	−14 34 5.0	2.30	wp701458n00	Blend	X D S	AGN, $z \simeq 1.2$ + star	
RX J0947.8+0741.....	09 47 50.5	+07 41 43.0	1.51	wp701587n00	Blend	S C	QSO, $z \simeq 0.63 + ?$	
RX J1010.2+5430.....	10 10 12.9	+54 30 09.6	1.41	wp900213	Group	N	V84 $z \simeq 0.045$	13
RX J1020.0+3915.....	10 20 02.4	+39 15 50.8	1.18	wp900528n00	Blend	X C	id pending	
RX J1024.3+6805.....	10 24 20.1	+68 05 05.1	2.60	wp800641n00	Cluster	N	A981, $z = 0.201$	14
RX J1031.3−1433.....	10 31 23.3	−14 33 40.6	1.18	rp700461n00	Blend	D S	Star + ?	
RX J1113.8+4017.....	11 13 48.5	+40 17 18.3	1.44	rp700855n00	Cluster	N	A1203, $z = 0.0795$	15
RX J1120.1+4318.....	11 20 07.5	+43 18 04.9	2.11	rp900383n00	Cluster	S C	$z = 0.60$	
RX J1142.2+1026.....	11 42 16.7	+10 26 46.9	1.27	wp600420	Cluster	N	A1356, $z = 0.0698$	16
RX J1143.7+5520.....	11 43 46.5	+55 20 13.6	1.98	rp600236n00	Blend	X D C	id pending	
RX J1204.0+2807.....	12 04 03.6	+28 07 03.6	4.49	wp700232	Cluster	N	MS1201.5, $z = 0.167$	17
RX J1204.1+2020.....	12 04 09.7	+20 20 40.5	2.04	rp800039	Galaxy	N	NGC4066, $z = 0.024$	18
RX J1210.4+3929.....	12 10 25.9	+39 29 07.6	14.30	wp700277	Blend	N C	QSO:MS1207.9, $z = 0.615 + ?$	19
RX J1211.1+3907.....	12 11 09.5	+39 07 44.4	2.14	rp600625n00	Blend	X D	Star + ?	

TABLE 1—*Continued*

Source (1)	R.A. (J2000) (2)	Decl. (J2000) (3)	cr_W (4)	Pointing (5)	ID (6)	ID Code (7)	Notes (8)	References (9)
RX J1211.2+3911.....	12 11 14.5	+39 11 41.1	1.52	wp700277	Cluster	N	MS1208.7, $z = 0.34$	20
RX J1220.3+7522.....	12 20 18.0	+75 22 10.2	4.65	rp700434	Galaxy	N	NGC4291, $z = 0.059$	21
RX J1222.1+7526.....	12 22 06.9	+75 26 16.8	1.17	rp700434	Cluster	N	MS1219.9, $z = 0.24$	22
RX J1222.5+2550.....	12 22 30.8	+25 50 26.7	36.93	wp200307	Blend	X D	2 Stars	
RX J1227.4+0849.....	12 27 27.6	+08 49 53.1	5.87	wp600587n00	Cluster	N	A1541, $z = 0.0895$	23
RX J1232.8+2605.....	12 32 48.3	+26 05 39.0	1.82	rp600162	Cluster	S C	$z = 0.22$	
RX J1241.5+3250.....	12 41 33.1	+32 50 22.9	2.38	rp600129a00	Cluster	S C	$z = 0.39$	
RX J1244.1+1134.....	12 44 08.2	+11 34 16.8	1.16	rp600017	Blend	X C	id pending	
RX J1250.4+2530.....	12 50 26.1	+25 30 17.6	1.71	wp900212	Galaxy	N	NGC4725, $z = 0.00402$	24
RX J1259.7−3236.....	12 59 45.4	−32 36 59.9	1.19	rp800384n00	Cluster	S C	$z = 0.076$	
RX J1308.5+5342.....	13 08 32.6	+53 42 19.3	1.25	wp300394n00	Cluster	S C	$z = 0.33$	
RX J1311.2+3228.....	13 11 12.3	+32 28 53.2	2.53	wp700216	Cluster	N C	MS1308.8, $z = 0.245$	25
RX J1311.8+3227.....	13 11 49.8	+32 27 40.4	1.47	wp700216	Cluster	S C	$z = 0.44$	
RX J1313.6−3250.....	13 13 41.0	−32 50 45.9	1.28	wp300219	Blend	X D	id pending	
RX J1334.3+5030.....	13 34 20.0	+50 30 54.2	1.36	rp800047	Cluster	S C	$z = 0.62$	
RX J1343.7+5538.....	13 43 45.2	+55 38 20.3	1.80	rp700922n00	Cluster	N	A1783, $z = 0.0766$	26
RX J1349.2−0712.....	13 49 12.3	−07 12 41.2	1.51	rp800637n00	Galaxy pair	N	part of HCG67, $z = 0.02406$	27
RX J1406.9+2834.....	14 06 55.1	+28 34 15.7	1.30	rp700061	Cluster	N S C	V154, $z = 0.117$	
RX J1412.4+4355.....	14 12 29.8	+43 55 31.2	2.32	wp700248	Blend	X S N C	AGN, $z = 0.095$ + ?	28
RX J1416.4+2315.....	14 16 26.6	+23 15 32.8	4.80	rp800401a01	Cluster	S C	$z = 0.138$	
RX J1417.9+5417.....	14 17 57.5	+54 17 51.3	1.26	wp150046	Blend	O C	AGN + Mstar	29
RX J1418.5+2510.....	14 18 31.4	+25 10 45.8	3.78	wp150071	Cluster	S C	V159, $z = 0.29$	
RX J1508.4+5537.....	15 08 24.6	+55 37 05.3	1.16	rp600119n00	Blend	D S C	Star + ?	
RX J1517.1+3140.....	15 17 08.4	+31 40 58.4	1.29	rp201018	Blend	X D S C	Star + ?	
RX J1524.6+0957.....	15 24 39.6	+09 57 44.8	1.64	rp701001n00	Cluster	S O C	V170, $z = 0.078$	30
RX J1525.3+4201.....	15 25 23.3	+42 01 00.0	1.26	rp701405n00	Blend	N C	QSO, $z = 1.189$ + ?	31
RX J1541.1+6626.....	15 41 10.3	+66 26 25.0	1.51	rp800511n00	Cluster	S C	$z = 0.245$	
RX J1543.7+6627.....	15 43 42.7	+66 27 42.3	1.25	rp800511n00	Blend	S C	QSO, $z = 1.4562$ + ?	
RX J1641.2+8233.....	16 41 13.9	+82 33 01.7	3.55	rp700098	Cluster	S N C	V183, $z = 0.195$	32

TABLE 1—*Continued*

Source (1)	R.A. (J2000) (2)	Decl. (J2000) (3)	cr_W (4)	Pointing (5)	ID (6)	ID Code (7)	Notes (8)	References (9)
RX J1701.3+6414.....	17 01 22.5	+64 14 08.3	1.98	wp701457n00	Cluster	N S C	V190, $z = 0.453$	33
RX J1705.6+6024.....	17 05 37.5	+60 24 11.0	1.46	rp701439n00	Id pending	C		
RX J1726.2+0410.....	17 26 14.4	+04 10 23.8	1.98	rp200522n00	Blend	X D	Star + ?	
RX J1730.6+7422.....	17 30 37.6	+74 22 23.8	3.20	wp701200	Galaxy	N S C	NGC6414, $z = 0.054$	
RX J1808.3+4542.....	18 08 20.9	+45 42 35.2	2.37	rp300103	Blend	X N	QSO:HB89:1806+456, $z = 0.83$ + ?	34
RX J1838.8−6502.....	18 38 48.8	−65 02 09.8	1.60	rp701020n00	Id pending			
RX J1845.6+7956.....	18 45 41.3	+79 56 34.5	2.23	rp700058	Blend	X D	Star:HD175938 + ?	
RX J2109.7−1332.....	21 09 47.8	−13 32 24.2	1.38	rp201007n00	Blend	S C	QSO + ?	
RX J2202.8−5636.....	22 02 52.9	−56 36 08.3	1.63	rp200559n00	Blend	X D	id pending	
RX J2215.2−2944.....	22 15 16.4	−29 44 29.2	1.95	rp701390n00	Blend	N	QS0: HB89:2212−299, $z = 2.7$ + ?	35
RX J2223.8−0206.....	22 23 48.8	−02 06 13.0	2.19	rp701018n00	Blend	S	AGN, $z = 0.0558$ + ?	
RX J2236.0+3358.....	22 36 00.3	+33 58 24.0	3.18	wp800066	Group	N	Stef.Quintet, $z = 0.0215$	36
RX J2237.0−1516.....	22 37 00.6	−15 16 08.0	1.68	wp201723n00	Cluster	S C	$z = 0.299$	
RX J2258.1+2055.....	22 58 08.4	+20 55 15.0	2.26	rp201282n00	Cluster	S N C	Z2255.5, $z = 0.288$	37
RX J2309.4−2713.....	23 09 27.9	−27 13 20.1	1.19	rp900323n00	Blend	S C	AGN, $z = 0.25$ + ?	
RX J2311.4+1035.....	23 11 25.9	+10 35 06.7	3.52	rp100578n00	Blend	S C	AGN, $z = 0.127$ + ?	
RX J2314.7+1915.....	23 14 44.0	+19 15 23.3	1.39	rp800488n00	Blend	S C	Cluster, $z = 0.28$ + Mstar	
RX J2353.5−1524.....	23 53 31.5	−15 24 51.2	1.18	wp701501n00	Blend	S C	QSO + Mstar	

NOTES.—Units of right ascension are hours, minutes, and seconds, and units of declination are degrees, arcminutes, and arcseconds. The ninety-four Extended sources in the Bright SHARC survey. Count rates (col. [4]) are quoted in units of 10^{-2} counts s^{-1}.

REFERENCES.—(1) Redshift taken from De Vaucouleurs et al. 1991, hereafter D91; (2) confirmation of redshift provided by P. Rosati 1999, private communication, and Ebeling et al. 2000; (3) D91; (4) Stocke et al. 1991, hereafter S91. (5) additional spectroscopy provided by I. Del Antonio; (6) additional spectroscopy provided by I. Del Antonio; (7) Abell et al. 1989; (8) D91; (9) additional redshift information available in Perlman et al. 1998; (10) Longhetti et al. 1998; (11) D91; (12) S91; (13) Carballo et al. 1995; (14) Huchra et al. 1990; (15) Slinglend et al. 1998; (16) Struble & Rood 1987; (17) S91; (18) D91. (19) S91; (20) S91; (21) D91; (22) S91; (23) Zabludoff et al. 1993; (24) D91; (25) S91; (26) Struble & Rood 1987; (27) Fairall et al. 1992; (28) additional redshift information available in Boyle et al. 1995; (29) spectroscopy provided by D. Turnshek and E. Monier; (30) spectroscopy provided by I. Del Antonio; (31) Perlman et al. 1998; (32) also known as EXSS 1646.5+8238 (Tucker et al. 1995); (33) also known as "Cluster B" (Reimers et al. 1997). (34) Hewitt & Burbidge 1993; (35) Hewitt & Burbidge 1993; (36) Hickson et al. 1992; (37) S91.

of-friends analysis with the (fainter) emission from a neighboring point source. (The X-ray surface brightness contours for this source show a secondary peak centered on the faint DSS object to the lower left of the source outline.) In other cases, the source outline, and/or the surface brightness contours, are indicative of blended emission but no obvious counterpart could be found on the DSS images, e.g., RX J0947.8+0741. When the DSS (or X-ray) images played a role in the identification of a source, a "D" (or "X") is listed in column (7) of Table 1.

A search of the NASA/IPAC Extragalactic Database (NED) has also provided useful information for several of the Bright SHARC extended sources, including some cluster redshifts e.g., for RX J1204.0+2807 (MS 1201.5, Gioia et al. 1990). When NED yielded information was used during the source identification, an "N" is listed in column (7) of Table 1.

Optical follow-up of Bright SHARC extended sources has been carried out at a number of telescopes; the 3.5 m ARC telescope at Apache Point Observatory, the Danish 1.5 m and 3.6 m telescopes at the ESO Southern Observatories, the 1.5 m telescope at the Cerro Tololo Inter-American Observatory, the 3.6 m Canada-France-Hawaii Telescope on Mauna Kea and the 4 m Mayall telescope at Kitt Peak National Observatory. Optical follow-up includes CCD imaging, long-slit spectroscopy and multi-object spectroscopy. Of the 94 extended sources, to date 57 have CCD images and 51 have been the target of spectroscopic follow-up. A "C" in column (7) of Table 1 indicates that a CCD image is available, whereas an "S" indicates spectroscopic follow up by the SHARC collaboration and an "O" indicates that spectroscopy came from private communications. To date, 91 of the 94 Bright SHARC extended sources have been identified; 37 clusters, 41 blends, nine galaxies and three galaxy groups. The symbols "+ ?" in column (8) indicate that the identification of one of the components of a blended source is unknown. We note that the distinctions between galaxies and groups (see § 7.4), and between groups and clusters, are not absolute at the low-luminosity end. For the 12 extended objects (nine galaxies and three groups) at redshifts less than $z = 0.07$, we based our classifications on the information provided by NED.

6. THE BRIGHT SHARC CLUSTER SAMPLE

The 37 clusters in the Bright SHARC are listed in Table 2. For each cluster, we list the source number (col. [1]), the cluster redshift (col. [2]), the hydrogen column density (in units of 1×10^{20} cm^{-2}, col. [3]), the major and minor axes (in units of 14.″947 pixels, cols. [4] and [5]), the off-axis angle of the cluster centroid (in units of 14.″947 pixels, col. [6]), the wavelet (cr_W) and total (cr_T) count rates [0.4–2.0 keV] (in units of 1×10^{-2} counts s^{-1}, cols. [7] and [8]), the percentage error on cr_T (δcr_T, col. [9]), the aperture containing 80% of the flux from a model cluster profile (r_{80}, col. [10], see § 6.1), the fraction of that aperture used to measure the cluster count rate (f_{80}, col. [11]), the total flux [0.5–2.0 keV] (f_{-13}, in units of 1×10^{-13} ergs s^{-1} cm^{-2}, col. [12]), the corresponding luminosity (L_{44}, in units of 1×10^{44} ergs s^{-1}, col. [13]), and the temperature used to derive the flux and luminosity (T, in units of keV, col. [14]). Various notes, including alternative cluster names and pointers to the information on the pointing target (if that target was a cluster) are given in column (15).

The redshift distribution ($\bar{z} = 0.266$) for the 37 Bright SHARC clusters is shown in Figure 3. The highest redshift, and most luminous, cluster in the sample is RX J0152.7 ($z = 0.83$). The lowest redshift cluster in the sample is RX J0321.9 ($z = 0.0696$). Twenty-one of the redshifts in Table 2 are presented here for the first time. These 21 include 17 clusters which have not been listed before in any published catalog and four clusters from the 160 deg^2 survey (V98). We describe below how the count rates (§ 6.1) and fluxes/luminosities (§ 6.2) were derived.

6.1. *Total Cluster Count Rate Derivation*

The method described in § 4, to measure wavelet count rates for all 10,277 sources in the Bright SHARC survey, was adopted because it was easy to apply to large numbers of sources. However, the method is not optimal for measuring cluster fluxes. This is because no correction is made for cluster flux falling outside the zero-crossing boundary. Moreover, when a portion of a cluster overlaps a masked out region (e.g., regions in the shadow of the support struts), the flux from that region will not be included in the count rate. Therefore, for the 37 sources identified with clusters of galaxies, we have performed a second count rate determination based on the method adopted by Holden et al. (1997). For each of the clusters, we derived an aperture for the flux measurement using a cluster model based on a modified isothermal sphere:

$$I = \frac{I_0}{[1 + (r/r_c)^2]^{3\beta - 1/2}}, \tag{2}$$

where I is the surface brightness at radius r. We used values for the slope ($\beta = 0.67$) and core radius ($r_c = 250$ kpc) which are typical for rich clusters (Jones & Forman 1992) and then converted the model from physical units to angular units using the cluster redshift. The cluster models were convolved with the appropriate off-axis PSPC PSF (Nichol et al. 1994b) so that the radius of a circular aperture, r_{80}, which contained $\simeq 80\%$ of the total model flux could be defined (for $\beta = 2/3$, $r_{80} = 24^{1/2} r_c$). The choice of r_{80} for the aperture represents a compromise between including a high fraction of the cluster flux and keeping down the number of contaminating sources within the region.

The 80% radii, r_{80}, are listed in column (10) of Table 2, in units of 14.″947 pixels. Since these radii could be quite large, up to 40 pixels, some of them overlapped other sources. If any $r < r_{80}$ pixels lay within the wavelet-defined boundary of another source, they were masked out from the cluster aperture. Also masked were any pixels that received less than half the exposure time of the central pixel in the count rate map. By reference to the cluster model, it was possible to correct for the fraction of cluster flux lying in these masked regions. In column (11) of Table 2, we list the fraction of the 80% aperture available for flux determination, f_{80}. The raw aperture count rates for each of the 37 clusters were measured by summing the flux in the unmasked $r < r_{80}$ pixels.

The corresponding background count rates were measured inside 120×120 pixel boxes centered on the cluster position. The background levels were measured in annuli with minimum radii of $1 \times r_{80}$ and maximum radii $3 \times r_{80}$. If these annuli overlapped any source boundaries, any low-exposure pixels, or the edges of the 120×120 pixel box, the pixels in those regions were excluded from the background calculations. In Appendix D we illustrate the masked out

TABLE 2

BRIGHT SHARC CLUSTER CATALOG

Source (1)	Redshift (2)	nH (3)	Major (4)	Minor (5)	Off-Axis (6)	cr_W (7)	cr_T (8)	δcr_T (%) (9)	r_{80} (10)	f_{80} (11)	f_{-13} (12)	L_{44} (13)	T (14)	Notes (15)
RX J0117.6−2238.....	0.207	1.51	8.82	6.32	86.91	1.255	2.285	9.2	18.36	0.943	2.594	0.4951	3	A2894
RX J0152.7−1357.....	0.83	1.42	11.4	4.99	57.22	1.716	2.440	5.6	9.900	1.000	2.930	8.2604	9	
RX J0221.1+1958.....	0.45	9.30	6.70	5.47	73.54	1.545	2.211	6.2	12.03	0.969	3.296	2.8661	6	
RX J0223.4−0852.....	0.163	3.18	8.86	4.98	43.25	1.202	3.036	7.7	21.09	0.994	3.706	0.4350	3	[a]
RX J0237.9−5224.....	0.133	3.08	8.56	5.53	69.94	2.324	6.107	5.3	24.63	0.906	7.495	0.5824	3	A3038
RX J0250.0+1908.....	0.12	9.40	13.5	5.92	57.00	1.426	1.576	15.3	26.49	0.997	2.242	0.1443	2	
RX J0256.5+6.00	0.36	5.33	7.40	6.82	83.87	3.614	5.692	4.9	13.44	0.998	7.549	4.1597	7	
RX J0318.5−0302.....	0.37	5.09	6.79	5.08	43.35	2.763	4.191	5.5	12.85	1.000	5.587	3.2819	6	[b]
RX J0321.9−5119.....	0.0696	2.46	6.93	5.36	73.91	6.180	17.10	2.4	40.23	0.916	20.72	0.4355	3	A3120[c]
RX J0426.1+1655.....	0.38	16.4	5.23	4.55	22.54	1.797	2.948	6.3	12.62	1.000	5.159	3.1969	6	
RX J0454.3−0239.....	0.26	5.24	10.4	5.92	85.65	1.594	2.732	8.0	16.01	0.914	3.564	1.0634	4	[d]
RX J0849.1+3731.....	0.230	3.07	8.42	7.47	52.64	1.295	2.052	11.3	16.84	0.991	2.525	0.5976	3	A708
RX J1024.3+6805.....	0.201	2.13	6.33	5.51	53.89	2.602	4.787	5.8	18.38	0.991	5.699	1.0100	4	A981[e]
RX J1113.8+4017.....	0.0795	1.80	12.6	4.36	88.73	1.440	5.879	6.1	36.39	0.913	6.696	0.1866	2	A1203
RX J1120.1+4318.....	0.60	2.15	5.33	4.88	48.43	2.117	2.728	8.1	10.63	1.000	3.285	5.0100	7	
RX J1142.2+1026.....	0.0698	3.33	6.15	5.88	40.27	1.272	4.245	10.8	40.04	0.927	5.182	0.1110	2	A1356
RX J1204.0+2807.....	0.167	1.69	6.16	4.56	29.50	4.492	10.60	3.2	20.93	0.997	12.38	1.4942	5	MS1201.5
RX J1211.2+3911.....	0.34	2.02	6.34	4.76	62.48	1.525	2.649	5.8	13.52	0.988	3.163	1.5948	5	MS1208.7
RX J1222.1+7526.....	0.24	2.88	5.14	4.48	31.01	1.175	1.353	20.5	16.28	1.000	1.630	0.4208	3	MS1219.9
RX J1227.4+0849.....	0.0895	1.70	9.48	7.97	74.61	5.872	19.75	2.5	33.15	0.983	22.57	0.7876	3	A1541
RX J1232.8+2605.....	0.22	1.36	10.4	5.72	73.53	1.828	3.577	8.0	17.47	0.932	4.136	0.8799	4	
RX J1241.5+3250.....	0.39	1.28	7.24	6.35	77.06	2.386	3.996	5.7	12.98	0.999	4.748	3.0995	6	
RX J1259.7−3236.....	0.076	5.92	7.68	4.80	77.70	1.198	4.058	11.7	37.59	0.884	5.222	0.1328	2	[f]
RX J1308.5+5342.....	0.33	1.59	8.57	6.20	44.76	1.254	1.732	10.7	13.62	1.000	1.978	0.9579	4	
RX J1311.2+3228.....	0.245	1.08	5.71	5.19	48.66	2.539	4.647	5.7	16.11	1.000	5.376	1.4223	4	MS1308.8
RX J1311.8+3227.....	0.43	1.08	5.62	5.52	73.97	1.472	2.029	9.4	12.22	0.913	2.375	1.9237	5	
RX J1334.3+5030.....	0.62	1.08	8.84	5.04	70.18	1.366	1.810	8.4	10.76	0.990	2.091	3.4606	6	[g]
RX J1343.7+5538.....	0.0766	1.05	12.8	6.60	68.94	1.808	9.228	4.9	37.31	0.946	10.32	0.2668	2	A1783
RX J1406.9+2834.....	0.117	1.40	6.68	5.01	28.69	1.304	3.625	7.3	26.93	0.987	4.085	0.2497	2	V154
RX J1416.4+2315.....	0.138	2.04	13.7	4.87	42.77	4.804	11.18	4.6	23.86	0.989	13.33	1.1066	4	[h]
RX J1418.5+2510.....	0.29	1.78	6.19	5.35	30.37	3.788	6.549	3.8	14.62	1.000	7.655	2.7618	6	V159
RX J1524.6+0957.....	0.078	2.88	5.53	5.14	16.07	1.646	2.236	29.8	36.70	0.914	2.371	0.0649	1	V170
RX J1541.1+6626.....	0.245	2.90	8.15	5.70	42.96	1.517	2.356	7.7	16.11	0.999	2.814	0.7578	3	[i]
RX J1641.2+8233.....	0.195	5.51	12.7	7.44	68.56	3.550	6.227	5.2	18.87	0.993	8.128	1.3550	4	V183
RX J1701.3+6414.....	0.453	2.51	5.62	4.71	13.16	1.986	3.302	4.7	11.62	0.997	3.965	3.4935	6	V190
RX J2237.0−1516.....	0.299	3.90	11.9	5.65	87.75	1.683	2.723	7.7	14.91	0.990	3.413	1.3525	4	
RX J2258.1+2055.....	0.288	4.91	5.74	4.81	51.96	2.262	4.428	6.1	14.76	0.997	5.694	2.0550	5	Z2255.5

NOTE.—The thirty-seven Bright SHARC clusters. Count rates (cols. [4] and [5]) are quoted in units of 10^{-2} counts s^{-1}.

[a] RX J0223.4 ($z = 0.163$) was detected in pointing rp800016n00, the central target of which was a wide angle radio (WAR) source. The cluster hosting this WAR source has a redshift of $z = 0.41$ (Nichol et al. 1994a). The redshift separation of the two clusters is $\delta z \simeq 0.247$.

[b] RX J0318.5 ($z = 0.37$) was detected in wp800555n00 which was pointed, accidentally, $\sim 40^\circ$ away in declination away from the listed target, A3112, which lies at 03 17 56−44 14 17 (Ebeling et al. 1996).

[c] RX J0321.9 (A3120, $z = 0.0696$) was detected in wp800371n00, the central target of which was a Couch et al. 1991 cluster at $z = 0.49$. The redshift separation of the two clusters is $\delta z = 0.42$.

[d] RX J0454.3 ($z = 0.26$) was detected in rp800229n00, the central target of which was cluster MS0451.6 ($z = 0.55$; Gioia & Luppino 1994). The redshift separation of the two clusters is $\delta z = 0.29$.

[e] RX J1024.3 (A981, $z = 0.201$) was detected in wp800641, the central target of which was cluster A998 ($z = 0.202$; Huchra et al. 1990). The redshift separation of the two clusters is $\delta z = 0.001$.

[f] RX J1259.7 ($z = 0.076$) was detected in rp800384n00, the central target of which was cluster A3537 ($cz = 5007$ km s^{-1}; Abell et al. 1989). The redshift separation of the two clusters is $\delta z = 0.059$.

[g] RX J1334.3 ($z = 0.62$) was detected in rp800047, the central target of which was cluster A1758 ($z = 0.2792$; Allen et al. 1992). The redshift separation of the two clusters is $\delta z = 0.34$.

[h] RX J1416.4 ($z = 0.138$) was detected in rp800401a01, the central target of which was galaxy 4C23.37 ($cz = 154$ km s^{-1}; De Vaucouleurs et al. 1991). The redshift separation of the two clusters is $\delta z = 0.137$.

[i] RX J1541.1 ($z = 0.245$) was detected in rp800511n00, the central target of which was A2125 ($z = 0.2465$; Struble & Rood 1987). The redshift separation of the two clusters is $\delta z = 0.0015$.

regions for the source and background apertures for each of the 37 Bright SHARC clusters. After subtraction of the appropriately scaled background, the total cluster count rates were derived by dividing by $(0.8 \times f_{80})$. The background-subtracted, aperture-corrected, total cluster count rates (cr_T) are listed in column (8) of Table 2. The 1 σ errors on the total cluster count rates are listed in column (9). These errors were calculated by adding in quadrature the counting errors on the cluster count rates and the background count rates. We draw attention to three SHARC clusters with anomalously high (>15%) count rates errors; RX J0250.0, RX J1524.6, and RX J1222.1. These clusters have much lower signal to noise values inside the cr_T apertures than in the cr_W apertures, demonstrating that the

adopted cluster model (eq. [2]) significantly over estimates the size of the aperture which encircles 80% of the source flux. The count rate errors are quoted as percentages since, in the absence of systematic errors in the count rate to flux/luminosity conversions (§ 6.2), they should also reflect the percentage errors on the flux (f_{-13}, col. [12]) and luminosity (L_{44}, col. [13]).

In Figure 2 we compare the initial wavelet count rates, cr_W (col. [7]), to the total aperture corrected count rates, cr_T. It can be seen that, as expected, the total count rate is systematically higher than the wavelet count rate. A least squares fit to the clusters at redshifts greater than $z = 0.15$ shows that the total count rate is typically 2.1 times higher than the wavelet value. At lower redshifts, the correction is higher because the clusters are significantly more extended than the $\sigma = 3$ pixel wavelet we used for source detection. It is encouraging that the wavelet count rate appears to be an unbiased measure of the total cluster count rate, since we have used the cr_W values to define the count rate limit of the Bright SHARC Survey.

6.2. *Luminosity Derivation*

We used the cr_T count rates listed in column (8) of Table 2 to determine fluxes and luminosities for each cluster. We note that we chose to present the fluxes and luminosities in the [0.5–2.0 keV] band, rather than in the Bright SHARC count rate band [0.4–2.0 keV], to allow easier comparison with other studies. Since the *ROSAT* PSPC provides only limited spectral resolution, we had to assume a spectral model for each cluster to make the conversion between measured cluster count rate and unabsorbed flux. As is typical in X-ray cluster analyses, we adopted an emission spectrum from hot, diffuse gas based on the model calculations of Raymond & Smith (1977). The integrated emission from a Raymond-Smith spectrum in the SHARC energy band (observer's rest frame) depends on several factors; the metallicity and temperature of the gas, the redshift of the cluster, and the absorption column along the line of sight. This means that the conversion between measured aperture count rate and cluster luminosity is nontrivial and must take into account the specific properties of each cluster. We note that, in most cases, the dominant source of error in the derived luminosities comes from the count rate uncertainty, which rises to 30% in the case of RX J1524.6. However, for those clusters with well-determined count rates (30 clusters have count rate errors of less than 10%) it is worth making the extra effort to reduce the systematic errors in the conversion between count rates, fluxes and luminosities.

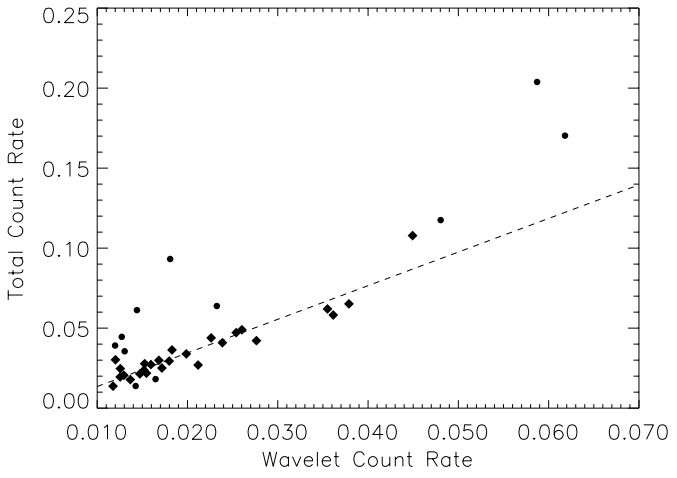

FIG. 2.—Wavelet count rate vs. the total count rate for each of the 37 clusters in the Bright SHARC sample. The low-redshift ($z < 0.15$) clusters are indicated by circles. A least squares fit to the $z > 0.15$ clusters (*diamonds*) is shown by the dotted line (slope = 2.1).

We have constructed a matrix of count rate to flux conversion factors as a function of temperature, redshift and absorbing column. (A single, canonical, value for the metallicity—one-third the solar value—was used throughout.) The conversion factors were derived using the "fakeit" command in XSPEC (version 10.00, Arnaud 1996) together with the appropriate *ROSAT* PSPC response function. Photoelectric absorption was included via the XSPEC "wabs" model, which is based on cross sections presented in Morrison & McCammon (1983). The neutral hydrogen column densities adopted for each cluster are listed in column (3) of Table 2. These values were derived using the AT&T Bell Laboratories 21 cm survey (Stark et al. 1992), for clusters north of $-40°$, and the values presented in Dickey & Lockman (1990) for clusters at lower declinations. In order to sample the observed distribution of cluster redshifts and column densities, and the expected distribution of cluster temperatures, we derived conversion factors over the following ranges; (i) $0.06 < z < 0.86$ (in increments of $\delta z = 0.05$), (ii) $0 < nH < 20 \times 10^{20}$ cm^{-2} (in increments of 1×10^{20} cm^{-2}), and (iii) $1 < T < 12$ keV (in increments of 1 keV). (When a cluster redshift or column density was not exactly matched by one of the matrix entries, linear interpolation was used.) As expected, the count rate to flux conversion varied most rapidly along the column density axis of this matrix, however, changing the redshift also had a measurable effect (by a factor of $\simeq 2$ over the range $0.08 < z < 0.8$). Estimates of the bolometric[6] and k-corrections were also derived, as a function of temperature, using XSPEC.

The luminosity derivation included an iteration to obtain an estimate of the X-ray temperature for each cluster, using the luminosity-temperature (L-T) relation presented in Arnaud & Evrard (1999). From a starting point of $T = 6$ keV an initial [0.5–2.0 keV] luminosity was derived. This luminosity was then converted into a pseudo bolometric luminosity, so that a temperature estimate (to the nearest integer in keV) could be derived. The new temperature was used to select a second count rate to flux conversion from the matrix and the process was repeated until convergence was reached. The temperature used in the final luminosity calculation is listed in column (14) of Table 2.

In the past, the luminosity-temperature (L-T) relation was not so well known and other groups have adopted a single temperature, usually 6 keV, for their luminosity calculations. Using the Arnaud & Evrard (1999) L-T relation, 6 keV corresponds to a cluster of $L_{44} \simeq 6$. Most of the clusters in Table 2 are significantly fainter than this, meaning that the use of a canonical temperature will yield inaccurate results, especially for the lowest luminosity clusters. This is illustrated by the faintest (and hence, coolest) cluster in our sample (RX J1524.6) which has a luminosity of $L_{44} = 0.065$ when a temperature of $T = 1$ keV is assumed and a luminosity of $L_{44} = 0.072$ when a tem-

[6] An energy range of 0.01–50 keV was used to calculate the (pseudo) bolometric corrections, which were found to be in excellent agreement with those presented in Fig. 2 of Borgani et al. (1999).

perature of $T = 6$ keV is assumed (an 11% effect). By contrast the effect is smaller (5%) for the hottest cluster in our sample; RX J0152.7 has a luminosity of $L_{44} = 8.26$ when a temperature of $T = 9$ keV is assumed and a luminosity of $L_{44} = 8.65$ when a temperature of $T = 6$ keV is assumed. It is worth mentioning that the L-T relation we use (Arnaud & Evrard 1999) was constructed from clusters known not to contain cooling flows. Another recent work (Allen & Fabian 1998) combines both noncooling flow and cooling flow clusters and fits a flatter slope to the L-T relation (2.4 compared to 2.9). Unfortunately, the poor photon statistics of the Bright SHARC cluster sample do not allow us to test for the presence of cooling flows, and so our choice of L-T relation will be inappropriate in some cases.

Finally, we note that the conversion between cluster count rate and cluster luminosity is a function of the adopted values of Hubble's constant and the deceleration parameter and that we have used $H_0 = 50$ km s^{-1} Mpc^{-1} and $q_0 = 0.5$ throughout.

7. DISCUSSION

In a companion paper (Nichol et al. 1999, hereafter N99) we use the Bright SHARC sample to examine evolution in the X-ray cluster luminosity function (XCLF). Future papers will go on to use these evolution results to constrain the density parameter Ω_m. It is appropriate, therefore, to discuss here some of the observational issues relevant to Ω_m analyses. These issues include systematic biases in the derived luminosities (§ 7.1) of the Bright SHARC clusters and any possible contamination (§ 7.2), or incompleteness (§ 7.3) in the Bright SHARC catalog. We also discuss the possible discovery of three "fossil groups" (§ 7.4) and our overlap with the 160 deg^2 survey of V98 (§ 7.5).

7.1. *Luminosity Bias in the Bright SHARC Cluster Sample*

A systematic bias in our luminosities would result in an over (or under) estimate of the number density of high-luminosity systems. To investigate whether such a systematic bias exists, we have compared the luminosities quoted in column (13) of Table 2 with published values for the six clusters we have in common with the EMSS (Gioia et al. 1990): RX J1024.3 (MS 1020.7 or A981), RX J1204.0 (MS 1201.5), RX J1211.2 (MS 1208.7), RX J1222.1 (MS 1219.9), RX J1311.2 (MS 1308.8), and RX J2258.1 (MS 2255.7 or Z2255.5). We have chosen to compare our luminosities for these clusters with those presented in Nichol et al. (1997, hereafter N97), rather than those presented in Henry et al. (1992), for two reasons. First, the luminosities quoted in N97 are in the *ROSAT* bandpass [0.5–2.0 keV] rather than the *Einstein* bandpass [0.3–3.5 keV]. Second, the N97 study used the SHARC pipeline to produce count rate maps. A comparison of the two sets of luminosities will, therefore, show if the methodology outlined in §§ 6.1 and 6.2 is robust (since a different methodology[7] was used in N97). We find our derived luminosities to differ by 0% for MS 1020.7, 1% for MS 1201.5, 5% for MS 1208.7, 26% for MS 1219.9, 2% for MS 1303.8, and 10% for MS 1219.9. These differences are all smaller than the 1 σ errors on the EMSS count rates quoted in N97. We note also that the luminosity we derive for RX J0152.7 is within 1% of the value derived by the WARPS collaboration in Ebeling et al. (2000).

We have also compared the fluxes quoted in column (12) of Table 2 with published values for the 11 clusters we have in common with the 160 deg^2 survey (V98, see § 7.3). In the fifth column of Table 3 we present the ratio of Bright SHARC to V98 fluxes. We find the Bright SHARC values to be systematically higher than those measured by V98, with an average flux ratio of 1.18. To understand this discrepancy, we have recalculated the Bright SHARC fluxes using the core radii and redshifts presented in V98. Except for RX J1641.2, the V98 core radii are all smaller than $r_c = 250$ kpc and, by using their values, we bring the average flux ratio down to 1.01 (sixth column).

We conclude that the methodology of §§ 6.1 and 6.2 is robust, although it has the disadvantage of over estimating the cluster flux if $r_c < 250$ kpc. Planned XMM observations of several Bright SHARC clusters will provide higher angular resolution and signal-to-noise images together with accurate estimates of the electron temperature. These observations will provide an important test of the methods described in §§ 6.1 and 6.2 since they will allow us to (i) more accurately excise contaminating sources in the cluster aperture, (ii) use fitted, rather than canonical, values for β, r_c and the ellipticity, (iii) be less sensitive to errors in the back-

[7] Differences between Bright SHARC and N97 include the use of the IRAF PROS package to set background apertures and the use of a constant temperature, $T = 6$ keV, for k-corrections and count rate to flux conversions.

TABLE 3

COMPARISON OF BRIGHT SHARC AND V98 FLUX MEASUREMENTS

Bright SHARC ID	V98 ID	Redshift	f_{-13}	Ratio[a]	Ratio[b]
RX J0237.9−5224.....	V28	0.1330	7.495	1.16	1.06
RX J0849.1+3731.....	V62	0.2300	2.525	1.72	1.48
RX J1204.0+2807.....	V112	0.1670	12.38	1.21	0.91
RX J1211.2+3911.....	V115	0.3400	3.163	1.19	0.83
RX J1308.5+5342.....	V132	0.3300	1.978	1.15	0.91
RX J1406.9+2834.....	V154	0.1170	4.085	1.58	1.22
RX J1418.5+2510.....	V159	0.2900	7.655	1.01	0.95
RX J1524.6+0957.....	V170	0.0780	2.371	0.78	0.83
RX J1641.2+8233.....	V183	0.1950	8.128	1.01	1.04
RX J1701.3+6414.....	V190	0.4530	3.965	1.03	0.92
RX J2258.1+2055.....	V213	0.2880	5.694	1.13	0.93
Average.....				1.18	1.01

[a] Ratios of the Bright SHARC fluxes (fourth column) to the V98 fluxes.

[b] Ratios of the recalculated Bright SHARC fluxes to the V98 fluxes, see § 7.1 for details.

ground calculation, and (iv) improve our spectral dependent count rate to flux conversions.

7.2. *Contamination of the Bright SHARC Cluster Sample*

The thorough, multiobject, spectroscopic follow-up of the Bright SHARC extended source list means that it is highly unlikely that any of the entries in Table 2 are misidentified contaminants. However, we stress that there are two clusters in that table which should *not* be used for studies of the cluster XCLF because their detections are not truly serendipitous: RX J1024.3 and RX J1541.1 were found in cluster pointings and lie at redshift separations from the pointing target of $\delta z < 0.002$, or $cz < 600$ km s^{-1}. These clusters are probably associated with the pointing target via the cluster correlation function (Romer et al. 1994; Nichol, Briel, & Henry 1994a). In addition, we feel that RX J1222.1 (MS 1219.9) warrants further study: This object is very compact, has a large count rate uncertainty (§ 6.1), and Gioia & Luppino (1994) note that its central galaxy has emission lines. It is possible, therefore, that the luminosity quoted in Table 2 is an overestimate due to AGN contamination. (Although, it should be noted that the presence of emission lines in the central galaxy could be attributed to cooling flow nebulosity or star formation; Crawford et al. 1999.) We note that the three clusters highlighted here (RX J1024.3, RX J1222.1, and RX J1541.1) have redshifts in the range $0.20 < z < 0.25$ and so were not used in the N99 analysis (which concentrated only on those clusters at $z > 0.3$).

7.3. *Incompleteness of the Bright SHARC Cluster Sample*

There are three possible ways in which the Bright SHARC cluster sample might be incomplete. First, there are those clusters that did not meet our selection criteria. Second, there is a possibility that some clusters were misidentified as contaminants. Third, there are the three extended sources which have yet to be identified.

We are using simulations to understand how the adopted selection criteria (§ 4) effects the completeness of the Bright SHARC cluster sample. We are in the process of carrying out a very thorough investigation of our selection function by adding many thousands of fake clusters (one at a time) to the pointings in our survey and then determining the fraction of these fake clusters that would have been selected as Bright SHARC cluster candidates. These simulations will provide us with the efficiency of cluster detection as a function of cluster parameters (e.g., redshift, luminosity, ellipticity, core radius etc.) and operational parameters (e.g., exposure time, off-axis angle, hydrogen column density, central target etc.). The results of these simulations will be presented elsewhere (Adami et al. 2000), but our preliminary findings are described in N99.

Let us now address possible cases where clusters might be misidentified as contaminants. We discuss first the two objects listed in Table 1 as blends of a cluster with another source, RX J0318.2 and RX J2314.7. The former, RX J0318.2, is a blend of a cluster with a QSO. (The cluster has the same redshift as the neighboring cluster RX J0318.8, $z = 0.37$). The surface brightness contours of RX J0318.2 are clearly dumbbell shaped, and so it has been possible to remove the QSO contribution from the total count rate. This object was also discovered as part of the Southern SHARC, and Burke (1998) has determined the total count rate and luminosity of this cluster to be $cr_T = 0.01362$ count s^{-1} and $L_{44} = 1.11$, respectively. Therefore, this cluster would not have made it into the Bright SHARC sample had it not been blended with the QSO and its exclusion for Table 2 is justified. By contrast, the boundary between the cluster and M star emission for RX J2314.7 is blurred. Hence, it is not possible to excise the M star flux to see if the cluster alone has a high enough count rate (and extent) to qualify as a Bright SHARC candidate. If the M star makes only a minimal contribution, less that 20%, to the total flux, then the cluster should have been included in Table 2: Assuming that all the RX J2314.7 flux comes from the cluster, the cluster would have a luminosity of $L_{44} = 1.31$.

As stated above, three of the 94 Bright SHARC extended sources remain unidentified. If all three were high-redshift, high-luminosity clusters, then there would be important implications for cluster evolution. In N99, we predict that the Bright SHARC survey should include 4.9 clusters with luminosities $L_{44} \geq 5$ in the redshift range $0.3 < z < 0.7$ (based on a simple extrapolation of the De Grandi et al. 1999b local XCLF). Since only one such cluster has been confirmed to exist in the Bright SHARC (RX J1120.1), we conclude in N99 that there may be evidence for evolution at luminosities brighter than $L_{44} = 5$. This evidence would effectively disappear if another three Bright SHARC clusters were added in this luminosity range. We stress, however, that it is very unlikely all these objects are clusters with luminosities brighter than $L_{44} = 5$; the CCD images of RX J0340.1 and RX J1705.6 are not consistent with the presence of distant clusters and RX J1838.8 is in a crowded star field (and so is most likely associated with a stellar X-ray source). We conservatively estimate that one these objects may be a cluster, given that the ratio of clusters to nonclusters among the other 91 identified sources is roughly 1:3. We have calculated that this cluster would have to reside at $z > 0.62$, $z > 0.57$ or $z > 0.51$, for RX J0340.1, RX J1705.6, and RX J1838.8, respectively, to have a luminosity greater than $L_{44} = 5$.

We also highlight candidate RX J1210.4. This object contains a QSO and has a compact X-ray surface brightness profile. Even though most of the flux from this source is probably coming the QSO, this object merits further study since a CCD image highlights a clustering of faint galaxies around the bright central object. The redshift of this source ($z = 0.615$) and its high count rate ($cr_W = 0.1430$) mean that if more than 18% of the count rate from this source was coming from an associated cluster, then this cluster would have a luminosity greater than $L_{44} = 5$.

For the various reasons outlined above, we have decided to continue the follow-up of the Bright SHARC in a variety of ways. As a first priority, we plan to identify the three remaining unidentified Bright SHARC extended sources (RX J0340.1, RX J1705.6, and RX J1838.8). We also plan to obtain identifications for at least one portion of the seven "id-pending" blends listed in Table 1 and to continue our campaign to obtain velocity dispersions for the Bright SHARC clusters. Moreover, we hope to obtain higher resolution X-ray images of complex sources such as RX J1210.4, RX J1222.1, and RX J2314.7 to help determine the contamination level.

7.4. *Fossil Groups and Dark Clusters in the Bright SHARC Survey*

We present evidence for the discovery of three new "fossil groups" (Ponman et al. 1994) or X-ray overluminous elliptical galaxies (OLEGs, Vikhlinin et al. 1999). These objects

are predicted to occur when a galaxy group relaxes to form a single elliptical galaxy. They are interesting because they provide invaluable insight into the processes of elliptical galaxy evolution, metal enrichment in the intracluster medium, and the dynamics of extended dark halos (Mulchaey & Zabludoff 1998). Their observational signatures would be an isolated cD or giant elliptical galaxy surrounded by a cool ($T \simeq 1$ keV), extended, X-ray halo. Two galaxies detected in the Bright SHARC survey appear to share these properties; RX J1730.6 (NGC 6414, $z = 0.05$) and RX J0327.9 (UGC 2748, $z = 0.03$). Applying the same method used to obtain total cluster count rates (§ 6.1), we have measured their luminosities to be $L_{44} = 0.158$ and $L_{44} = 0.056$, respectively.[8] In addition to these two galaxies, one of the Bright SHARC clusters, RX J0321.9 (A3120, $z = 0.0696$, $L_{44} = 0.43$), also appears to display "fossil group" characteristics. We highlight these objects here since they are ideal targets for follow-up studies at X-ray and optical wavelengths. We have estimated the "fossil group" space density to be $\sim 2 \times 10^{-6}$ Mpc^{-3} under the assumption that the Bright SHARC is 100% efficient in detecting extended sources in the redshift range $0.02 < z < 0.08$ and at luminosities of $L_{44} > 0.1$.

In addition to estimating the space density of "fossil groups," we can comment on the space density of "dark clusters" or "failed clusters." These objects are theorized to have cluster-like masses and to radiate in the X-rays but to have an underluminous galactic component (Tucker, Tananbaum, & Remillard 1995; Hattori et al. 1997). We have successfully identified 91 of the 94 Bright SHARC extended sources and have found no evidence for "dark clusters." To avoid detection in the Bright SHARC, these objects either must have a lower space density than rich clusters and "fossil groups" or they must be intrinsically faint and evolve rapidly (to avoid detection at low redshift). In either case, "dark clusters" are unlikely to be a significant contribution to the mass of the universe.

7.5. *Comparison with the* 160 deg^2 *Survey*

As pointed out by N99, it may be possible to combine the Bright SHARC with the 160 deg^2 survey (V98) to maximize the area available for high-redshift cluster searches. The motivation for this is demonstrated by Figure 3, which shows several gaps in the redshift coverage of our survey. Even though we are able to find high-luminosity clusters out to at least $z = 0.83$, we find none at $z \simeq 0.5$ or $z \simeq 0.7$. The only way to guarantee more $L_{44} > 3$ cluster detections would be to search over a wider area. The combination of the two surveys would yield a search area of $\simeq 260$ deg^2, since only 44% (or $\simeq 78$ deg^2) of the Bright SHARC Survey overlaps with the 160 deg^2 survey. (There are 201 pointings in common between the 160 deg^2 and Bright SHARC Surveys; A. Vikhlinin 1999, private communication).

There are 13 sources in common between the Bright SHARC and the 160 deg^2 surveys. Of these 13, five clusters have not been followed up spectroscopically by either survey but rely on literature redshifts (RX J1010.2,[9] RX J1204.0, RX J1211.2, RX J1311.2, RX J2258.1). An additional three clusters have both Bright SHARC and V98 redshifts (RX J0849.1, RX J1406.9, RX J1701.3); with the two redshifts being in agreement in all cases. We have also been able to provide spectroscopic information for five 160 deg^2 sources which previously relied on photometric redshifts; RX J0237.9 (V28), RX J0947.8 (V75), RX J1418.5 (V159), RX J1524.6 (V170), and RX J1641.2 (V183). We have identified RX J0947.8 as a blend, the main component of which is a QSO[10] at $z = 0.63$ (Burke 1998). We confirm that the other four sources are clusters and we find that the photometric redshifts listed in V98 are good estimates of the true redshift, with the largest error being $\delta z = 0.065$ for RX J1641.2. This cluster has been shown to be at $z = 0.195$, giving it a luminosity of $L_{44} = 1.355$. It is not, therefore, a high-redshift, high-luminosity, cluster, as previously suggested by Vikhlinin et al. (1998b), based on the upper limit of the estimated redshift ($z_{\rm est} = 0.26^{+0.04}_{-0.07}$).

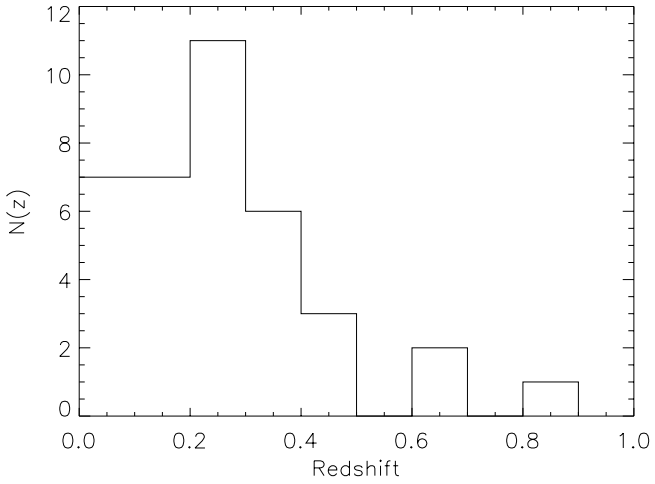

FIG. 3.—Redshift distribution of the 37 clusters in the Bright SHARC

In addition to the 13 sources described above, 77 other V98 clusters were detected in the 201 pointings common to the two surveys. Most of these clusters are too faint to have been included in the Bright SHARC sample, only nine have wavelet count rates greater than the Bright SHARC threshold ($cr_W = 0.01163$). Of these nine, seven were not included in the Bright SHARC because they did not meet our filling factor criterion ($f < 1.3$), one was detected at an off-axis distance less than our threshold of 2.5 and one did not meet our extent criterion. Conversely, two clusters (RX J0256.5 and RX J1311.8) in Table 2 are not listed in V98, despite falling in common pointings, because they lie beyond the V98 off-axis limit of 17.5. These examples demonstrate how differing survey selection criteria produce differing cluster samples and that detailed simulations are required to determine a survey's selection function.

There are eight confirmed $L_{44} > 3$ clusters in the Bright SHARC; RX J0152.7, RX J0256.5, RX J0318.5, RX J0426.1, RX J1241.5, RX J1120.1, RX J1334.3, and RX J1701.3. The presence of so many $L_{44} > 3$ clusters in the Bright SHARC has allowed us to show that the XCLF is nonevolving up to $L_{44} \simeq 5$ (N99). It is important to note that, even after the combination of Bright SHARC and 160 deg^2 surveys, the areal coverage available for high-redshift cluster searches

[8] Assuming an absorbed Raymond Smith spectrum with an electron temperature of $T = 1$ keV.

[9] RX J1010.2 was not included in Table 2 because its redshift ($z = 0.045$) is too low, i.e., $z < 0.07$.

[10] Subsequent observations by Vikhlinin et al. have shown that this QSO most likely resides on the outskirts of a cluster at the same redshift (A. Vikhlinin 1999, private communication).

will still be only about one-third that of the EMSS at the bright end (Henry et al. 1992). This means that we will probably have to wait until larger area surveys are made available, e.g., from the *XMM* satellite (Romer et al. 2000) to make definitive statements about XCLF evolution at $L_{44} > 5$.

We acknowledge financial support from NASA grants NAG5-2432 (A. R., R. P., C. A., and M. U.), NAG5-6548 (R. N.), NAG5-3202 (B. H.), and GO-06838.01-95A (B. H.). And also from a NASA Space Consortium grant through Aerospace Illinois (A. M., K. C., B. H.), the CMU undergraduate research initiative (A. J. M.), the NSF Center for Astrophysical Research in Antartica (B. H.), NSF grant AST-9256606 (B. H.) and PPARC (D. B.). This research has made use of: (i) Data obtained through the High-Energy Astrophysics Science Archive Research Center Online Service, provided by the NASA-Goddard Space Flight Center. (ii) The Digitized Sky Survey, which was produced at the Space Telescope Science Institute under US Government grant NAG W-2166. (iii) The NASA/IPAC Extragalactic Database (NED), which is operated by the Jet Propulsion Laboratory, Caltech, under contract with the National Aeronautics and Space Administration. (iv) The "APM Catalogues at AAO" web server, author Micheal Drinkwater. (v) The APS Catalog of POSS I and the APS Image Database, which are supported by the National Science Foundation, the National Aeronautics and Space Administration, and the University of Minnesota. We offer special thanks to Jim DeVeny and the support staff at the ARC, CFHT, CTIO, ESO, and KPNO telescopes, and also to Alain Blanchard, Francisico Castander, Ian Del Antonio, Paul Lynam, Eric Monier, Francis Falbo, Tim Kimball, Marc Postman, Patricia Purdue, Connie Rockosi, Rachid Sadat, Steve Snowden, Jeffrey Tran, Dave Turnshek, Pedro Viana, Alexey Vikhlinin, and an anonymous referee.

APPENDIX A

Table 4 shows the 460 *ROSAT* PSPC pointings in the Bright SHARC survey.

TABLE 4

ROSAT PSPC Pointings in the Bright SHARC Survey

Pointing (1)	R.A. (J2000) (2)	Decl. (J2000) (3)	b (deg) (4)	Time (s) (5)	Pointing Target (6)
rp800469n00	00 02 28.8	+31 28 48.0	−30.2	13977	NGC 7805
rp700467n00	00 03 24.0	−26 03 36.0	−79.2	35368	Q0000−26
rp700101	00 08 16.8	+20 41 24.0	−41.0	24608	Mrk 335
wp800386n00	00 09 31.2	−33 54 36.0	−78.7	18363	Sculptor/Phoenix N
wp800388n00	00 11 19.2	−36 25 12.0	−77.4	22751	Sculptor/Phoenix S
rp800253n00	00 18 33.6	+16 26 24.0	−45.7	33636	CL 0016+16
wp400322	00 19 50.4	+21 57 00.0	−40.3	10954	RX J0019.8+2156
rp800483n00	00 22 52.8	+04 24 00.0	−57.7	24905	CL 0020
rp300016	00 30 4.8	+26 17 24.0	−36.3	25539	PG 0027+260
rp800486n00	00 31 31.2	+08 25 48.0	−54.1	19391	HCG 2
wp800387n00	00 31 38.4	−35 43 12.0	−80.4	13824	Sculptor/Phoenix ref
rp600244n00	00 36 00.0	+39 45 00.0	−23.0	30785	M31 Pos 2
rp700377	00 46 14.4	+01 04 12.0	−61.7	10823	Q0043+0048
rp600245n00	00 47 28.8	+40 30 00.0	−22.3	9657	M31 Pos 3
rp700331	00 48 45.6	+31 57 36.0	−30.9	22694	Mrk 348
rp700275n00	00 52 4.8	−29 05 24.0	−88.0	24088	SGP 2
rp900496a01	00 55 00.0	−28 19 48.0	−88.5	18034	SGP 3
rp701223n00	00 57 28.8	−27 38 24.0	−88.5	45513	GSGP 4
rp700424	00 57 48.0	+30 21 00.0	−32.5	25916	NGC 315
wp700528	00 58 4.8	−27 38 24.0	−88.4	18145	SGP 4
wp701194	01 03 38.4	−30 09 00.0	−85.9	12314	0101−304
rp201488n00	01 09 48.0	+19 39 36.0	−43.0	13499	HD 6903
rp700794n00	01 11 28.8	−38 04 48.0	−78.2	10094	NGC 424
rp800292n0	01 14 45.6	−48 30 00.0	−68.1	11458	Abell 2889
rp100376n00	01 18 36.0	−22 55 12.0	−82.5	15533	WFC focus check GD 695
rp800473a01	01 20 43.2	−34 02 24.0	−80.6	7460	NGC 491
wp701048	01 24 31.2	+03 48 00.0	−58.0	12463	520
rp700976	01 24 45.6	+09 18 36.0	−52.6	10686	MS 0122.1+0903
wp800645n00	01 26 2.4	−00 08 24.0	−61.7	12827	Group 3
rp800487n00	01 26 7.2	+34 40 48.0	−27.6	14221	HCG 10
wp800358	01 27 31.2	−04 40 12.0	−65.9	8917	HCG 12
wp200208	01 36 43.2	−18 22 12.0	−76.3	25642	UV Ceti
wp701499n00	01 39 40.8	+17 52 48.0	−43.4	16146	PKS 0136+176
rp701407n00	01 39 57.6	+01 31 48.0	−59.0	14936	0137+012

TABLE 4—*Continued*

Pointing (1)	R.A. (J2000) (2)	Decl. (J2000) (3)	b (deg) (4)	Time (s) (5)	Pointing Target (6)
rp300043n00	01 41 00.0	−67 53 24.0	−48.5	13250	BL HYI
rp700108	01 43 57.6	+02 21 00.0	−57.9	11369	Mrk 573
rp600005n00	01 53 00.0	−13 44 24.0	−70.3	22826	NGC 720
wp201325	01 57 48.0	+37 40 48.0	−23.3	14159	NGC 752
wp600422	02 01 12.0	−31 43 48.0	−74.1	13725	01590−3158
wp300359n00	02 03 48.0	+29 59 24.0	−30.3	10362	RX J0203.8+2959
rp300003	02 06 52.8	+15 18 00.0	−43.7	24206	TT Arietis
rp700432n00	02 07 50.4	+02 43 12.0	−54.9	13555	NAB 0205+024
rp700027a01	02 09 28.8	−39 30 36.0	−69.6	16319	Q0207−398
rp800114n00	02 09 33.6	−10 09 36.0	−64.9	14482	Arp 318
rp700316	02 09 38.4	+35 48 −0.0	−24.4	13308	0206+35
rp900352n00	02 17 19.2	−17 45 36.0	−68.1	9646	G192−67
wp900147	02 22 24.0	+19 53 24.0	−38.0	26437	MBM 7
rp800016n00	02 23 21.6	−09 03 00.0	−61.7	13415	
rp800482n00	02 33 40.8	+00 45 00.0	−52.8	26014	CL 0231
rp120100n00	02 34 21.6	−43 47 24.0	−63.4	13122	PSPC particle background
rp700350n00	02 35 7.2	−04 01 48.0	−56.1	9554	0232−042
rp300201n00	02 36 12.0	−52 19 12.0	−58.1	14581	WW Hor
rp701356n00	02 37 12.0	−52 15 36.0	−58.0	23179	ESO 198−G24/ WW Hor
rp600003n00	02 39 55.2	−34 31 12.0	−65.6	9783	Fornax
rp600520n00	02 41 4.8	−08 15 00.0	−57.9	11848	NGC 1052
rp800508n00	02 41 7.2	+08 44 24.0	−45.3	13875	S49−128
rp700920	02 49 19.2	+19 18 00.0	−35.4	12876	Mrk 372
rp701403n00	02 55 12.0	+00 10 48.0	−49.6	10731	NGC 1144
wp900138	02 57 4.8	+19 50 24.0	−34.0	25896	MBM 12
wp800566n00	03 03 31.2	−15 40 48.0	−57.3	12604	HCG 22
rp150052n00	03 14 12.0	−23 15 36.0	−57.5	15967	EF Eri
rp701036n00	03 15 9.6	−55 13 48.0	−51.7	45465	The Marano Field
rp600131n00	03 17 19.2	−41 06 36.0	−57.0	16631	NGC 1291
wp800555n00	03 17 57.6	−02 57 00.0	−47.4	12729	A 3112
rp600504n00	03 18 14.4	−66 30 00.0	−44.6	13998	NGC 1313
rp700437n00	03 22 40.8	−37 12 36.0	−56.6	23313	Fornax A
wp800371n00	03 23 12.0	−51 05 24.0	−52.7	20694	J1780 (5BL)
rp800307n00	03 23 24.0	−53 37 12.0	−51.5	21007	Field B-3
rp600006n00	03 26 48.0	−21 19 48.0	−54.2	27605	NGC 1332
rp700099m01	03 28 26.4	+02 48 36.0	−41.7	24508	H0323+022
rp800306n00	03 29 52.8	−53 07 48.0	−50.9	9981	Field B-2
wp800367a01	03 32 57.6	−39 06 36.0	−54.4	14937	J2175 (23C)
wp300079	03 37 55.2	−25 21 00.0	−52.7	51925	EXO 033319−2554.2
rp900495n00	03 42 9.6	−44 54 36.0	−51.7	45907	QSF 1
wp900632n00	03 42 12.0	−44 07 48.0	−51.9	44480	QSF 3
rp150082n00	03 42 14.4	−44 07 48.0	−51.9	22562	QSF 3
rp200107m01	03 52 43.2	+17 38 24.0	−27.2	27121	V471 Tau
rp800308	03 57 16.8	−53 06 36.0	−47.1	11738	Field C-1
rp700271n00	04 05 33.6	−13 08 24.0	−42.6	9755	0403−132
rp700825a01	04 09 21.6	+12 17 24.0	−27.8	13956	0406+121
rp800171n00	04 12 55.2	−65 51 00.0	−40.4	20586	F 1557
rp900242n00	04 14 16.8	−12 44 24.0	−40.5	9826	NGC 1535
wp201748n00	04 14 26.4	+12 26 24.0	−26.8	15950	Hyades field G3
rp200912a01	04 15 28.8	+16 40 12.0	−23.9	17815	Hyades C
wp600623n00	04 15 28.8	−55 37 12.0	−43.8	14870	NGC 1553/49
rp800089n00	04 16 2.4	−11 32 24.0	−39.6	10271	A 483
wp600456n00	04 20 00.0	−54 56 24.0	−43.3	16925	NGC 1566
rp200776n00	04 20 52.8	+13 51 36.0	−24.7	23044	Hyades field F1
wp200441	04 21 12.0	+14 42 00.0	−24.1	11734	Hyades, position 1
rp200442n00	04 21 12.0	+17 31 48.0	−22.3	17954	Hyades, position 2
rp201370a01	04 21 28.8	+18 25 12.0	−21.7	11768	Hyades field F4
rp700026	04 22 12.0	−38 45 00.0	−44.9	14886	Q0420−388
rp200020n00	04 24 50.4	+15 06 00.0	−23.2	34058	Hyades field #1
wp200777	04 25 36.0	+15 56 24.0	−22.5	15717	Hyades field F2
rp201369n00	04 26 24.0	+16 51 00.0	−21.8	13409	Hyades field G1
wp201368	04 30 4.8	+15 38 24.0	−21.8	14024	Hyades field F3
rp800471n00	04 30 45.6	+00 24 36.0	−30.6	8173	NGC 1588
rp200911a01	04 31 24.0	+12 23 24.0	−23.6	10110	Hyades B
rp200444n00	04 32 28.8	+14 42 00.0	−22.0	12355	Hyades, position 4

TABLE 4—*Continued*

Pointing (1)	R.A. (J2000) (2)	Decl. (J2000) (3)	b (deg) (4)	Time (s) (5)	Pointing Target (6)
wp900143	04 34 14.4	−14 39 00.0	−36.9	9261	MBM 20
wp201747n00	04 34 36.0	+15 30 00.0	−21.1	18782	Hyades field G2
rp180042n00	04 37 16.8	−47 15 00.0	−41.9	9507	PSR J0437−4715
rp200980n00	04 37 43.2	+11 19 12.0	−23.0	9449	VLM Hyades 2
rp180069n00	04 37 52.8	−02 25 12.0	−30.5	12180	SNR shell Voges
rp700028	04 40 16.8	−43 33 00.0	−41.5	10132	PKS 0438−436
rp900017	04 40 55.2	−16 30 36.0	−36.1	21306	EDS-PSPC
rp701021n00	04 45 43.2	−59 15 00.0	−38.9	18943	NGC 1672
wp300221n00	04 53 24.0	−42 13 48.0	−39.1	11673	RX J0453.4−4214
rp800229n00	04 54 12.0	−03 01 12.0	−27.3	12532	MSS 0451.6−0305
wp600436n00	04 54 14.4	−53 21 36.0	−38.7	22362	NGC 1705
wp701557n00	05 02 7.2	+03 31 48.0	−22.3	11372	MS 0459+0327
rp700826n00	05 03 21.6	+02 03 00.0	−22.8	11258	0500+019
rp700233n00	05 05 50.4	−28 35 24.0	−34.4	18705	0503−286
rp600094n00	05 07 43.2	−37 30 36.0	−35.8	10599	NGC 1808
rp200523n00	05 11 40.8	−45 01 12.0	−36.0	14538	LHS 29
wp800368n00	05 13 33.6	−48 18 36.0	−35.8	22205	J2001 (21C)
rp700422	05 16 12.0	+00 09 00.0	−20.9	23392	AKN 120
rp300193a01	05 29 26.4	−32 49 12.0	−30.6	20102	TV Columbae
wp300130a01	05 29 26.4	−58 54 36.0	−33.4	14132	RX J0529.4−5855
rp300334n00	05 31 36.0	−46 24 00.0	−32.6	32514	RE 0531−461
rp400246n00	05 32 50.4	−66 22 12.0	−32.5	14050	4U 0532−664
rp300023n00	05 43 19.2	−41 01 48.0	−29.7	13301	H0542−407
wp201245n00	05 57 2.4	−75 40 12.0	−29.5	17149	K1-27
rp701359n00	05 57 40.8	−38 28 48.0	−26.4	13260	3A0557−383
rp300111	06 10 33.6	−48 44 24.0	−26.5	10933	4U0601−49
rp701216n00	06 15 36.0	+71 02 24.0	22.7	15400	Markarian 3
wp201603n00	06 41 19.2	+82 16 12.0	26.5	27227	SV CAM
rp700210n00	07 21 52.8	+71 19 48.0	28.0	17336	S5 0716+71
rp200450n00	07 25 33.6	+29 29 24.0	19.8	10951	NGC 2371−2
rp600536n00	07 36 55.2	+65 36 00.0	29.1	8707	NGC 2403
rp700112	07 42 40.8	+65 10 48.0	29.7	18358	Mrk 78
wp180036n00	07 51 12.0	+18 07 12.0	21.0	13508	Unknown
wp300388n00	07 51 16.8	+14 44 24.0	19.7	21059	RE 0751+14
rp180046n00	07 51 24.0	+17 30 36.0	20.8	8723	GRO J0752+1
rp700315	07 58 28.8	+37 47 24.0	28.8	15463	0755+37
rp600169n00	08 13 14.4	+45 59 24.0	32.9	14050	MK 86
wp600431n00	08 19 16.8	+70 42 36.0	32.7	8359	HOL II
wp200453	08 26 52.8	+26 37 48.0	31.7	14808	DX Cnc
rp900349n00	08 28 43.2	+09 19 48.0	25.8	7283	G213+26
rp400020	08 38 48.0	+36 31 12.0	36.4	9782	GBS 0839+37
rp200654n00	08 41 16.8	+64 22 12.0	36.0	28342	PI**1 UMa
wp800370n00	08 47 40.8	+17 54 −0.0	33.4	16948	F1767 (10TC)
rp700546n00	08 48 19.2	+37 40 12.0	38.5	10400	E0845+378
rp900009	08 49 12.0	+44 50 24.0	39.1	70219	Lynx.3A
rp800019	08 49 14.4	+44 28 48.0	39.1	15244	
rp700887n00	08 53 7.2	+13 52 48.0	33.1	18002	0850+140
rp900239n00	08 55 4.8	+17 04 48.0	34.8	14171	VLB
rp701375n00	08 58 7.2	+27 51 00.0	38.7	14410	3C 210
rp700436	08 58 40.8	+14 09 00.0	34.4	20342	3C212
rp700120	09 05 31.2	+34 07 48.0	41.5	15240	B2 0902+343
rp900327a01	09 06 52.8	+33 39 36.0	41.7	28869	ZEL
rp201382n00	09 09 31.2	+54 24 00.0	41.6	32344	XY UMa
rp700329	09 09 33.6	+42 54 00.0	42.8	21113	3C216
wp700211	09 21 36.0	+62 15 36.0	40.9	19212	S4 0917+62
wp600204	09 21 57.6	+50 59 24.0	44.1	12049	NGC 2841
rp700882n00	09 22 14.4	+74 59 24.0	35.5	12222	0917
wp700262	09 25 12.0	+52 17 24.0	44.3	8567	Mrk 110
wp800557n00	09 30 7.2	+34 18 −0.0	46.5	15613	HGR 24
wp600165	09 34 2.4	+55 14 24.0	44.8	15018	I Zw 18
rp600207n00	09 35 52.8	+61 21 00.0	42.8	15072	UGC 5101
rp700387	09 41 4.8	+38 54 00.0	48.8	15720	0937+391
rp800102	09 42 55.2	+46 59 24.0	48.2	11851	A851
wp701458n00	09 45 43.2	−14 19 48.0	28.7	18102	NGC 2992
wp701587n00	09 47 45.6	+07 25 12.0	42.2	10605	3C227

TABLE 4—*Continued*

Pointing (1)	R.A. (J2000) (2)	Decl. (J2000) (3)	b (deg) (4)	Time (s) (5)	Pointing Target (6)
wp701554n00	09 49 40.8	+29 55 12.0	50.2	10196	PG 0946+301
rp701214n00	09 49 45.6	+73 14 24.0	38.0	8591	4C73.08
rp701367n00	09 50 48.0	+39 27 00.0	50.7	11866	PG 0947+396
rp600514n00	09 52 19.2	+71 45 36.0	39.1	7928	M82-North
wp800359n00	10 00 21.6	−19 39 00.0	27.5	12625	HCG 42
rp700319	10 01 57.6	+55 40 48.0	48.3	16284	NGC 3079
wp600178	10 02 00.0	−08 09 36.0	35.8	13605	09595−0755
rp600174n00	10 03 7.2	−26 09 36.0	23.0	17535	NGC 3109
rp300222n00	10 07 36.0	−20 16 48.0	28.1	8891	RX J1007.6−2017
wp900214	10 10 12.0	+50 45 00.0	51.4	15111	Survey field 5
wp700265	10 10 14.4	+51 45 00.0	51.1	22032	Survey field 4
wp700263	10 10 14.4	+52 45 00.0	50.6	12911	Survey field 3
wp900213	10 10 16.8	+54 45 00.0	49.8	15452	Survey field 4
wp700264	10 10 16.8	+53 45 00.0	50.2	15762	Survey field 2
rp900215n00	10 10 19.2	+55 45 00.0	49.3	15728	Survey field 6
rp600051	10 18 16.8	+41 25 12.0	55.6	15109	NGC 3184
wp900400a01	10 19 16.8	+52 45 00.0	51.9	11869	Lockman Spur A
wp600575n00	10 19 55.2	+45 33 00.0	54.8	12624	NGC 3198
wp900528n00	10 20 40.8	+39 15 00.0	56.5	9039	HVC 1
rp700996n00	10 23 31.2	+19 51 36.0	55.4	18545	NGC 3227
rp700540n00	10 24 33.6	+47 09 00.0	55.0	15840	10214+4724
wp800641n00	10 26 16.8	+67 56 24.0	43.7	10711	A998
wp900401a01	10 27 14.4	+53 29 24.0	52.6	15031	Lockman Spur B
wp900529n00	10 28 16.8	+38 58 48.0	57.9	8241	HVC 2
rp800315n00	10 30 9.6	−03 09 36.0	44.4	9307	MKW 2
wp701544n00	10 31 19.2	+50 53 24.0	54.4	8740	RXJ 10313+5053
rp700461n00	10 31 55.2	−14 16 48.0	36.5	13364	HE 1029−1401
rp900149	10 35 7.2	+54 14 24.0	53.2	16124	UMa Cloud 1
wp201243n00	10 37 4.8	−00 08 24.0	47.7	17856	PG 1034+001
rp800423n00	10 40 48.0	+67 11 24.0	45.2	9402	A1061
rp700384	10 42 45.6	+12 03 36.0	56.3	9698	1040+123
rp700883n00	10 43 19.2	+31 31 12.0	61.8	20631	1040+31
rp201020n00	10 45 21.6	+45 34 12.0	58.9	10597	TX UMa
wp800366a01	10 46 4.8	−00 24 00.0	49.1	18321	J1834 (5BC/8BL/22CR)
rp700999a02	10 46 24.0	−00 21 00.0	49.2	14526	BJS 855
wp600280n00	10 46 33.6	+63 14 24.0	48.5	7840	NGC 3359
rp300158n00	10 47 14.4	+54 18 36.0	54.6	10942	EK UMa
rp600261n00	10 49 50.4	+33 00 00.0	63.1	15163	Arp 270
wp300234a01	10 51 36.0	+54 04 48.0	55.2	11016	EK UMa
wp900029a04	10 52 4.8	+57 22 12.0	53.1	42207	The Lockman Field
rp900329n00	10 58 12.0	+64 29 24.0	48.5	7853	UMa 5
wp300291n00	11 02 40.8	+25 04 48.0	65.5	42588	ST LMI
rp500157n00	11 02 52.8	+60 53 24.0	51.5	16189	G290.1−0.8
wp180019n00	11 04 00.0	−18 00 00.0	37.8	13046	Too HE 1104−18AB
rp700872n00	11 06 48.0	+72 34 12.0	42.4	9885	NGC 3516
wp600464a01	11 09 57.6	−37 32 24.0	21.0	19192	NGC 3557
rp201019n00	11 13 12.0	−26 28 12.0	31.4	10415	TT Hya
rp700855n00	11 14 38.4	+40 37 12.0	65.9	13841	1111+408
rp600263n00	11 16 55.2	+18 02 24.0	66.4	22941	NGC 3607
rp700358	11 18 16.8	+07 46 12.0	60.6	13920	1115+080
rp600537n00	11 18 55.2	+13 05 24.0	64.2	13587	NGC 3623
wp700228	11 19 9.6	+21 19 12.0	68.2	22014	1116+215
rp700010	11 20 16.8	+13 35 24.0	64.7	13581	NGC 3628
rp800646a01	11 21 4.8	+03 14 24.0	57.7	12728	Group 4
rp900383n00	11 21 14.4	+43 17 24.0	65.6	8960	M1-X2
wp800537n00	11 21 28.8	+34 19 48.0	69.4	18613	A 1228
wp700510	11 24 43.2	+38 45 36.0	68.4	6687	1122+39
wp600570n00	11 28 2.4	+78 59 24.0	37.3	8215	VII Zw 403
wp900384n00	11 28 43.2	+43 00 36.0	66.9	7975	M1-X3
rp700372n00	11 29 16.8	−04 24 00.0	52.7	16283	1126−041
rp900148	11 31 50.4	+63 50 24.0	51.0	16259	UMa Cloud 2
rp900336n00	11 35 21.6	+59 43 12.0	54.8	7734	UMa 12
rp200091	11 36 33.6	+29 48 00.0	73.3	29402	GD 140
rp900150	11 37 45.6	+61 13 12.0	53.7	17123	UMa Cloud 3
rp701357n00	11 38 9.6	−37 49 48.0	22.8	19273	NGC 3783

TABLE 4—*Continued*

Pointing (1)	R.A. (J2000) (2)	Decl. (J2000) (3)	b (deg) (4)	Time (s) (5)	Pointing Target (6)
wp701201n00	11 39 12.0	+33 01 12.0	73.3	10400	MS 1136.5+3413
wp600420	11 42 9.6	+10 16 48.0	66.5	11414	11395+1033
rp600236n00	11 43 12.0	+55 04 12.0	59.4	18678	NGC 3921
wp300367n00	11 45 7.2	+72 21 −0.0	43.8	11409	DO Dra
wp300287n00	11 46 50.4	+28 44 24.0	75.6	16198	RE 1149+28
rp700833n00	11 50 19.2	+24 18 00.0	75.9	10074	1147+245
rp600533n00	11 51 2.4	−28 48 36.0	32.2	22352	N3923
rp700055	11 57 55.2	+55 27 00.0	60.0	45906	NGC 3998
wp701202	12 01 14.4	−03 40 48.0	56.8	13246	MS 1158.6−0323
wp600468a02	12 01 55.2	−18 52 48.0	42.4	16629	NGC 4038/9
wp700557	12 03 12.0	+44 33 00.0	70.0	25553	NGC 4051
rp800039	12 04 9.6	+20 13 12.0	77.1	15198	N79−299A
rp201367m01	12 04 24.0	−03 40 12.0	57.1	47791	PG 1159−035
wp700232	12 04 43.2	+27 54 00.0	79.6	24408	1202+281
wp700557m01	12 06 45.6	+44 20 24.0	70.5	19417	NGC 4051
wp700277	12 10 31.2	+39 24 36.0	75.0	32886	NGC 4151
rp600625n00	12 11 33.6	+39 01 12.0	75.4	11791	MS 1209+3917
wp800421n00	12 14 21.6	+13 05 24.0	73.4	13975	Group 1
rp600130	12 15 4.8	+33 12 00.0	80.0	21457	NGC 4203
rp600189n00	12 16 43.2	+69 28 12.0	47.3	11859	NGC 4236
wp600417a01	12 17 9.6	+07 11 24.0	68.4	10275	NGC 4235
wp700221	12 17 50.4	+30 07 12.0	82.0	21345	B2 1215+30
rp700970n00	12 18 26.4	+30 02 24.0	82.1	15004	Mrk 766 field
wp600166	12 19 9.6	+03 51 36.0	65.4	11656	MK 49
rp700425n00	12 19 24.0	+05 49 12.0	67.3	18879	NGC 4261
rp700864a01	12 20 33.6	+33 43 12.0	80.6	17386	3C 270.1
wp701056	12 21 21.6	+30 10 48.0	82.7	10572	2A 1218+304
wp700223	12 21 31.2	+28 13 48.0	83.2	13924	ON 231
rp700434	12 21 43.2	+75 18 36.0	41.6	11569	Mrk 205
wp200307	12 23 00.0	+25 57 00.0	83.5	16076	COM 15
rp600009	12 24 26.4	+07 19 12.0	69.1	14424	NGC 4365
wp600587n00	12 26 28.8	+09 01 12.0	70.9	17704	NGC 4410
rp600242a01	12 27 43.2	+01 36 00.0	63.8	24024	Giovanelli-Haynes CL
wp300034	12 30 7.2	+69 12 00.0	47.8	14528	4 Dra
wp900137	12 30 43.2	+41 38 24.0	74.8	30154	NGC 4490
rp700435	12 32 2.4	+20 09 36.0	81.7	10349	TON 154
rp600162	12 33 55.2	+26 16 12.0	85.9	11463	NGC 4565
rp600518n00	12 34 2.4	+07 42 00.0	70.1	17974	NGC 4526
rp300194n00	12 34 55.2	+37 37 48.0	78.9	8184	AM CVN
rp600595a02	12 35 57.6	+27 57 36.0	86.4	16379	NGC 4559
wp600415a01	12 36 21.6	+25 58 48.0	86.4	9716	NGC 4565
rp700355	12 36 24.0	+00 54 36.0	63.5	21614	QNY 1
wp600437a01	12 36 48.0	+13 10 12.0	75.6	17534	NGC 4569
rp600258n00	12 40 00.0	−11 37 12.0	51.1	10749	NGC 4594
wp701524n00	12 41 43.2	+35 03 36.0	81.8	12551	12393+3520
rp600129a00	12 42 7.2	+32 32 24.0	84.2	16871	NGC 4631
rp600017	12 43 43.2	+11 33 36.0	74.3	12834	NGC 4649
wp600450	12 43 43.2	+16 24 00.0	79.1	9765	3C 275.1/NGC 4651
wp600416	12 43 57.6	+32 10 12.0	84.7	16407	NGC 4656
rp600532n00	12 45 9.6	−00 27 36.0	62.3	14452	NGC 4666
rp800324a01	12 47 26.4	−42 06 36.0	20.7	13024	Centaurus Cluster ST
rp600262a02	12 48 36.0	−05 48 00.0	57.0	38119	NGC 4697
rp700375n00	12 49 14.4	−05 59 24.0	56.8	11042	Q1246−0542
wp900212	12 51 14.4	+25 39 36.0	88.5	17701	NGC 4725/NGC 4747
rp300093n00	12 52 24.0	−29 15 00.0	33.6	15171	EX Hydrae
wp800393a01	12 53 33.6	+15 42 36.0	78.5	12653	3C 277.2
rp201514n00	12 55 33.6	+25 53 24.0	88.4	13754	LOTR 5
wp700208	12 56 14.4	+56 52 12.0	60.2	22691	Mrk 231
rp700073	12 56 57.6	+47 20 24.0	69.7	42417	3C280
rp800374n00	12 58 26.4	−28 26 24.0	34.4	11219	Abell 3535
wp600164	12 59 00.0	+34 51 36.0	82.1	14876	NGC 4861
rp800384n00	13 01 2.4	−32 25 48.0	30.3	11869	A 3537
wp300394n00	13 07 52.8	+53 51 36.0	63.0	10083	RE 1307+535
wp700216	13 10 28.8	+32 21 00.0	83.3	12274	B2 1308+32
rp700376	13 11 36.0	−05 52 48.0	56.6	12020	Q1309−056

TABLE 4—*Continued*

Pointing (1)	R.A. (J2000) (2)	Decl. (J2000) (3)	b (deg) (4)	Time (s) (5)	Pointing Target (6)
wp300219	13 13 16.8	−32 59 24.0	29.6	13857	RX J1313.3−3259
wp600191	13 15 50.4	+42 01 48.0	74.2	9485	NGC 5055
rp100308n00	13 16 24.0	+29 06 00.0	84.1	18327	WFC Main Grid HZ 43
rp900325n00	13 17 43.2	+44 54 00.0	71.4	8322	G107+71
wp800556n00	13 17 55.2	+33 24 36.0	81.5	9415	HGR 23
rp800238n00	13 24 48.0	+30 34 48.0	81.9	24338	CL 1322
wp600419	13 25 19.2	−38 24 36.0	23.9	19171	13224−3809
wp600458n00	13 29 36.0	+58 25 12.0	58.0	14061	NGC 5204
rp800047	13 32 31.2	+50 29 24.0	65.3	16056	Abell 1758
wp700283	13 34 36.0	+37 54 36.0	75.9	67805	Deep Survey
rp600534n00	13 39 55.2	−31 38 24.0	30.1	31386	NGC 5253
rp300285n00	13 41 2.4	+51 54 00.0	63.5	13744	UX UMa
wp701063	13 42 50.4	+27 04 48.0	78.5	9326	CFHT field A/2
rp701000a01	13 43 43.2	−00 15 00.0	59.8	20927	BJS 864
rp800369a01	13 44 4.8	−00 10 48.0	59.9	17661	J1836 (3CR/23T)
rp700922n00	13 44 43.2	+55 53 24.0	59.6	16467	Mrk 273
rp300028	13 48 55.2	+07 57 36.0	66.4	25698	PG 1346+082
rp800637n00	13 49 2.4	−07 12 36.0	52.9	15127	HCG 67
rp600270n00	13 49 14.4	+60 11 24.0	55.4	28864	NGC 5322
wp701500n00	13 54 7.2	−02 05 24.0	57.1	14783	PKS 1351−018
rp700392	13 56 2.4	+18 22 12.0	72.7	11288	Mrk 463
rp201037n00	13 56 9.6	+25 55 12.0	75.4	12292	ZZ Boo
rp800109n00	13 59 50.4	+62 31 12.0	52.8	19735	CL 1358+62
wp700227	14 06 21.6	+22 24 00.0	72.3	9827	1404+226
rp700117	14 06 43.2	+34 10 48.0	72.3	22279	3CR 294
rp700061	14 06 57.6	+28 27 00.0	73.2	24803	1404+286
wp400134n00	14 12 33.6	+59 10 12.0	55.0	12188	GRB 910219
wp700248	14 13 48.0	+44 00 00.0	66.3	23464	1411+442
wp600462	14 15 33.6	+36 13 48.0	69.9	12689	NGC 5529
rp700122	14 15 45.6	+11 29 24.0	64.7	26380	Q1413+1143
rp800401a01	14 15 57.6	+23 07 12.0	70.4	8219	4C23.37
wp150071	14 18 00.0	+25 08 24.0	70.4	16982	NGC 5548
rp700865	14 19 7.2	+06 28 48.0	60.6	9270	3C 298
wp150046	14 19 45.6	+54 23 24.0	58.3	9866	OQ 530
wp800528n00	14 20 26.4	−09 19 48.0	47.6	9907	Shakhbazian GRO. 328
wp200329	14 28 43.2	+33 10 48.0	68.1	25509	LHS 2924
wp600448	14 34 52.8	+48 40 48.0	60.6	11309	Mark 474/NGC 5682
rp701002n00	14 45 16.8	+09 58 48.0	58.1	12753	1442+101
rp800518n00	14 52 12.0	+18 49 48.0	61.0	12043	Abell 1991
wp201536n00	15 01 57.6	+40 23 24.0	60.0	10229	Beta Boo
rp170001n00	15 02 7.2	+66 12 36.0	46.0	21551	Calibration Source
wp700257	15 04 2.4	+10 26 24.0	54.6	17606	Mrk 841
rp600119n00	15 06 31.2	+55 46 12.0	52.4	11467	NGC 5866
rp200905n00	15 13 33.6	+38 34 12.0	58.2	8451	SS Bootis
rp200965n00	15 14 48.0	+44 01 48.0	56.6	7780	PG 1513+442
wp600585n00	15 15 24.0	+55 31 12.0	51.5	7237	NGC 5905
wp600190	15 15 55.2	+56 19 12.0	51.0	16684	NGC 5907
rp201018	15 18 12.0	+31 39 00.0	57.8	18174	U Crb
rp701001n00	15 24 24.0	+09 58 12.0	50.1	8305	1522+101
rp701405n00	15 26 7.2	+41 40 12.0	55.3	10363	NGC 5929
rp701411n00	15 34 55.2	+23 29 24.0	53.0	20969	Arp 220
rp700897n00	15 38 45.6	−03 22 48.0	39.4	8198	CGCG 022−021
rp800511n00	15 41 16.8	+66 15 36.0	42.9	14104	A2125
rp201006n00	15 42 4.8	−19 28 12.0	27.7	9490	LHS 54
rp701373n00	15 49 50.4	+21 25 48.0	49.1	14910	3C 324
wp701213	15 52 9.6	+20 06 00.0	48.2	13831	3C326
wp701526n00	15 57 2.4	+63 50 24.0	42.8	9002	15564+6359
rp200459n00	15 58 36.0	−24 49 48.0	21.1	8709	HR 5942
rp800003	15 58 55.2	+33 23 24.0	49.3	26663	GC 1556+335
rp800103n00	16 00 36.0	+41 32 24.0	48.9	9416	1559+417
rp800239	16 04 28.8	+43 13 12.0	48.0	25963	CL 1603
wp600588n00	16 05 12.0	+20 32 24.0	45.4	13724	Mrk 297
rp300021n00	16 05 45.6	+25 51 36.0	46.7	23460	MS 1603.6+2600
wp600421n00	16 15 21.6	+68 23 24.0	39.0	9448	16155+6831
wp900381n00	16 15 52.8	+59 42 00.0	42.5	7972	HVC 1

TABLE 4—*Continued*

Pointing (1)	R.A. (J2000) (2)	Decl. (J2000) (3)	b (deg) (4)	Time (s) (5)	Pointing Target (6)
wp701589n00	16 17 43.2	+32 22 12.0	45.3	9172	3C332
rp700213n00	16 17 45.6	+06 04 12.0	36.7	10911	E1615+061
wp170154	16 29 33.6	+78 04 48.0	33.5	34402	Unknown
rp700098	16 32 31.2	+82 32 24.0	31.1	13633	NGC 6251
wp701552n00	16 33 4.8	+41 57 36.0	42.8	11503	RXJ 16331+4157
rp200721n00	16 34 24.0	+57 09 00.0	40.9	39879	CM Dra
rp201446n00	16 40 55.2	+53 41 24.0	40.6	17510	GD 356
rp701409n00	16 43 48.0	+17 15 36.0	35.7	14488	1641+173
rp900166n00	16 50 00.0	+60 12 00.0	38.2	19265	Draco Cloud
wp900207	16 50 36.0	+61 04 48.0	38.0	17668	Draco Nebula HVC Interf
wp900586n00	16 52 4.8	+68 12 36.0	35.9	8252	IVC-A 3
wp900591n00	16 56 43.2	+52 56 24.0	38.4	13979	LVC 2
rp900494n00	16 57 00.0	+69 03 00.0	35.3	12311	Low-contrast cloud 1
rp900169n00	16 57 12.0	+62 33 00.0	36.9	16321	MBM 41
rp400374n00	16 57 50.4	+35 20 24.0	37.5	17880	Her X-1
wp800530n00	16 59 43.2	+32 36 36.0	36.6	9964	Abell 2241
wp701457n00	17 01 00.0	+64 11 24.0	36.1	20818	HS 1700+6416
rp701439n00	17 04 40.8	+60 44 24.0	36.3	12779	3C 351
wp900211	17 05 4.8	+59 37 12.0	36.5	25282	HI-filament
rp900493n00	17 07 00.0	+53 12 00.0	36.8	17057	High-contrast cloud 1
rp700875n00	17 08 43.2	+71 07 12.0	33.7	29154	Draco Survey field
wp300387n00	17 12 55.2	+33 31 12.0	34.1	13550	V795 Her
rp800017	17 19 31.2	+49 58 48.0	34.9	28623	
rp701080n00	17 19 38.4	+48 04 12.0	34.8	11523	1718+481
wp800395	17 24 19.2	+50 57 36.0	34.2	16356	3C 356
wp701200	17 26 12.0	+74 31 12.0	31.7	8405	RX J1726.2+7431
rp200522n00	17 26 31.2	+04 08 24.0	20.7	12616	HD 157999
rp180014n00	17 46 14.4	+62 27 00.0	31.3	10787	Too Q1746+624
wp701523n00	17 48 38.4	+68 41 24.0	30.8	20292	Mrk 507
wp170075	17 57 55.2	+66 22 48.0	30.0	45962	Unknown
rp100378n00	18 00 00.0	+66 33 00.0	29.8	45872	WFC background Nep S1
wp700489	18 06 50.4	+69 49 12.0	29.1	8093	3C 371
rp300103	18 07 31.2	+45 51 36.0	26.4	12340	DQ Her
wp400043	18 11 45.6	+31 24 36.0	21.6	14334	GRB 790325B
rp300067a01	18 16 14.4	+49 52 12.0	25.8	17550	AM Her
rp701415n00	18 36 55.2	−59 24 00.0	−21.3	11208	IRAS 18325−5926
rp701020n00	18 38 55.2	−65 22 12.0	−23.2	15481	ES 0103−G35
rp700058	18 42 7.2	+79 46 12.0	27.0	11268	3C 390.3
rp201505n00	18 42 38.4	+55 32 24.0	23.2	23256	HD 173524
wp201597n00	18 53 4.8	−50 10 48.0	−20.7	21302	PZ Tel
rp300314n00	19 03 36.0	+68 33 00.0	24.0	12985	H1907+690
rp900338n00	19 24 50.4	−29 14 24.0	−19.6	26562	1921−293
wp300272n00	19 35 48.0	−46 40 48.0	−26.6	21369	RE 1938−46
rp701410n00	19 44 55.2	+77 06 00.0	23.4	11206	Q 1946+77
rp300232n00	19 47 40.8	−42 00 36.0	−27.7	8361	V3885 SGR
wp700488	20 09 26.4	−48 49 48.0	−32.6	11403	PKS 2005−489
wp800536n00	20 35 57.6	−25 16 48.0	−33.3	19263	A 3698
rp201763n00	20 37 16.8	+75 35 24.0	20.0	15746	VW Cep (Phase 0.00)
rp700547n00	20 37 31.2	−22 42 36.0	−32.8	11089	E2034−228
wp300218n00	20 38 14.4	−01 21 00.0	−24.2	20295	AE AQR
wp201374a02	20 47 45.6	−36 35 24.0	−38.2	28766	HD 197890
wp700538	20 52 2.4	−57 04 12.0	−38.7	18728	IC 5063
rp701025n00	20 56 4.8	−19 56 24.0	−36.0	10705	2053−201
wp300389n00	21 07 55.2	−05 16 12.0	−32.6	28927	RE 2107−05
rp201007n00	21 09 19.2	−13 14 24.0	−36.4	17360	LHS 65
rp900133n00	21 14 24.0	−67 47 24.0	−38.2	22239	PAVO field
rp700006n00	21 14 52.8	+06 07 48.0	−28.0	9778	PG 2112+059
wp201753a01	21 31 2.4	+23 20 24.0	−20.0	13278	RE 2131+23
wp800336a01	21 39 7.2	−42 51 36.0	−48.2	13416	UKRO−287−1
wp800573n00	21 40 14.4	−23 39 36.0	−46.9	9599	MS 2137.3−2353
rp800150a01	21 46 33.6	+04 13 48.0	−35.4	12612	21 Hour field
rp600512n00	21 52 43.2	−48 15 00.0	−49.6	25344	NGC 7144
wp800419a01	22 02 4.8	−31 58 12.0	−53.0	13266	Hickson 90
rp200559n00	22 02 57.6	−56 45 00.0	−48.0	13764	
wp700516	22 03 4.8	−18 55 12.0	−50.5	22781	MT field

TABLE 4—*Continued*

Pointing (1)	R.A. (J2000) (2)	Decl. (J2000) (3)	b (deg) (4)	Time (s) (5)	Pointing Target (6)
rp600175n00	22 09 7.2	−27 48 36.0	−54.1	13345	22062−2803
wp701191n00	22 13 00.0	−17 10 12.0	−52.1	9549	RX J2213.0−1710
rp701390n00	22 15 16.8	−29 59 24.0	−55.7	7626	Q2212−299
rp600235n00	22 20 48.0	−24 40 48.0	−56.1	17424	NGC 7252
rp701018n00	22 23 45.6	−02 13 12.0	−46.7	9509	3C445
rp900337n00	22 25 48.0	−04 57 00.0	−48.8	14821	2223−052
rp700873n00	22 35 45.6	−26 03 00.0	−59.7	23579	NGC 7314
wp800066	22 36 12.0	+34 00 36.0	−20.9	19793	Stephan's Quintet
wp201723n00	22 38 31.2	−15 18 36.0	−56.9	12512	GJ 866
rp800467n00	22 46 43.2	−65 02 24.0	−47.2	10933	NGC 7358
wp300135	22 49 40.8	−27 06 36.0	−62.9	8767	TY PSA
wp201552n00	22 50 00.0	+24 36 00.0	−30.5	16152	Mu Peg
wp800334n00	22 52 55.2	−21 33 36.0	−62.5	16727	RX J2252.9−213
rp900339n00	22 53 57.6	+16 09 00.0	−38.1	16352	2251+158
wp701630n00	22 54 4.8	−17 34 48.0	−61.3	14730	MR 2251−179
rp400293	22 54 19.2	+29 03 36.0	−27.1	19102	GRB 910814
rp600266n00	22 57 9.6	−36 27 36.0	−64.1	31005	IC 1459
rp201282n00	22 57 28.8	+20 46 12.0	−34.7	9836	51 Peg
wp701204n00	22 57 40.8	−36 56 24.0	−64.0	8396	MS 2254.9−3712
rp700423	23 03 14.4	+08 52 12.0	−45.4	18757	NGC 7469
rp600177n00	23 04 36.0	−51 28 12.0	−58.4	14527	23016−5144
wp701250n00	23 04 43.2	−08 41 24.0	−58.7	17022	MCG-2-58-22
wp201339n00	23 05 24.0	−35 52 12.0	−65.8	10612	Gliese 887
rp900323n00	23 08 40.8	−27 25 48.0	−67.2	8537	G026−67
rp100578n00	23 12 21.6	+10 46 48.0	−45.1	9765	WFC SPEC/FLUX BPM 97895
wp600544n00	23 13 40.8	+14 01 12.0	−42.5	17880	Mrk 316
rp400144n00	23 14 00.0	−49 39 36.0	−60.7	18446	GRB 790406
rp800488n00	23 15 24.0	+18 58 48.0	−38.3	14711	HCG 93
wp300220n00	23 16 2.4	−05 27 00.0	−58.6	13838	RX J2316.1−0527
wp600439	23 20 31.2	+17 13 48.0	−40.4	10780	III Zw 102
wp200322	23 25 21.6	+23 24 00.0	−35.3	24386	HR 8905
wp701045a01	23 36 21.6	+02 09 36.0	−55.5	9365	Arp 284
wp701205n00	23 43 31.2	−14 55 12.0	−70.0	11248	MS 2340.9−1511
wp701501n00	23 54 28.8	−15 13 12.0	−72.1	12017	PKS 2351−154
wp600386n00	23 57 50.4	−32 35 24.0	−77.1	13045	NGC 7793
wp800372a01	23 59 16.8	−32 17 24.0	−77.5	16598	F1637 (23TL)

NOTE.—Units of right ascension are hours, minutes, and seconds, and units of declination are degrees, arcminutes, and arcseconds.

APPENDIX B

Table 5 shows the 178 *ROSAT* PSPC pointings excluded from the Bright SHARC Survey.

TABLE 5

ROSAT PSPC POINTINGS EXCLUDED FROM THE BRIGHT SHARC SURVEY

Pointing (1)	R.A. (J2000) (2)	Decl. (J2000) (3)	b (deg) (4)	Time (s) (5)	Pointing Target (6)	Reject Code (7)
wp800343	00 14 19.2	−30 23 24.0	−81.2	13714	A 2744	X
rp600107n00	00 15 9.6	−39 13 12.0	−75.7	18080	NGC 55	O
rp300007	00 24 7.2	−72 04 48.0	−44.8	59419	47 Tucanae	M
rp201045	00 39 19.2	+30 51 36.0	−31.9	27475	S And	O
wp600079	00 39 36.0	+40 24 00.0	−22.4	46905	M31 west pos. 1	O
wp600064	00 41 2.4	+40 46 12.0	−22.0	47219	M31 east pos. 1	O
rp800250n00	00 41 50.4	−09 18 00.0	−72.0	8460	A85	X
wp600068	00 42 26.4	+41 08 24.0	−21.7	30688	M31 east pos. 7	O
wp600067	00 43 55.2	+41 30 36.0	−21.3	27262	M31 west pos. 6	O
wp201327n00	00 44 24.0	+85 19 48.0	22.4	13307	NGC 188	O
wp600066	00 45 21.6	+41 52 48.0	−20.9	30729	M31 east pos. 4	O

TABLE 5—*Continued*

Pointing (1)	R.A. (J2000) (2)	Decl. (J2000) (3)	b (deg) (4)	Time (s) (5)	Pointing Target (6)	Reject Code (7)
rp500249n00	00 46 40.8	−73 12 36.0	−43.9	17315	SMC SNR 0045−733	M
rp600121	00 46 48.0	+41 58 12.0	−20.8	42463	M31POS 1	O
wp600065	00 46 48.0	+42 15 00.0	−20.6	28465	M31 west pos. 3	O
rp600087a00	00 47 36.0	−25 17 24.0	−87.9	11531	NGC 253	O
wp600196	00 50 43.2	−73 13 48.0	−43.8	23566	SMC Region B	M
wp201094n00	00 50 48.0	−74 46 48.0	−42.3	62382	CF Tuc	M
wp600453n00	00 54 28.8	−72 45 36.0	−44.3	16516	SMC Region E	M
rp600025a01	00 54 52.8	−37 41 24.0	−79.4	36997	NGC 300	O
rp800251n00	00 56 16.8	−01 15 00.0	−64.0	13386	A119	X
wp600195	00 58 12.0	−72 16 48.0	−44.8	26146	SMC Region A	M
rp700884	00 58 24.0	+26 52 12.0	−35.9	19348	0055+26	X
rp800319n00	01 02 40.8	−21 52 48.0	−84.1	15657	A133	X
rp500250n00	01 04 38.4	−72 04 48.0	−45.0	19481	SMC SNR 0103−726	M
wp600452a01	01 05 55.2	−72 33 00.0	−44.5	16030	SMC Region D	M
wp600106	01 07 24.0	+32 24 36.0	−30.3	28791	NGC 383	X
rp800276n00	01 09 55.2	−45 55 48.0	−70.8	19370	DC 0107−46	X
rp600197n00	01 13 24.0	−72 49 12.0	−44.2	21403	SMC Region C	M
rp400022n00	01 17 4.8	−73 26 24.0	−43.5	15610	SMCX-1	M
rp600254a01	01 23 38.4	+33 15 00.0	−29.1	12645	NGC 507	X
rp600541n00	01 25 31.2	+01 45 36.0	−59.9	11794	NGC 533	X
rp800316	01 25 52.8	−01 22 48.0	−62.9	20792	A194	X
rp600023	01 33 50.4	+30 39 36.0	−31.3	34892	M33	O
rp800507n00	01 56 24.0	+05 37 48.0	−53.6	13044	S49−140	X
rp900250a01	02 17 12.0	−74 06 00.0	−41.7	46071	Magellanic Bridge	M
rp900251n00	02 22 00.0	−75 33 00.0	−40.2	12412	Magellanic Bridge	M
rp800226n00	02 57 40.8	+06 01 48.0	−44.9	22512	Abell 400	X
rp600127n00	03 36 31.2	−34 58 48.0	−54.0	17350	NGC 1380	X
rp600133n00	03 38 28.8	−23 01 48.0	−52.1	17427	NGC 1395	X
rp600043n00	03 38 28.8	−35 27 00.0	−53.6	30232	N1399	X
wp800083	03 38 38.4	+09 58 12.0	−35.0	9274	2A0335+096	X
rp600163n00	03 40 12.0	−18 34 48.0	−50.3	18842	NGC 1407	X
rp200557	03 44 24.0	+24 47 24.0	−23.4	26774	Pleiades NW	O
rp200068	03 46 48.0	+23 54 00.0	−23.7	41007	Pleiades field #1	O
rp200008	03 47 00.0	+24 09 00.0	−23.4	35875	Pleiades Center	O
rp200556	03 50 9.6	+24 21 36.0	−22.8	20965	Pleiades NE	O
wp800193	04 13 24.0	+10 28 12.0	−28.2	22075	Abell 478	X
wp800552n00	04 31 9.6	−61 28 48.0	−40.1	12980	A 3266	X
rp800277	04 38 55.2	−22 06 00.0	−38.4	16919	Abell 500	X
rp200997	04 45 28.8	−03 15 00.0	−29.3	8676	Mu Eri	O
rp800278	04 48 12.0	−20 27 36.0	−35.9	16276	Abell 514	X
rp800086n00	04 48 43.2	−20 35 24.0	−35.8	11939	F1652	X
rp500263n00	04 55 21.6	−67 09 00.0	−36.0	11765	N9	M
rp500258n00	04 55 43.2	−68 39 00.0	−35.5	11612	N86	M
rp900320n00	04 56 33.6	−66 28 48.0	−36.0	15539	N11	M
rp200921n00	04 58 19.2	−75 16 48.0	−33.2	23300	HD 32918	M
rp600098n00	05 00 4.8	−66 25 48.0	−35.7	9997	Region C	M
rp200056	05 09 9.6	−08 45 00.0	−26.6	25187	Lambda Eridani	O
wp500052	05 13 55.2	−67 20 24.0	−34.2	15430	DEM 105	M
rp400080n00	05 14 7.2	−40 02 24.0	−35.0	9887	0512−40	O
rp400263a01	05 20 28.8	−71 57 36.0	−32.6	12257	LMC X-2	M
wp600578n00	05 26 24.0	−66 13 48.0	−33.1	10218	Region E	M
rp500138a02	05 26 36.0	−68 49 48.0	−32.7	14011	N144	M
rp200692n00	05 30 45.6	−65 54 36.0	−32.7	41469	LMC X-4 and AB DOR	M
rp800523n00	05 32 24.0	−11 33 00.0	−22.7	13543	A545	X
rp500100a00	05 35 28.8	−69 15 36.0	−31.9	17000	SN 1987A	X
wp600100	05 35 38.4	−69 16 12.0	−31.9	21894	Region F	M
rp300335n00	05 36 12.0	−70 45 00.0	−31.6	9789	2 New S. Soft Srcs	M
rp500131n00	05 38 33.6	−69 06 36.0	−31.6	15200	N157	M
rp800246n00	05 45 31.2	−25 54 00.0	−25.2	10154	A548S	X
rp400012n00	05 46 45.6	−71 09 00.0	−30.7	18216	CAL 87	M
rp800463n00	05 48 38.4	−25 28 12.0	−24.4	11586	A548 N	X
rp100406n00	06 00 00.0	−66 33 00.0	−29.8	17847	WFC Background Sep S1	M
rp800154n00	06 01 43.2	−39 58 48.0	−26.0	11820	SC 0559−40	X
wp200638	06 48 12.0	−61 55 48.0	−24.0	10010	HR 2550	O

TABLE 5—*Continued*

Pointing (1)	R.A. (J2000) (2)	Decl. (J2000) (3)	b (deg) (4)	Time (s) (5)	Pointing Target (6)	Reject Code (7)
wp200328	07 34 36.0	+31 53 24.0	22.4	89618	YY Gem	O
rp600542n00	08 20 36.0	+21 04 12.0	28.6	21337	NGC 2563	X
rp800022	08 31 2.4	+65 51 00.0	34.7	34417	Abell 665	X
wp300133	08 50 24.0	+11 49 12.0	31.7	10098	CV in M67	O
rp201326n00	08 51 24.0	+11 49 48.0	31.9	11577	M 67	O
rp600451n00	09 08 00.0	−09 59 24.0	24.3	10440	G0905−098	X
rp800318n00	09 18 4.8	−12 05 24.0	25.0	16719	Hydra A	X
wp600547n00	09 19 48.0	+33 45 00.0	44.3	16901	NGC 2832	X
rp180015n00	09 55 24.0	+69 00 36.0	40.9	15364	M81	O
rp600382n00	09 55 31.2	+69 04 12.0	40.8	23577	M81	O
wp180035n00	09 55 33.6	+69 04 12.0	40.8	15712	Unknown	O
wp600576n00	09 55 50.4	+69 19 48.0	40.7	14690	M81/M82 group	X
wp600110	09 55 52.8	+69 40 48.0	40.5	23531	M82	X
wp800572n00	10 17 31.2	+59 34 48.0	48.2	12044	A959	X
rp200076	10 19 38.4	+19 52 12.0	54.5	24542	AD Leo	O
rp800491n00	10 22 9.6	+38 31 12.0	56.9	10652	R1022.1+3831	X
rp800200n00	10 36 43.2	−27 31 48.0	26.4	13593	Abell 1060	X
rp800135n00	10 39 21.6	−27 19 48.0	26.9	17967	TOL 1037−271	X
wp800410n00	10 40 43.2	+39 57 00.0	60.1	10106	Abell 1068	X
wp200213	11 14 7.2	+20 31 12.0	66.8	19218	Delta Leo	O
rp600223a01	11 14 12.0	−38 11 24.0	20.8	18799	MS 1111.9−3754	X
rp800153	11 44 40.8	+19 42 36.0	73.0	17600	A1367	X
rp100366n00	11 49 4.8	+14 34 12.0	70.8	16154	WFC UV Leak B. Leo	O
rp800127	12 04 26.4	+01 54 00.0	62.3	9735	MKW 4	X
rp600519n00	12 05 26.4	+02 05 24.0	62.6	19736	NGC 5838	X
wp600444n00	12 06 38.4	+28 10 12.0	80.0	13943	NGC 4104	X
wp600546n00	12 18 57.6	+47 18 36.0	68.8	22095	NGC 4258	O
rp701404n00	12 25 45.6	+12 39 36.0	74.3	9349	NGC 4388	X
wp600105	12 26 12.0	+12 57 00.0	74.6	20052	NGC 4406	X
rp600248n00	12 29 48.0	+08 00 00.0	70.1	24579	NGC 4472	X
wp800187	12 30 50.4	+12 23 24.0	74.4	9233	M 87	X
wp600586n00	12 35 36.0	+12 28 12.0	74.8	12088	NGC 4552	X
rp800522n00	12 36 55.2	+63 10 48.0	53.8	15293	A1576	X
rp600016	12 42 50.4	+02 41 24.0	65.4	11935	NGC 4636	X
rp800322n00	12 44 36.0	−41 03 36.0	21.7	16931	Centaurus Cluster WE	X
rp800323n00	12 50 12.0	−40 31 12.0	22.3	19998	Centaurus Cluster NR	X
rp800321a01	12 53 2.4	−41 34 12.0	21.3	12174	Centaurus Cluster EA	X
wp800098	12 53 7.2	−09 13 12.0	53.6	17779	Hickson 62	X
rp800009	12 57 43.2	+27 36 00.0	88.5	20080	Coma 5	X
rp800006	12 59 45.6	+27 48 00.0	88.0	20864	Coma 2	X
rp800005	12 59 45.6	+27 58 12.0	87.9	21371	Coma 1	X
rp800013	13 00 31.2	+28 07 48.0	87.7	21204	Coma 9	X
wp800411	13 03 43.2	−24 15 00.0	38.5	12793	Abell 1664	X
rp800295n00	13 11 24.0	+39 12 00.0	77.2	7752	Abell 1691	X
rp800248	13 11 31.2	−01 20 24.0	61.1	13726	A1689	X
rp800020	13 15 24.0	−16 22 48.0	46.1	27193	WP 23	X
rp800375n00	13 22 57.6	−31 43 12.0	30.6	12247	Abell 3556	X
wp800416a01	13 23 19.2	−31 30 36.0	30.8	11511	Shapley 8 (Offset)	X
rp800076n00	13 27 55.2	−31 29 24.0	30.7	29114	A3558	X
rp600158n00	13 29 52.8	+47 12 00.0	68.5	23254	N5194/N5195	O
wp800553n00	13 30 52.8	−01 51 36.0	59.4	11184	A 1750	X
rp800237n00	13 33 38.4	−31 40 12.0	30.3	17448	A3562	X
rp800252n00	13 35 21.6	+41 00 00.0	73.4	12388	A1763	X
rp600268a01	13 36 38.4	−33 58 12.0	27.9	14536	IC 4296	X
wp600188a02	13 37 00.0	−29 52 12.0	31.9	22899	M83	O
rp300333a01	13 42 9.6	+28 22 48.0	78.7	13140	NGC 5272	O
wp700145	13 48 36.0	+26 22 12.0	77.2	20375	1E1346+26	X
rp800055	13 48 52.8	+26 37 12.0	77.1	25701	Abell 1795	X
rp800105	13 48 55.2	+26 35 24.0	77.1	34684	Abell 1795	X
rp800485n00	13 53 40.8	+40 19 48.0	71.5	11904	HCG 68	X
rp800243	14 01 48.0	−11 09 00.0	48.0	14213	A1837	X
wp600108	14 03 9.6	+54 20 24.0	59.7	33859	M101	O
rp150018n00	14 15 40.8	+19 11 24.0	69.1	15732	Alpha Bootis	O
rp800518a01	14 54 31.2	+18 38 24.0	60.4	20489	Abell 1991	X

TABLE 5—*Continued*

Pointing (1)	R.A. (J2000) (2)	Decl. (J2000) (3)	b (deg) (4)	Time (s) (5)	Pointing Target (6)	Reject Code (7)
rp200510n00	15 00 57.6	−08 31 12.0	42.5	14358	Delta Lib	X
rp800249n00	15 10 55.2	+05 45 00.0	50.5	9577	A2029	X
wp800184	15 23 4.8	+08 36 36.0	49.6	9125	A2063	X
wp201558n00	15 34 40.8	+26 43 12.0	53.7	16162	HR 5793	O
rp900170n00	15 49 36.0	−03 19 12.0	37.3	9635	MBM 37	O
wp800415	15 58 21.6	+26 58 12.0	48.6	18719	Abell 2142 (Offset)	X
rp800129n00	16 04 57.6	+23 55 48.0	46.4	18477	AWM 4	X
rp800517n00	16 05 26.4	+17 47 24.0	44.4	11196	A2151	X
wp800363	16 27 16.8	+40 55 48.0	43.9	8961	A 2197	X
wp800644n00	16 28 38.4	+39 33 00.0	43.6	35984	A2199	X
rp800413n00	16 29 38.4	+58 31 48.0	41.1	7936	Abell 2208	X
wp800097	16 35 48.0	+66 12 36.0	38.1	36694	A2218	X
wp800571n00	16 40 24.0	+46 42 36.0	41.4	8437	A2219	X
rp300181	16 41 40.8	+36 27 36.0	40.9	39207	NGC 6205	O
wp900590n00	16 48 57.6	+53 36 00.0	39.4	15940	LVC 1	X
wp600583n00	16 57 57.6	+27 51 36.0	35.9	10399	NGC 6269	X
wp800341	16 59 31.2	+78 31 48.0	31.9	8676	A2256 Region 4	X
rp800163n00	17 01 40.8	+78 56 24.0	31.7	8891	A2256 Region 2	X
wp100110	17 03 36.0	+78 43 12.0	31.7	16680	XRT/PSPC Spec/FL A	X
rp800512n00	17 12 28.8	+64 03 00.0	34.9	11568	A2255	X
wp600582n00	17 14 14.4	+43 40 48.0	35.4	18165	NGC 6329	X
rp300180n00	17 17 7.2	+43 08 24.0	34.8	37298	NGC 6341	O
rp201066n00	17 56 36.0	+51 29 24.0	29.2	16792	Gamma Draconis	O
rp200941n00	18 45 24.0	−64 52 12.0	−23.7	15960	HR 7012	O
rp800256n00	18 47 16.8	−63 19 48.0	−23.5	10384	SC 1842−63	X
wp400302n00	19 40 00.0	−30 57 36.0	−23.2	18035	NGC 6809	O
rp800234n00	20 12 31.2	−56 49 12.0	−33.3	11463	A3667	X
rp800227a01	21 51 57.6	−15 37 48.0	−46.9	16647	Abell 2382	X
wp800570n00	21 53 36.0	+17 41 24.0	−27.8	8452	A2390	X
wp800344n00	21 56 4.8	+01 19 48.0	−39.1	12853	A 2397	X
wp800378n00	22 49 48.0	−64 22 12.0	−47.9	11493	A 3921	X
wp800397n00	23 13 57.6	−42 43 48.0	−64.8	12376	Sersic 159−03	X
wp800568n00	23 17 16.8	+18 43 12.0	−38.7	28678	HCG 94	X
rp600134	23 20 31.2	+08 12 36.0	−48.3	18371	Pegasus I Cluster	X
rp800014a01	23 38 28.8	+27 01 48.0	−33.0	8715	Abell 2634	X
wp800333a01	23 44 16.8	−04 22 12.0	−62.1	9261	RX J2344.3−042	X
rp800320	23 44 55.2	+09 10 48.0	−50.2	17977	A2657	X
wp800357	23 47 26.4	−02 18 36.0	−60.8	12457	HCG 97	X
rp800420n00	23 54 9.6	−10 24 00.0	−68.5	14591	A2670	X

NOTES.—Units of right ascension are hours, minutes, and seconds, and units of declination are degrees, arcminutes, and arcseconds. (X) An extended X-ray source covers most of the field of view. (O) An extended optical source covers most of the field of view. (M) The pointing is close ($<6°$) to the Magellanic clouds.

APPENDIX C

Figures 4–97 show the Digitized Sky Survey images of the 94 bright SHARC extended sources, with wavelet source boundaries overlaid. Each image is 400″ × 400″ in size.

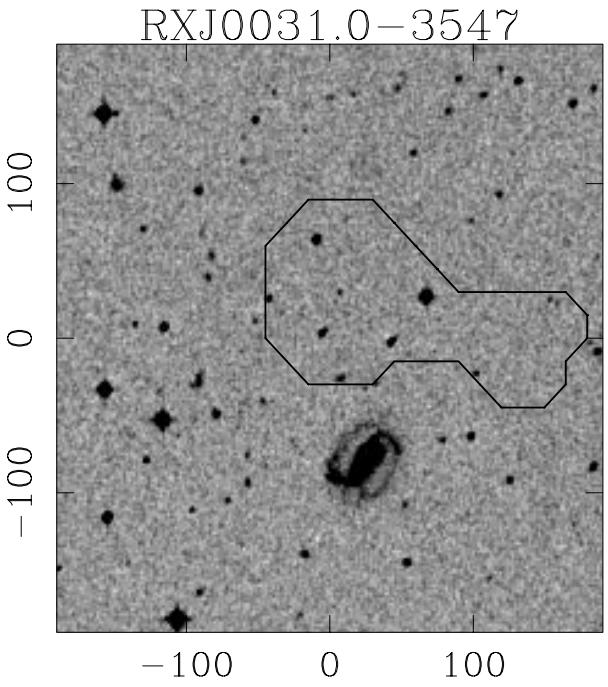

FIG. 4.

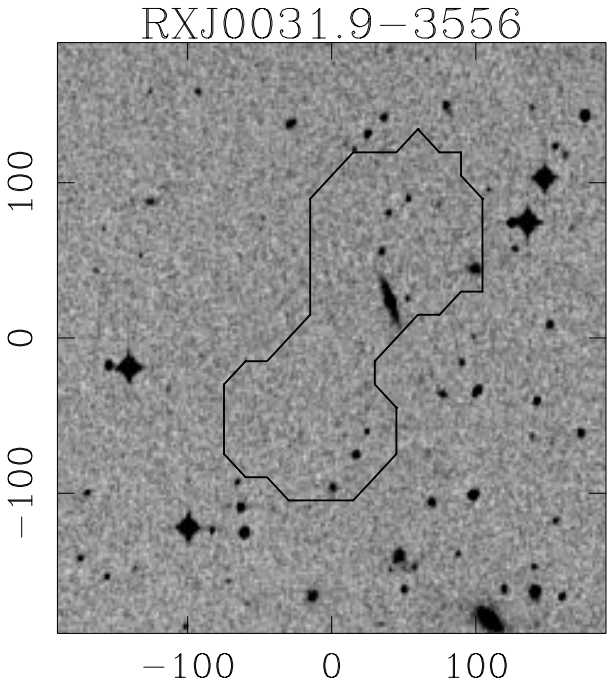

FIG. 5.

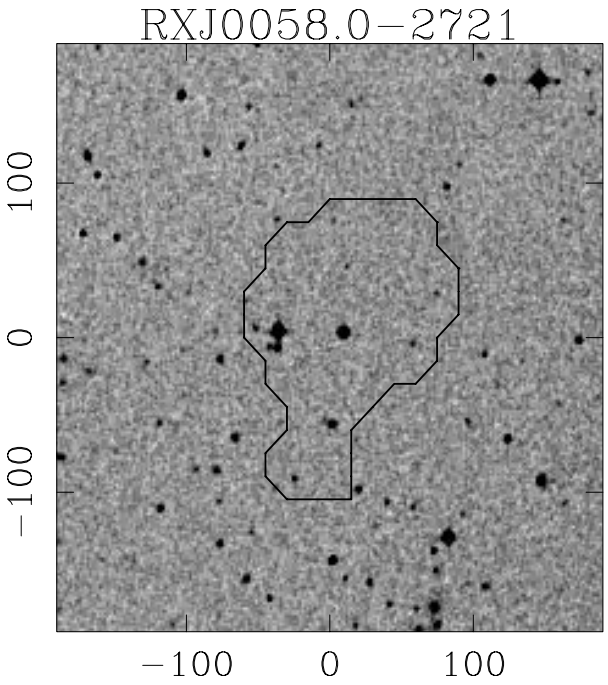

FIG. 6.

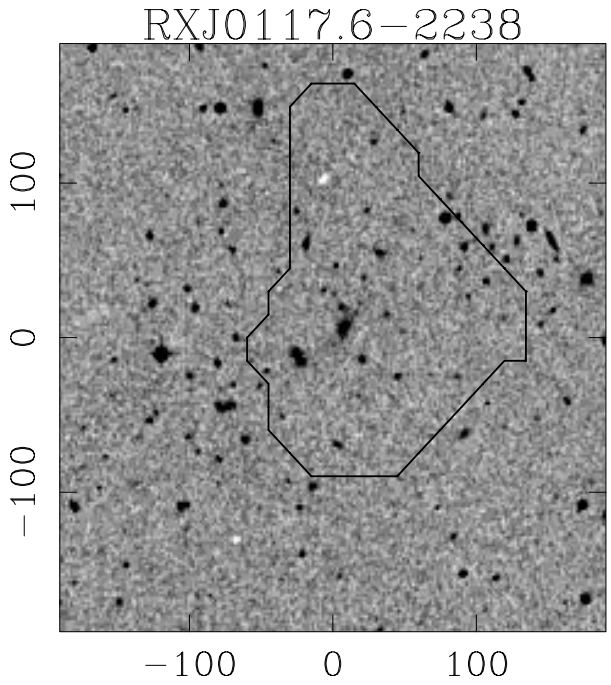

FIG. 7.

Figs. 4–97 show the Digitized Sky Survey images of the 94 bright SHARC extended sources, with wavelet source boundaries overlaid. Each image is 400″ × 400″ in size.

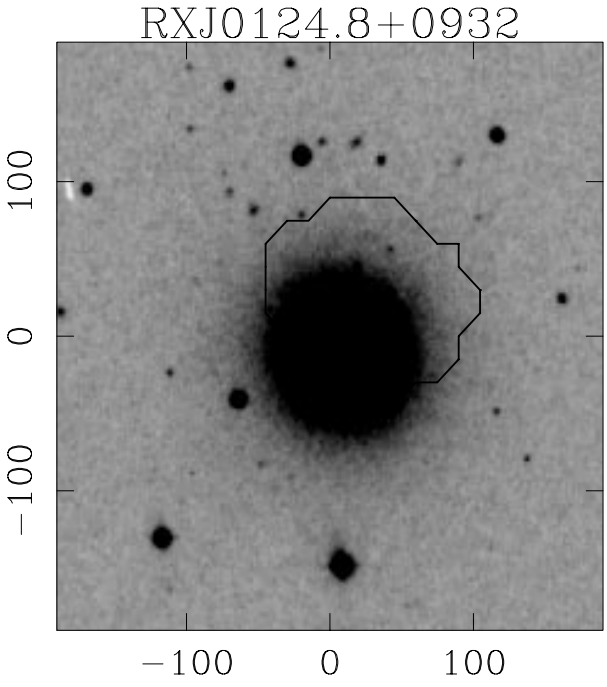

FIG. 8.

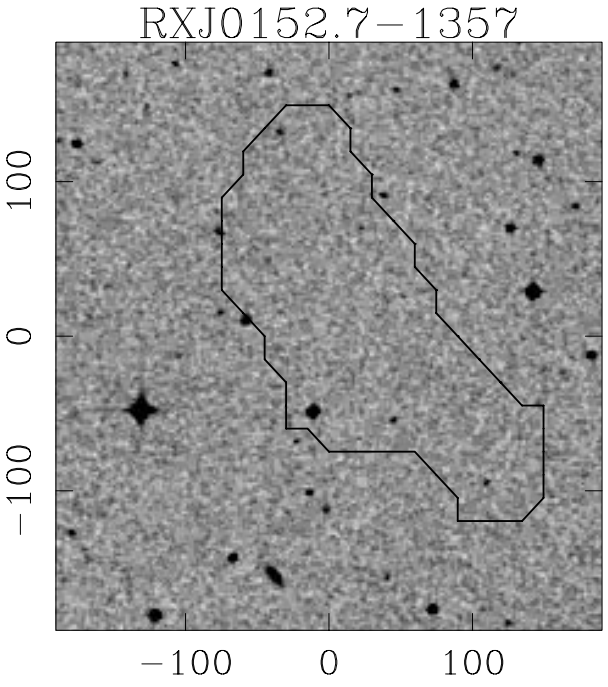

FIG. 9.

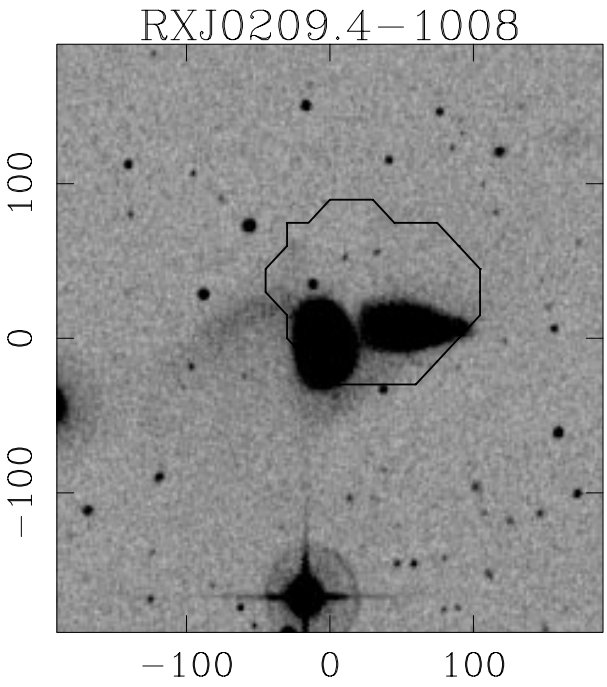

FIG. 10.

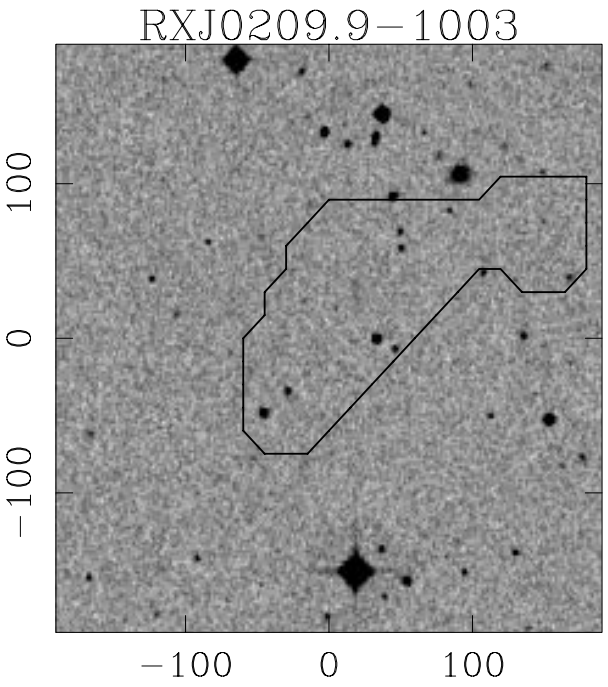

FIG. 11.

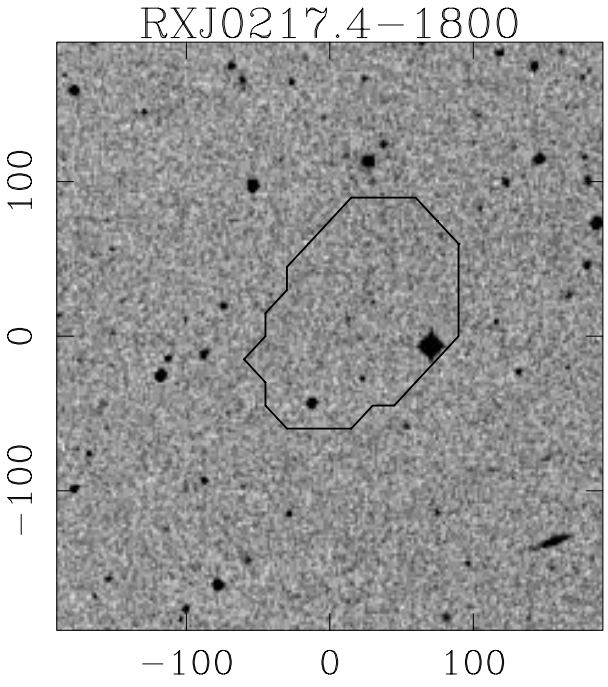

FIG. 12.

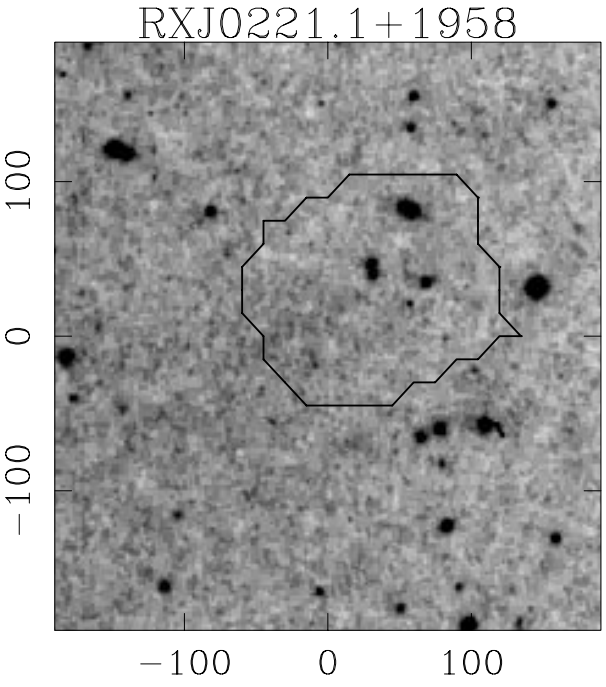

FIG. 13.

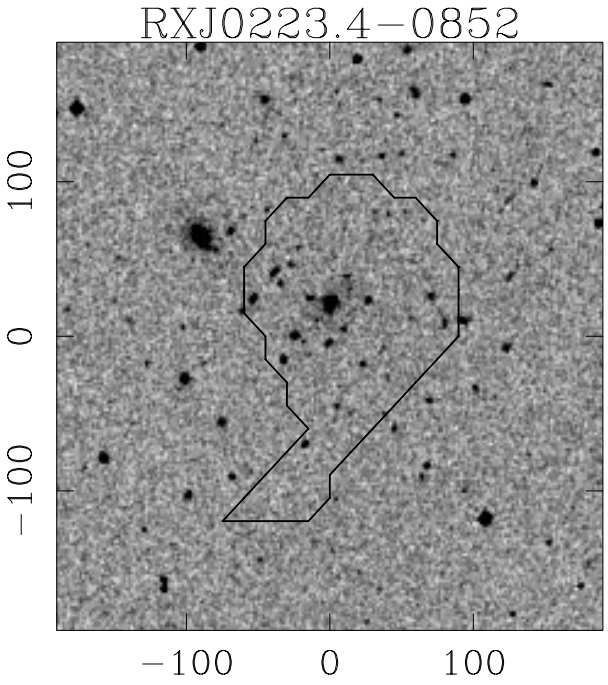

FIG. 14.

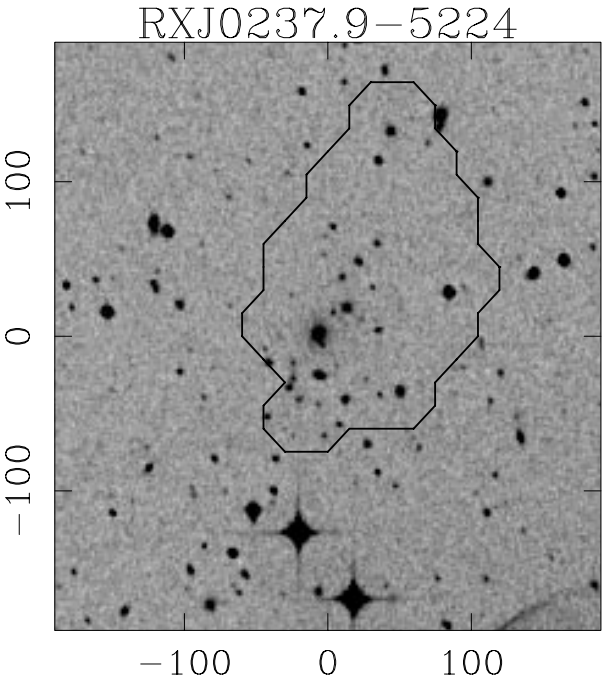

FIG. 15.

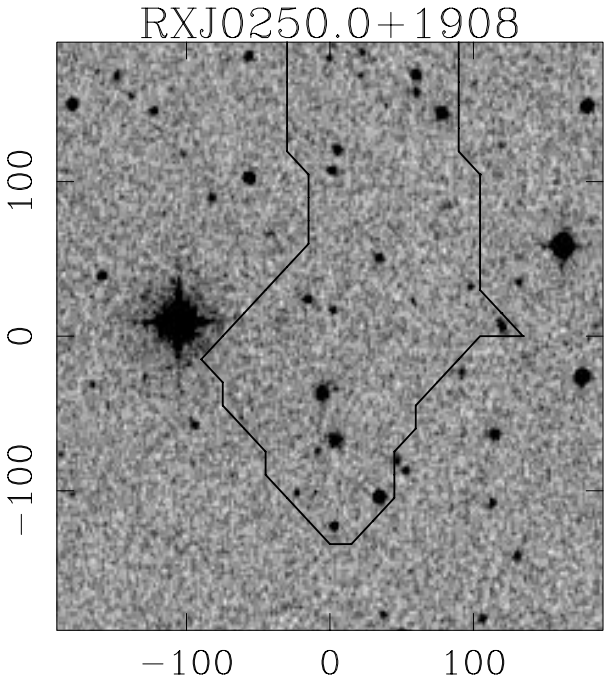

FIG. 16.

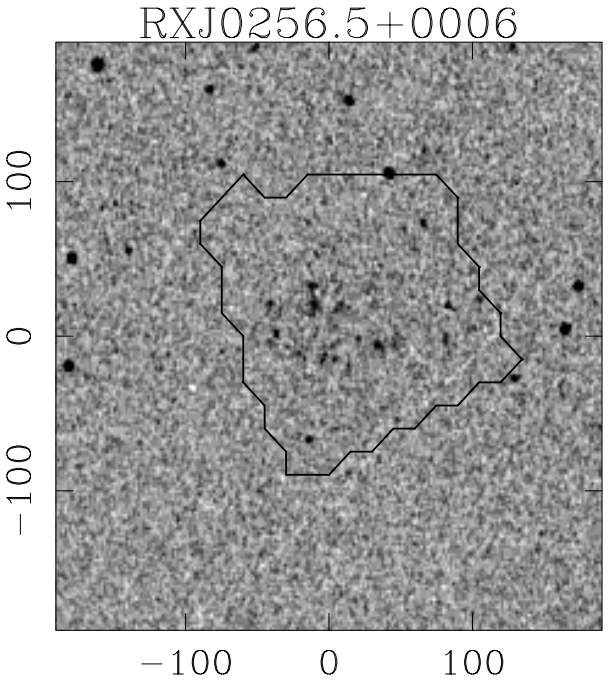

FIG. 17.

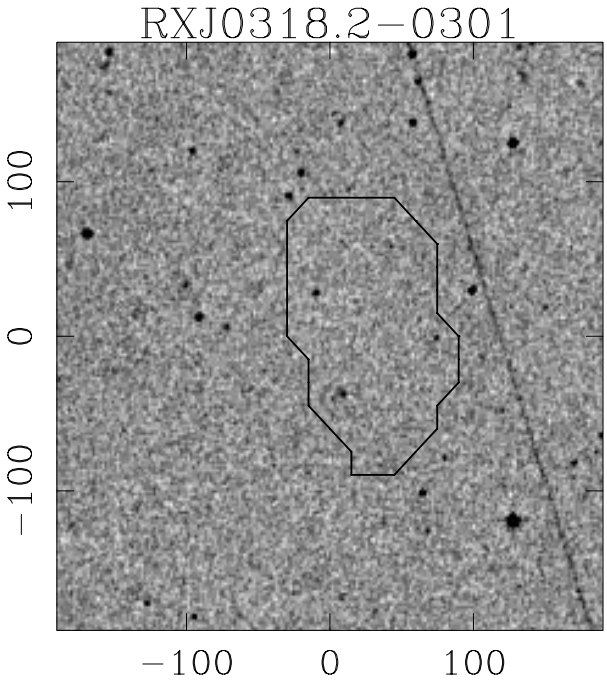

FIG. 18.

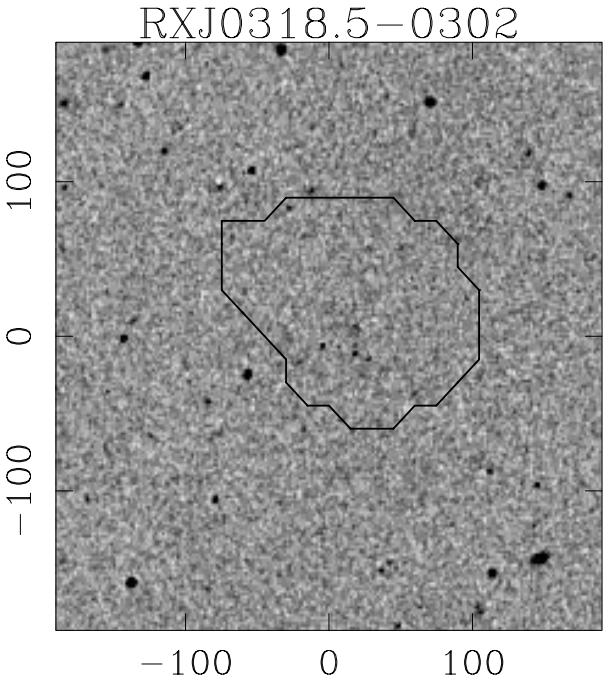

FIG. 19.

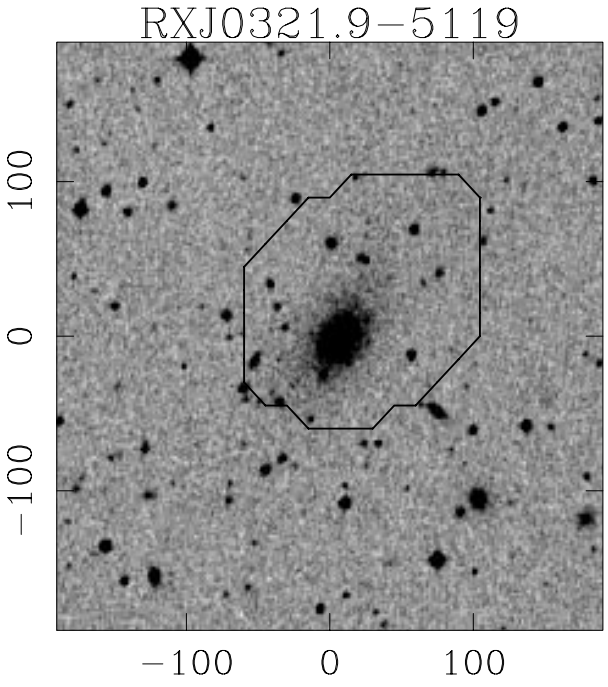

FIG. 20.

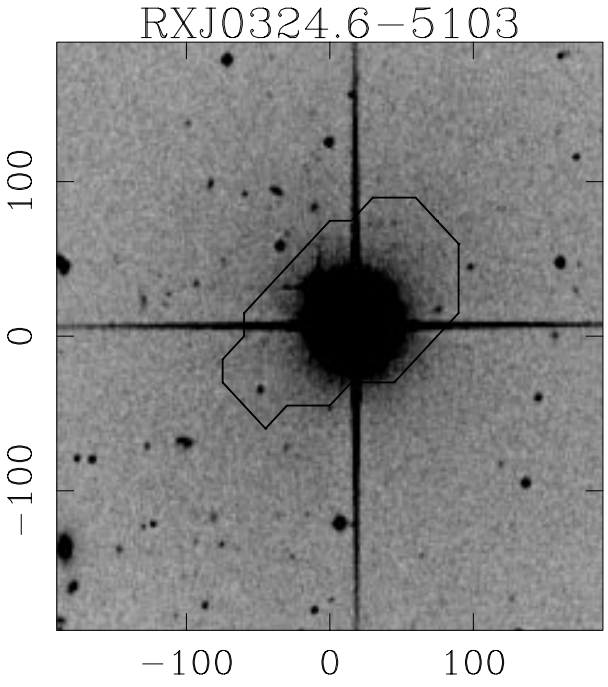

FIG. 21.

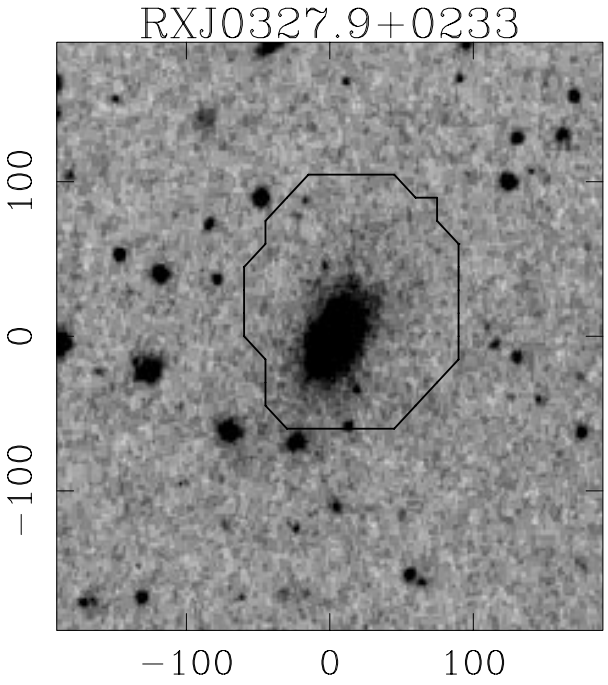

FIG. 22.

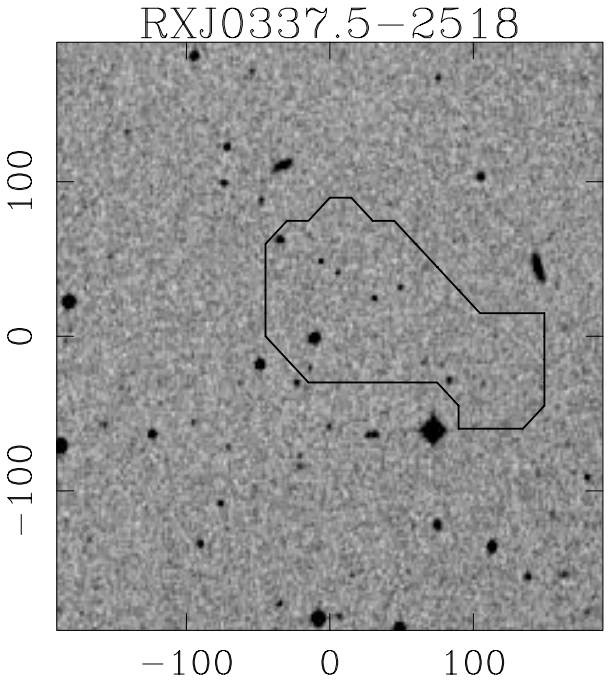

FIG. 23.

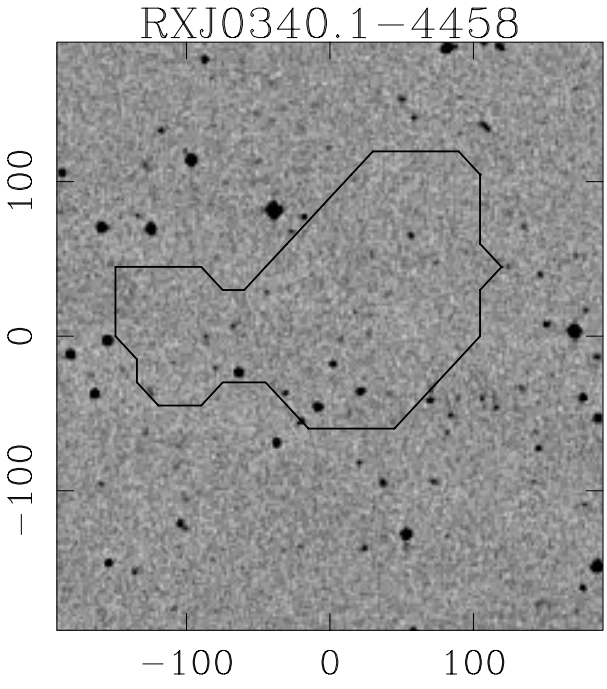

FIG. 24.

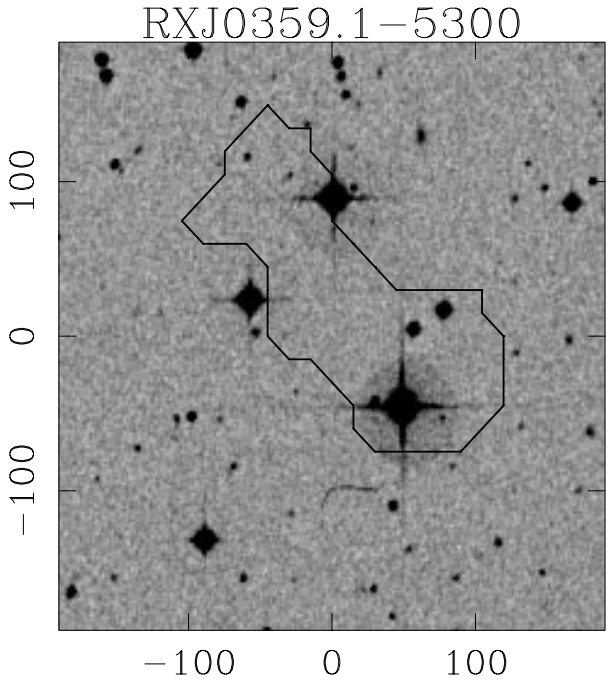

FIG. 25.

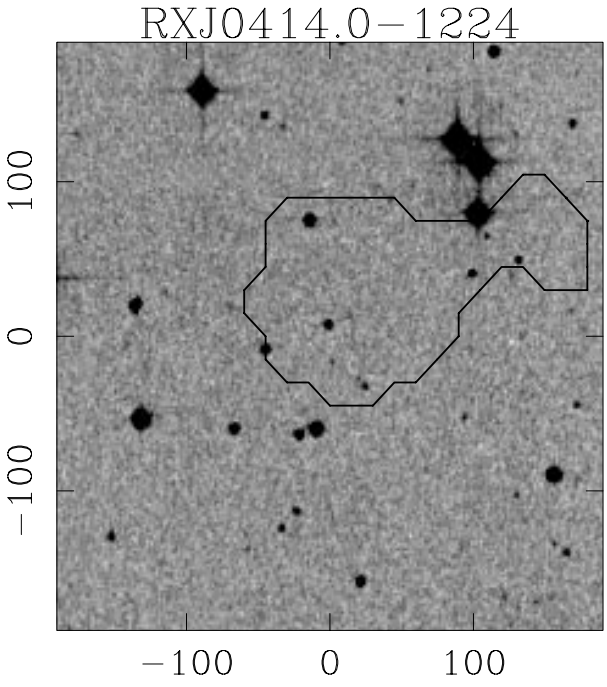

FIG. 26.

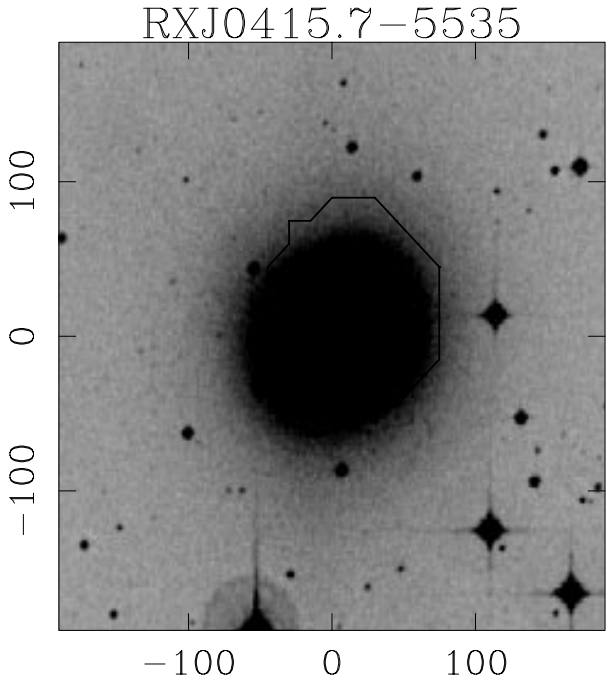

FIG. 27.

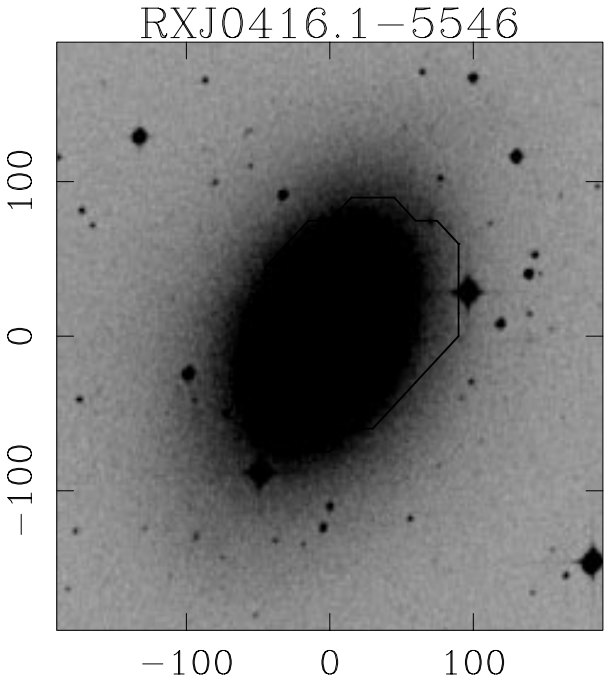

FIG. 28.

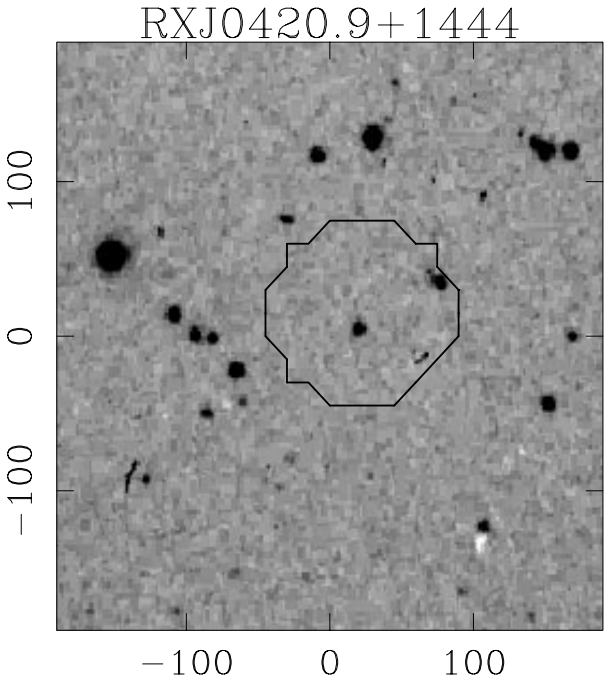

FIG. 29.

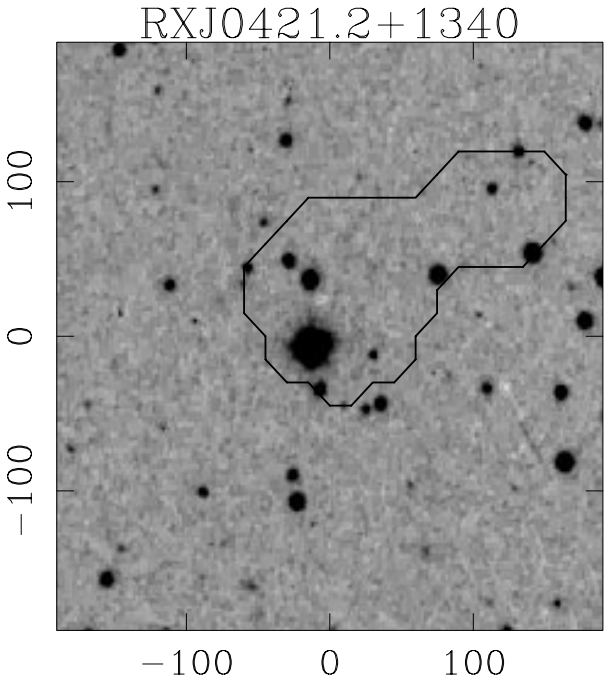

FIG. 30.

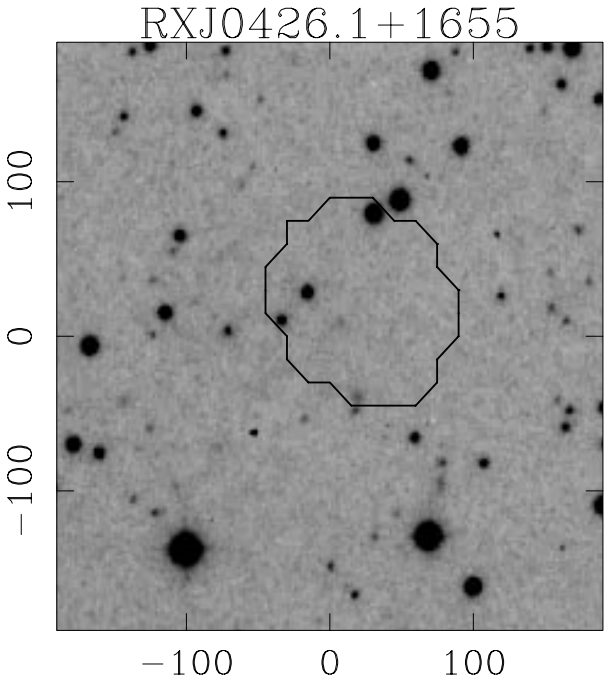

FIG. 31.

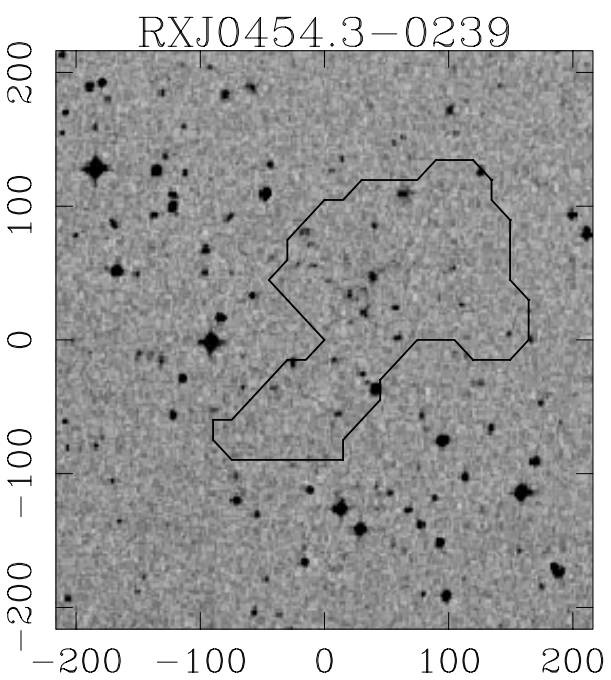

FIG. 32.

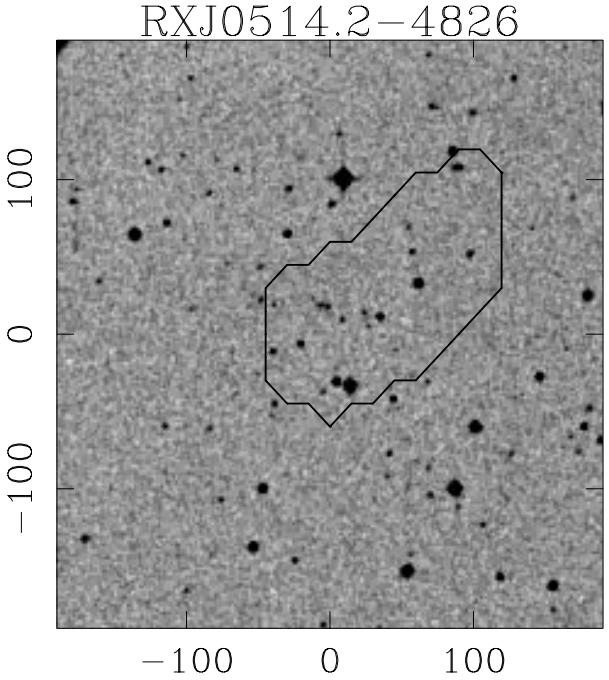

FIG. 33.

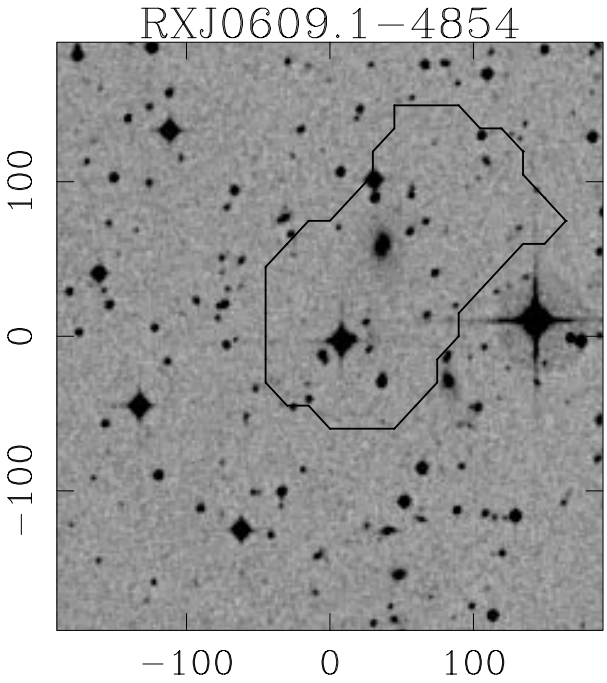

FIG. 34.

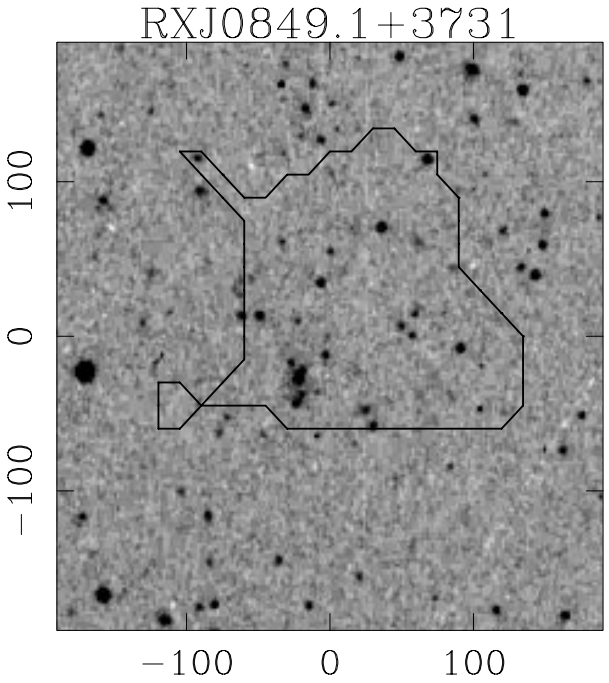

FIG. 35.

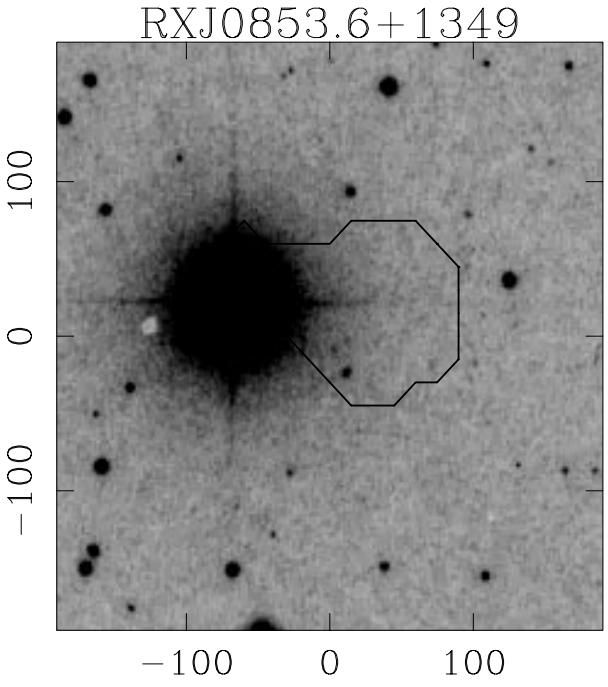

FIG. 36.

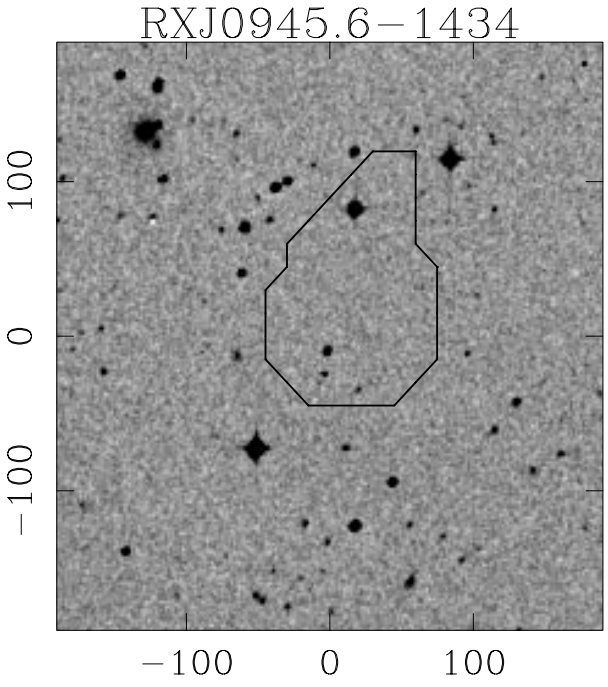

FIG. 37.

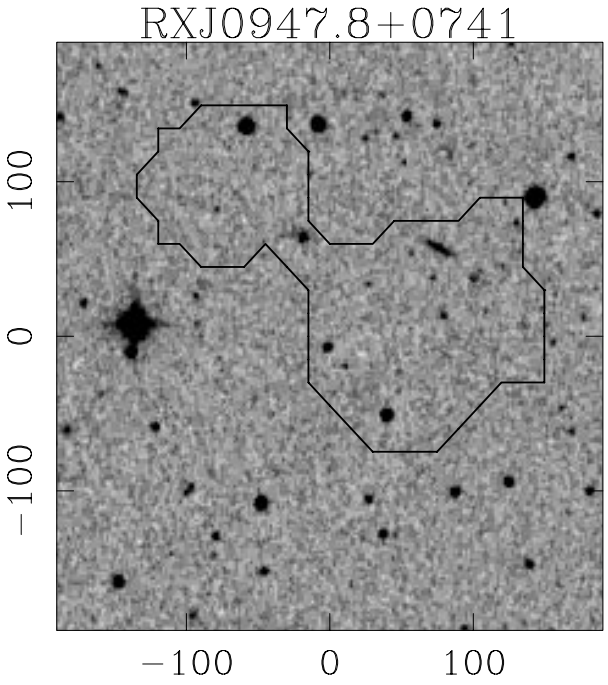

FIG. 38.

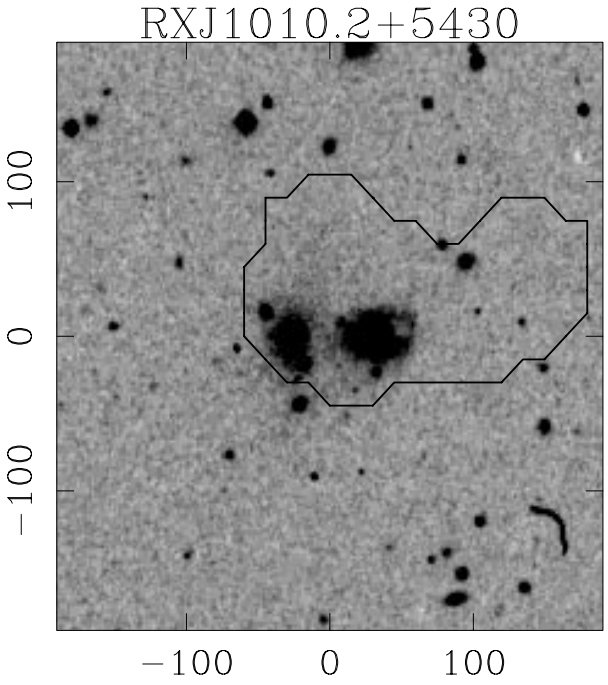

FIG. 39.

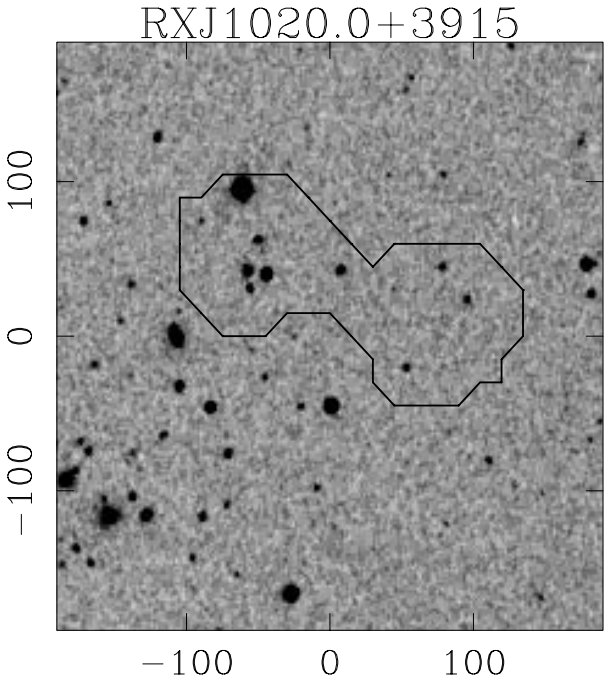

FIG. 40.

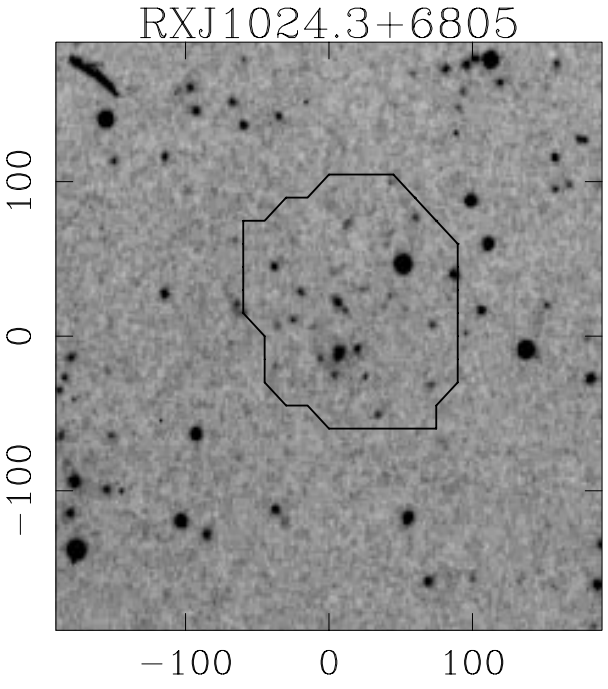

FIG. 41.

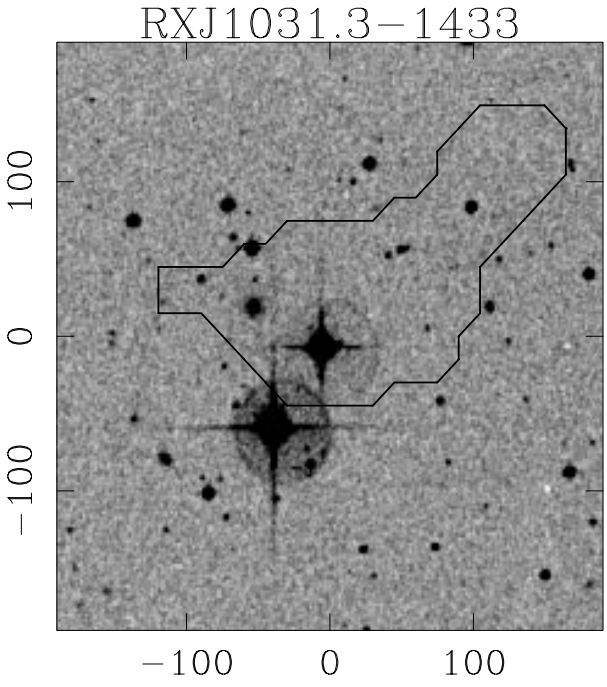

FIG. 42.

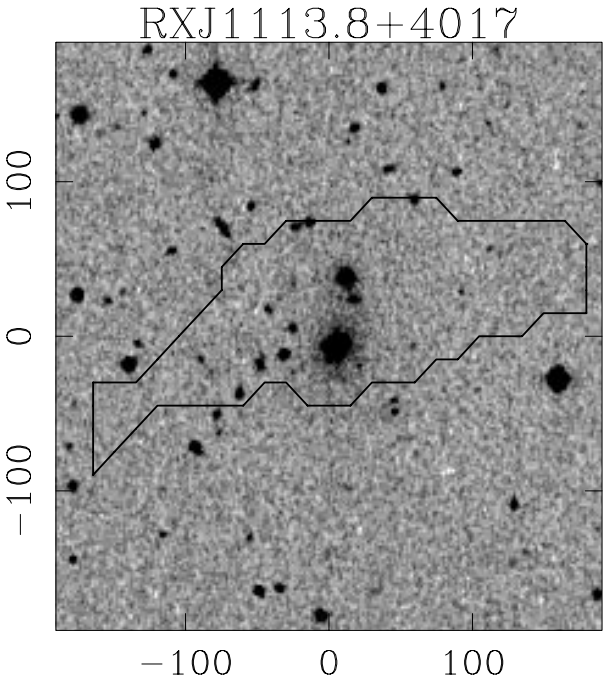

FIG. 43.

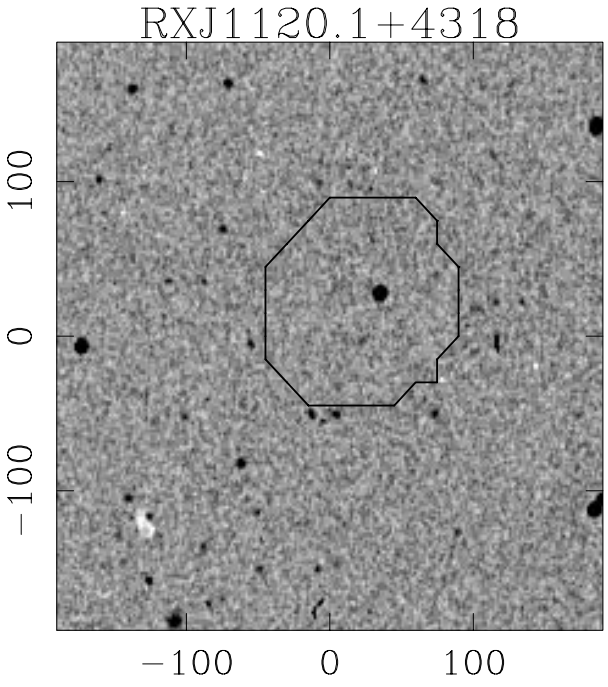

FIG. 44.

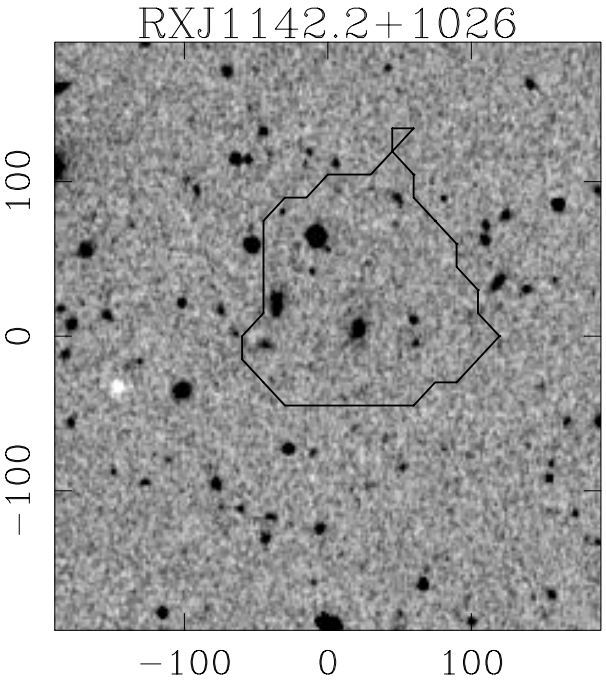

FIG. 45.

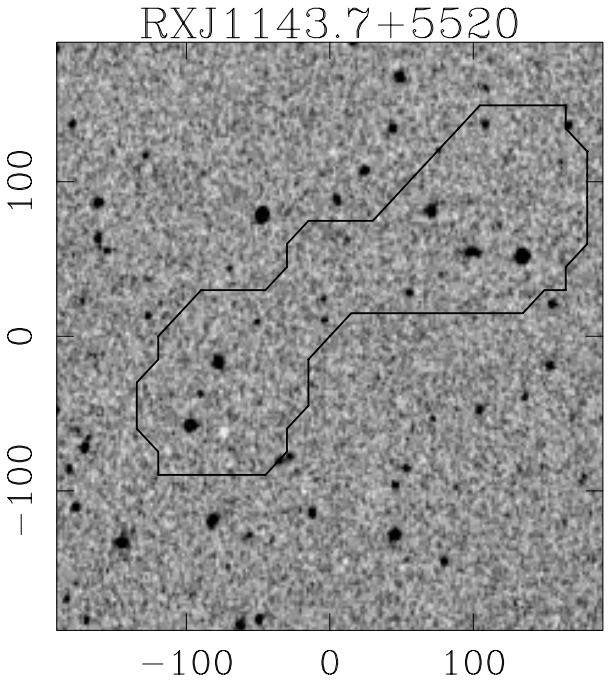

FIG. 46.

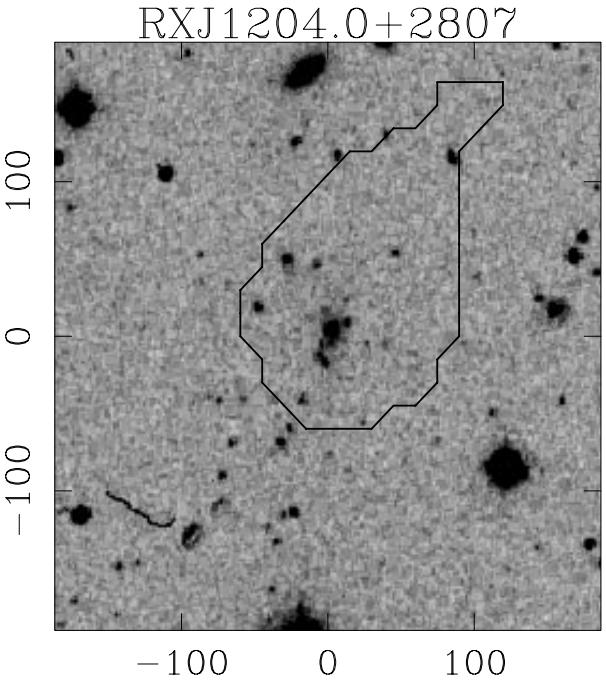

FIG. 47.

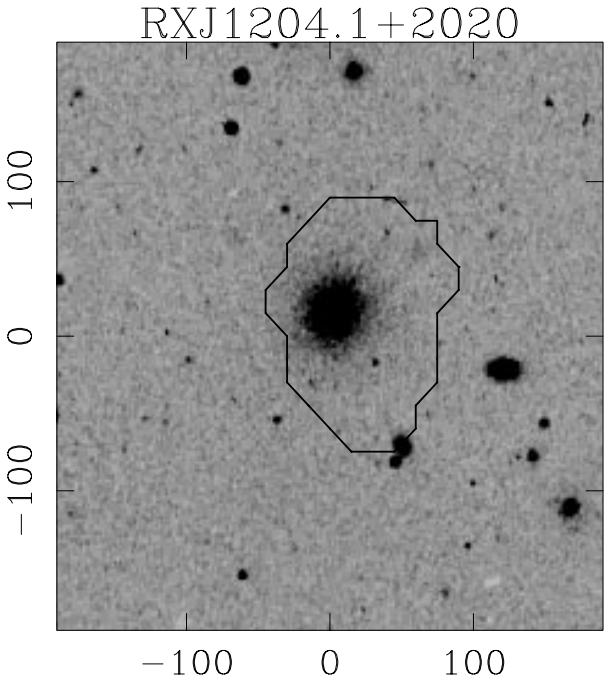

FIG. 48.

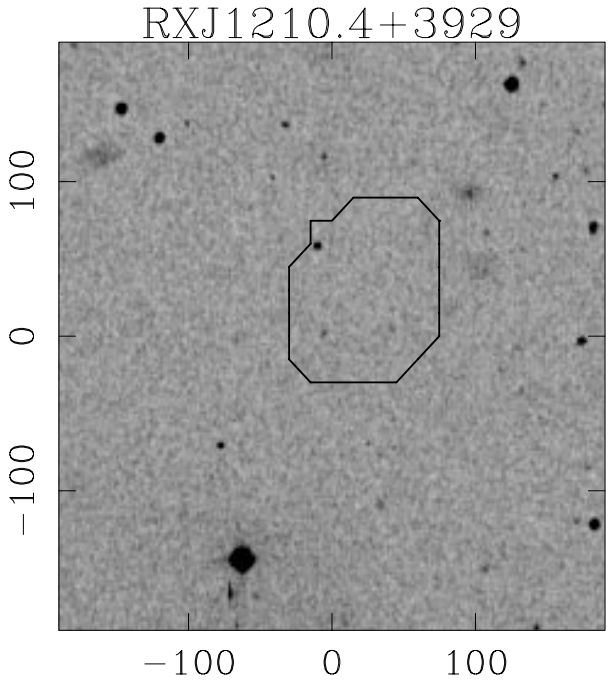

FIG. 49.

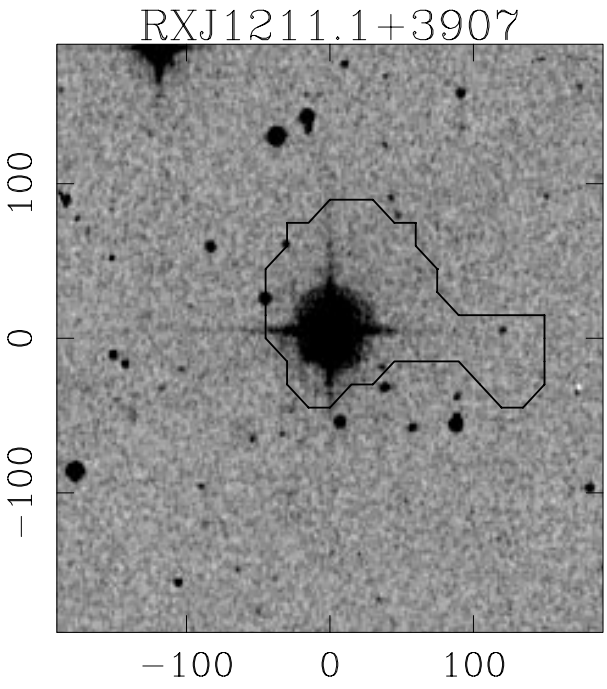

FIG. 50.

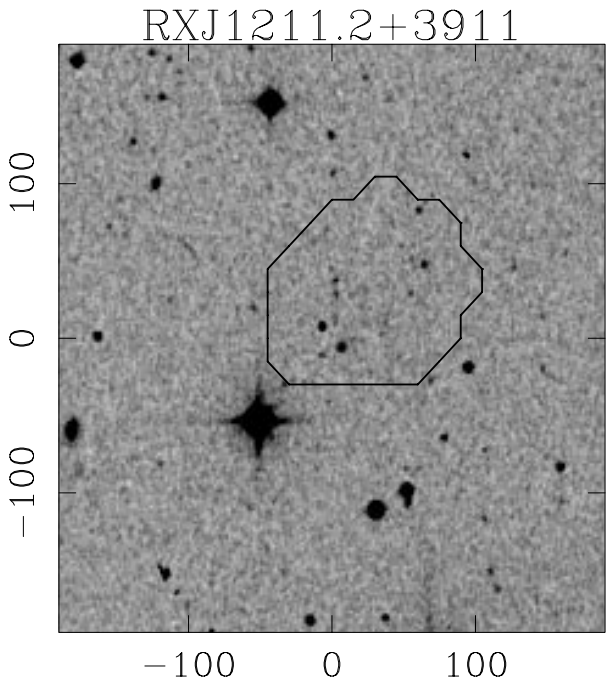

FIG. 51.

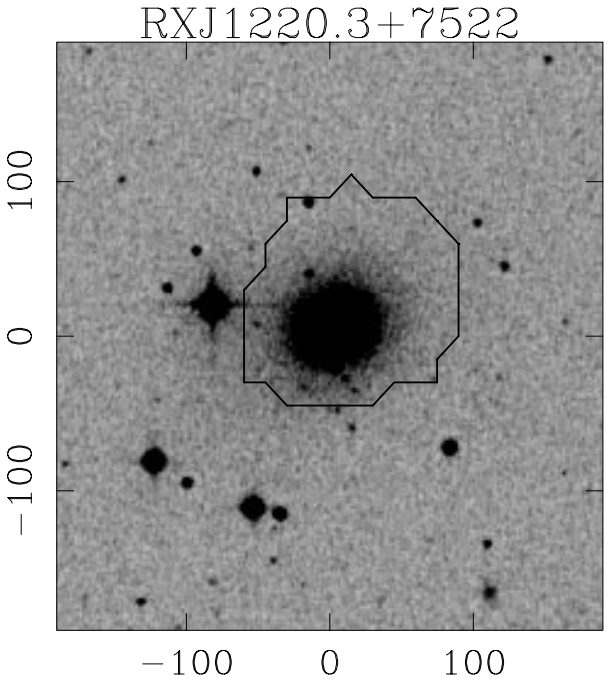

FIG. 52.

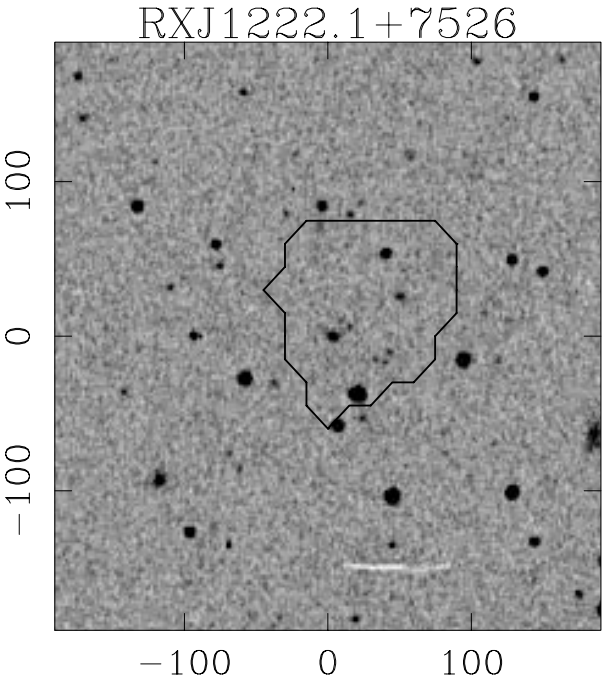

FIG. 53.

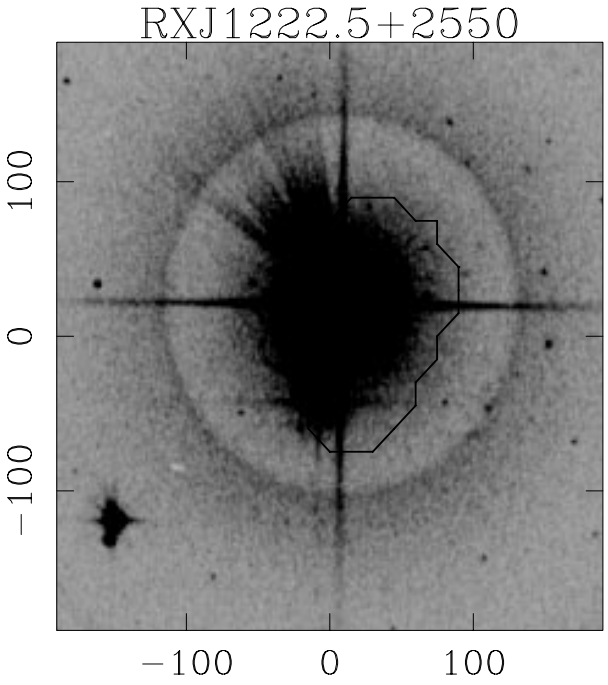

FIG. 54.

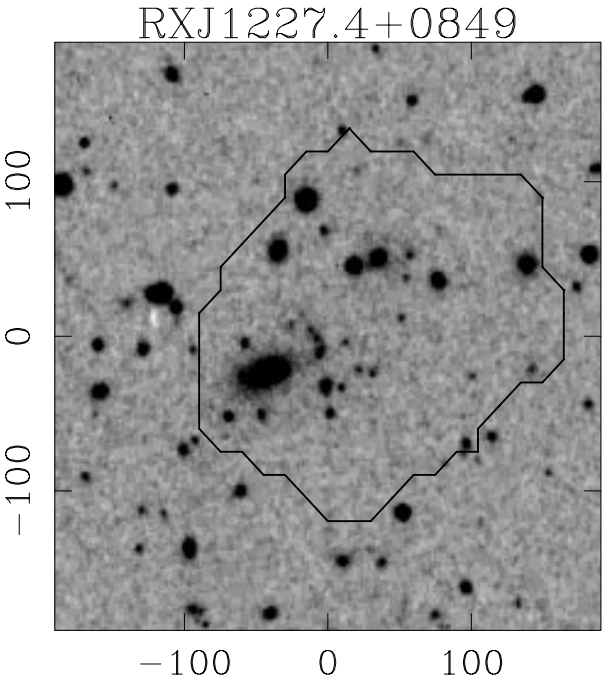

FIG. 55.

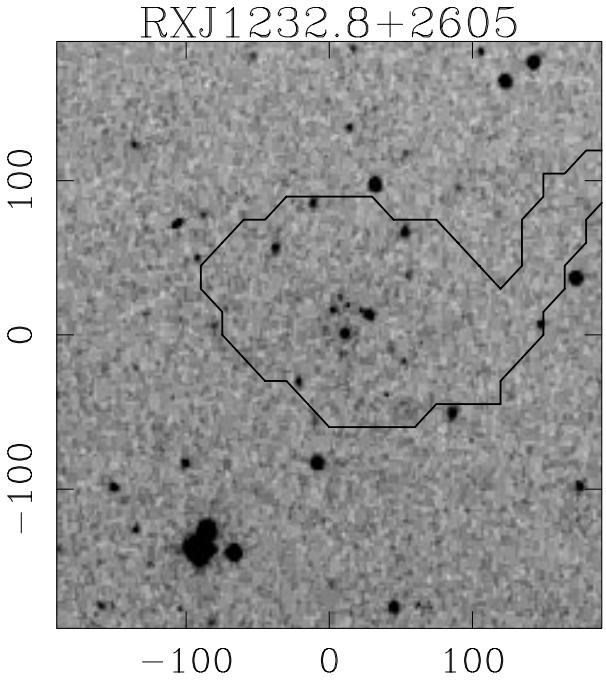

FIG. 56.

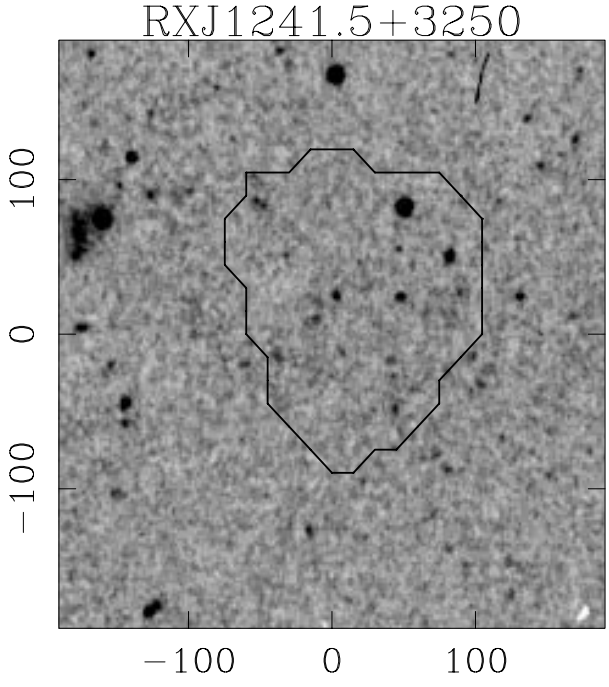

FIG. 57.

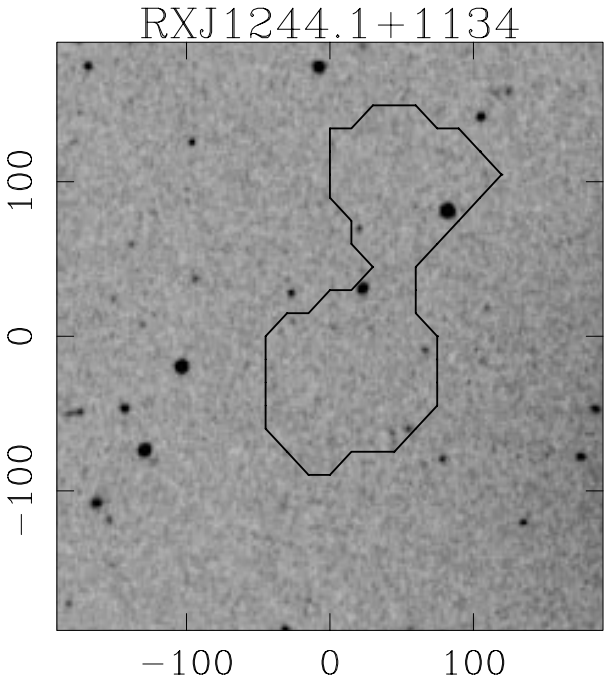

FIG. 58.

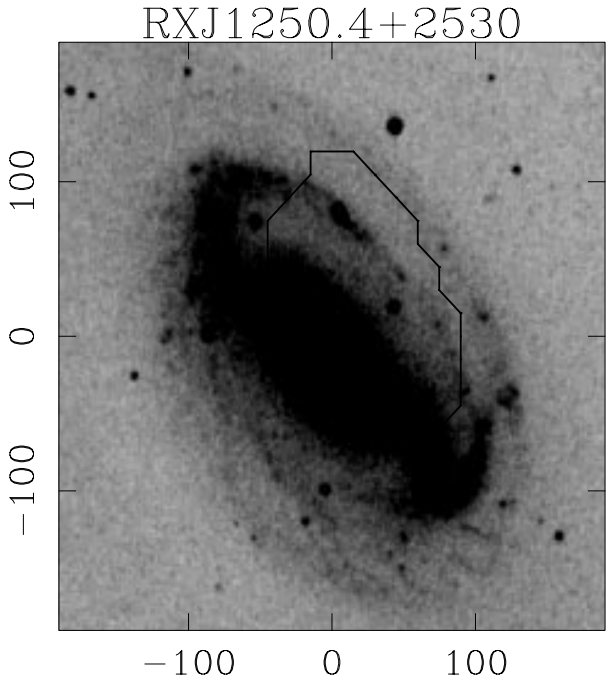

FIG. 59.

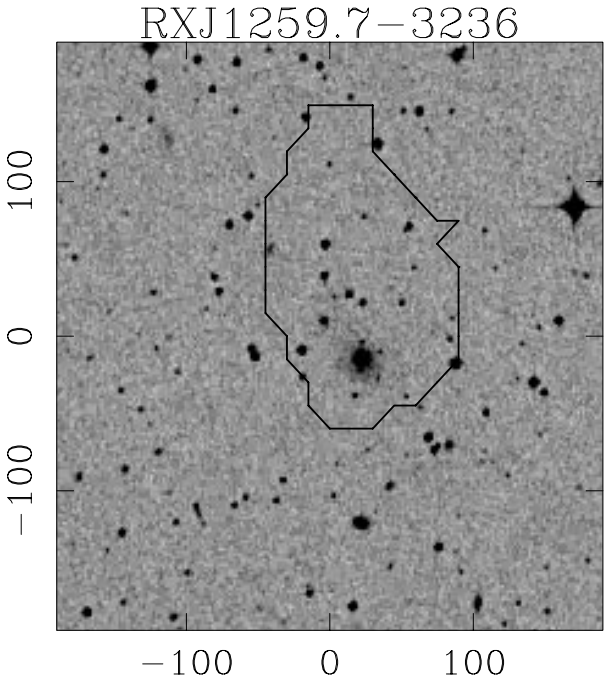

FIG. 60.

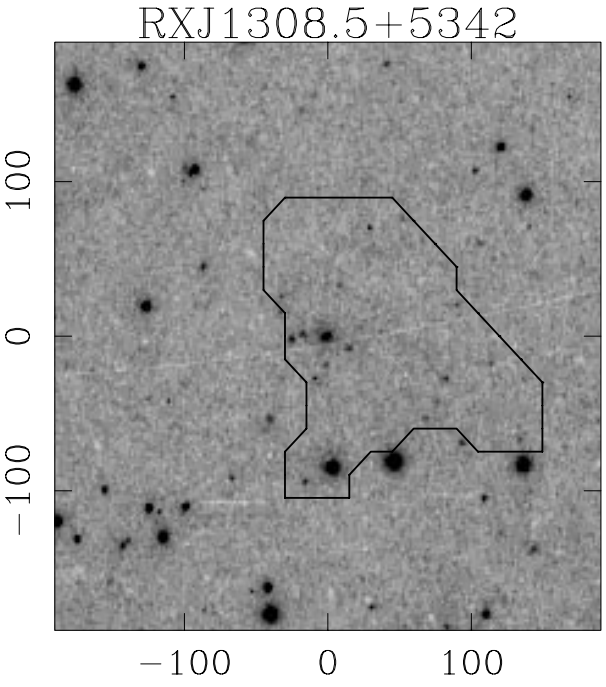

FIG. 61.

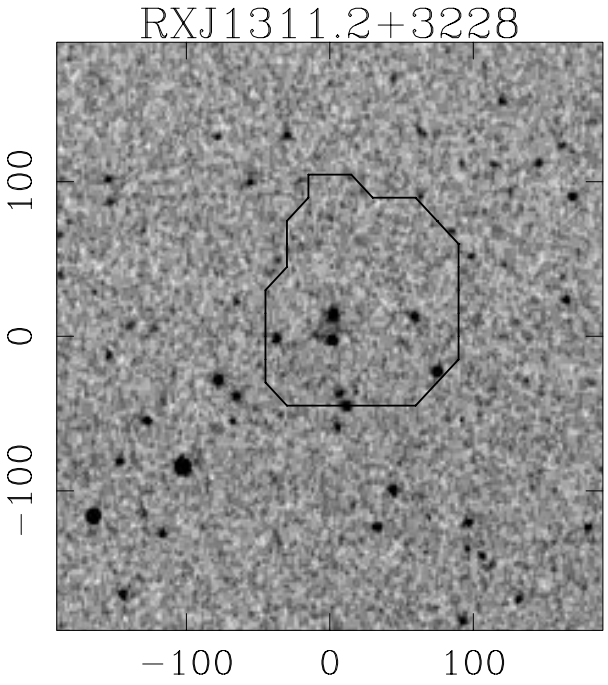

FIG. 62.

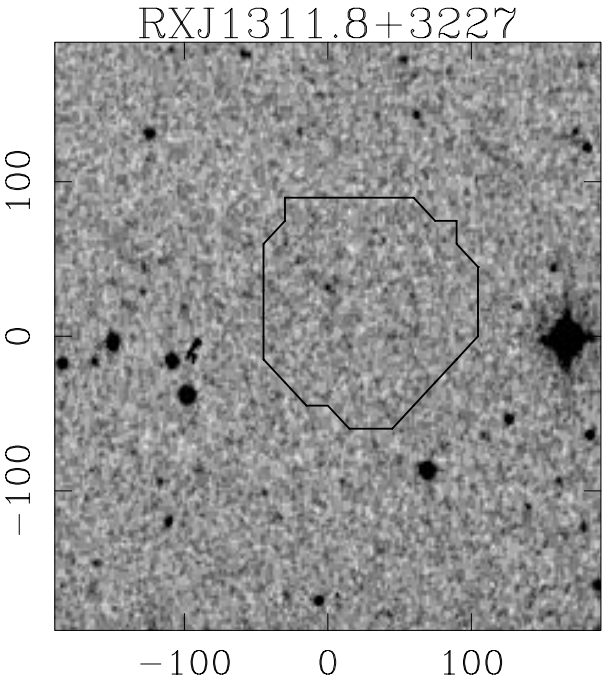

FIG. 63.

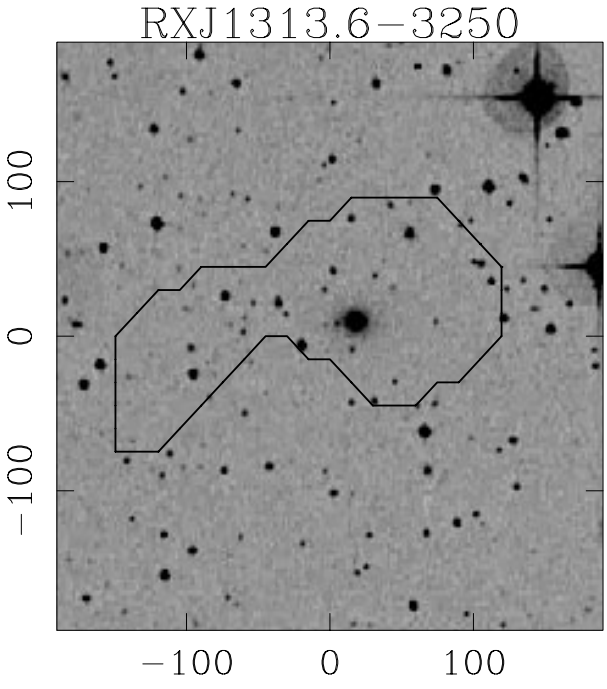

FIG. 64.

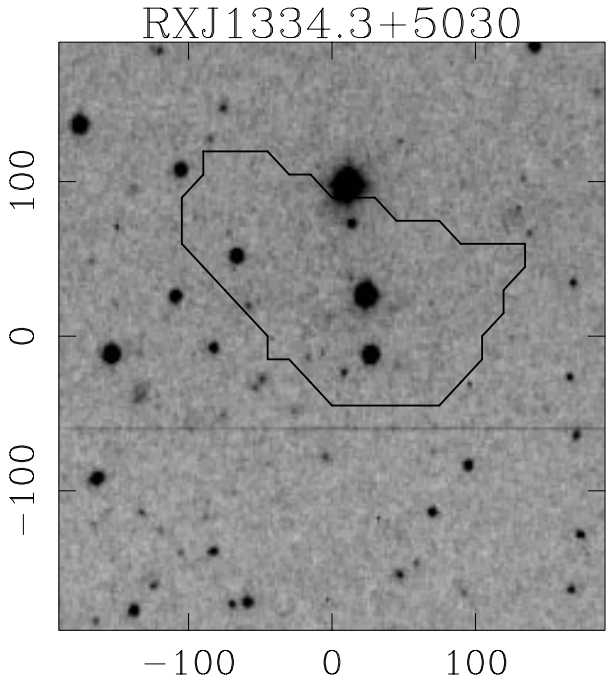

FIG. 65.

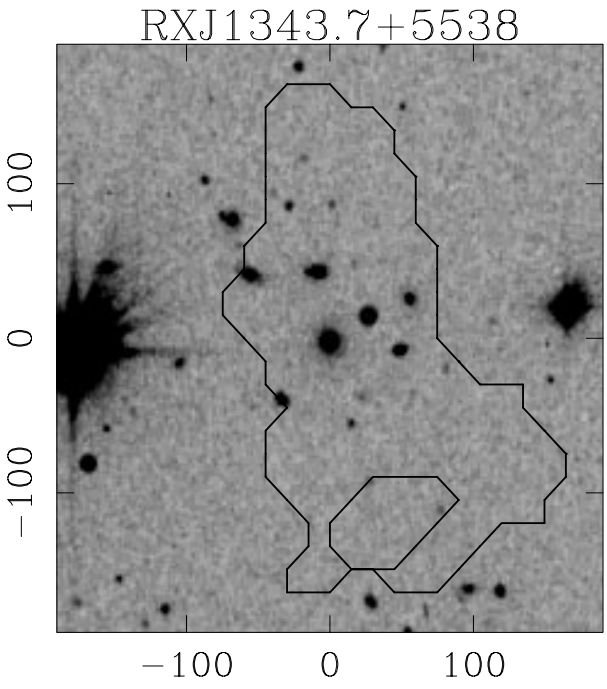

FIG. 66.

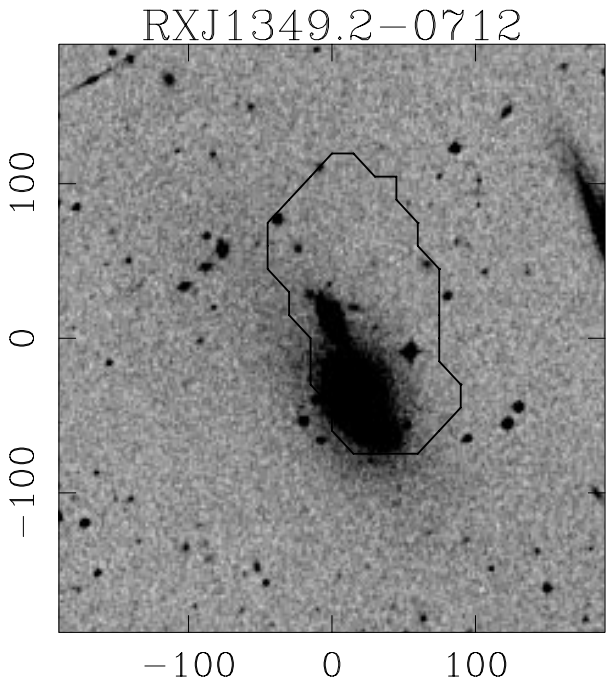

FIG. 67.

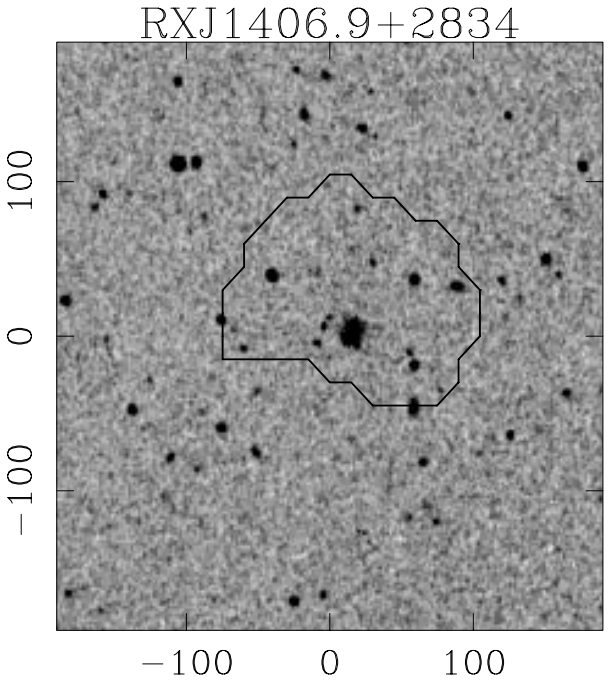

FIG. 68.

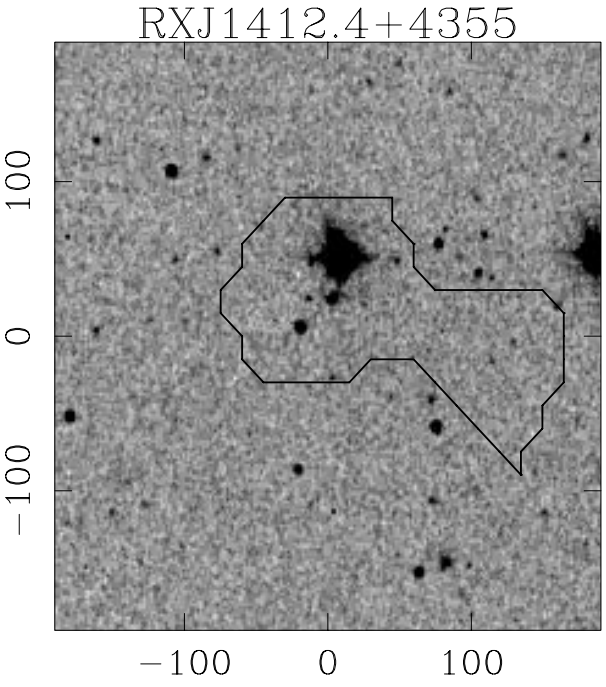

FIG. 69.

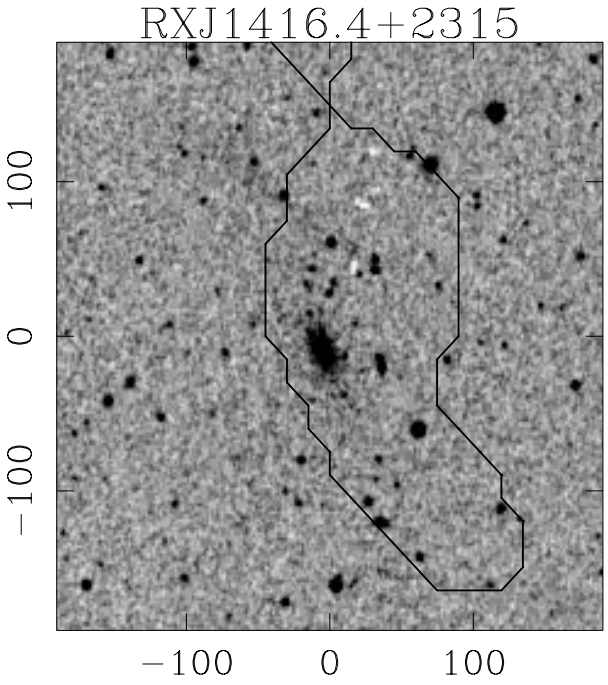

FIG. 70.

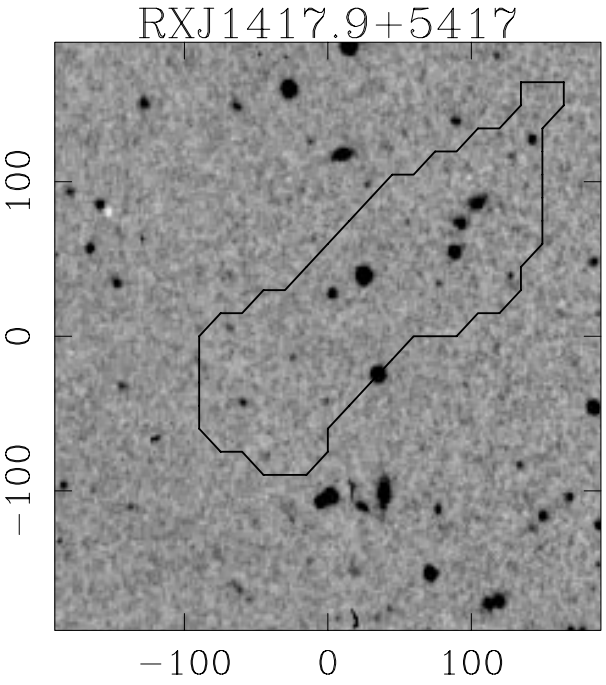

FIG. 71.

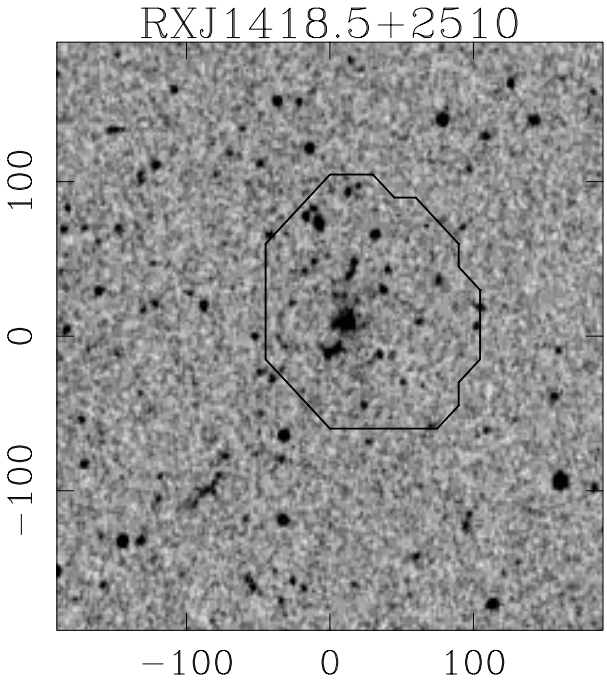

FIG. 72.

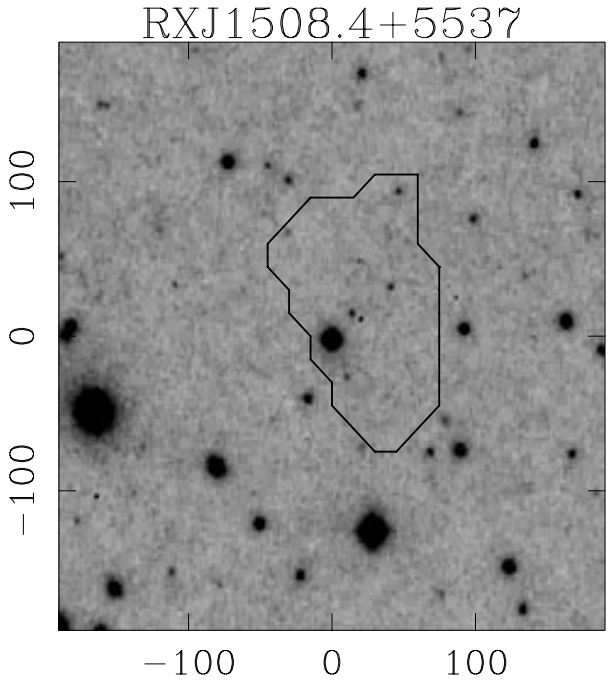

FIG. 73.

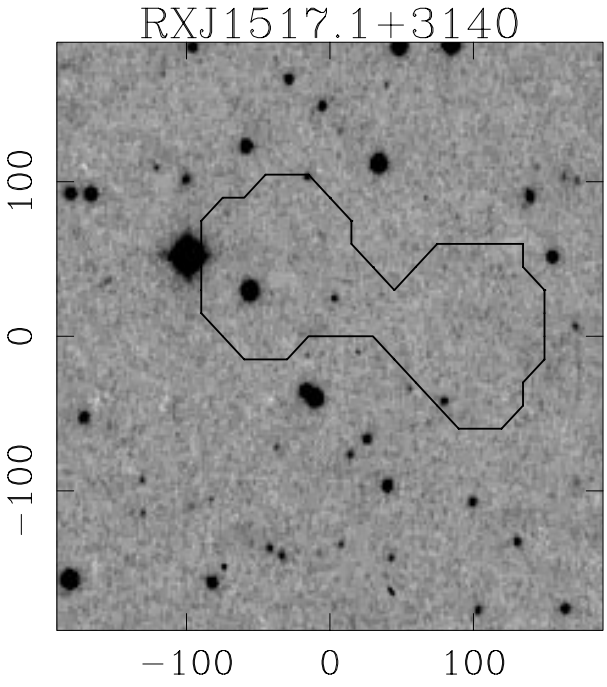

FIG. 74.

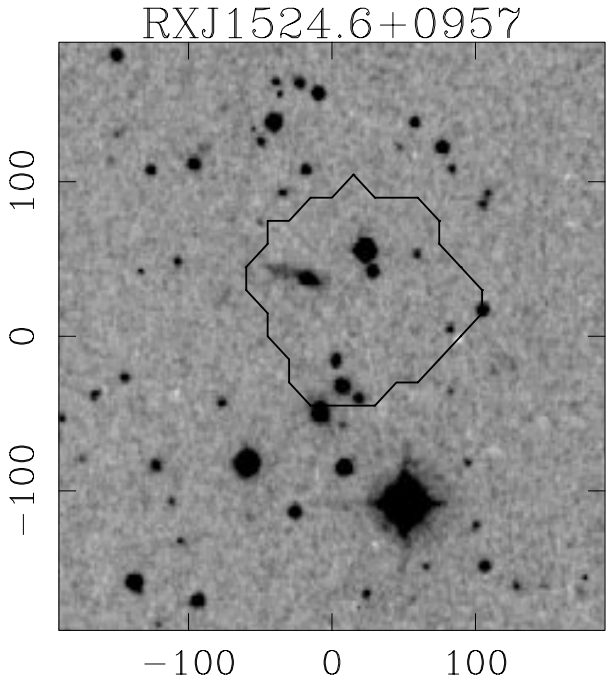

FIG. 75.

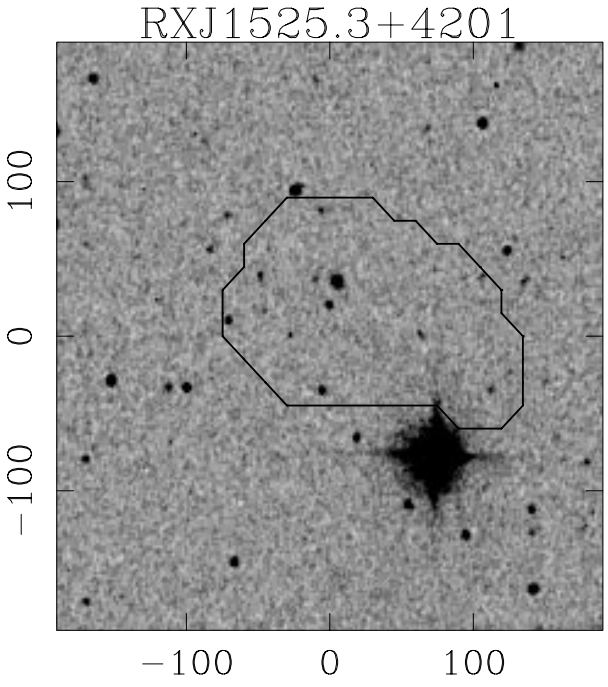

FIG. 76.

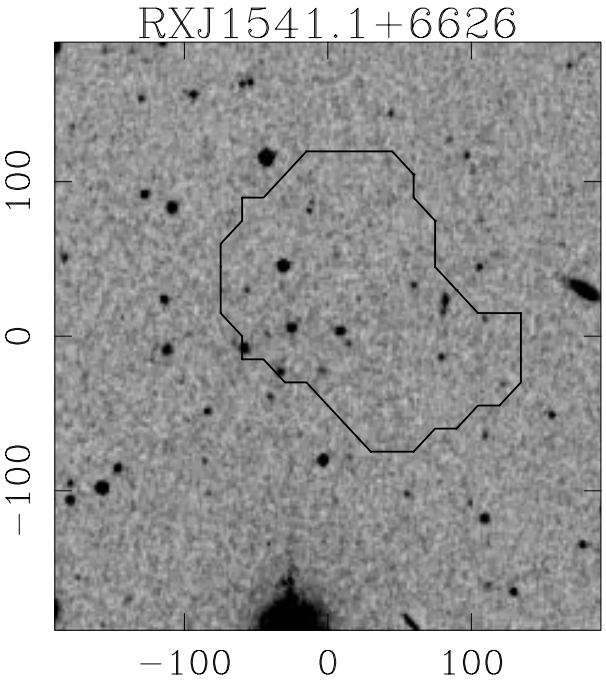

FIG. 77.

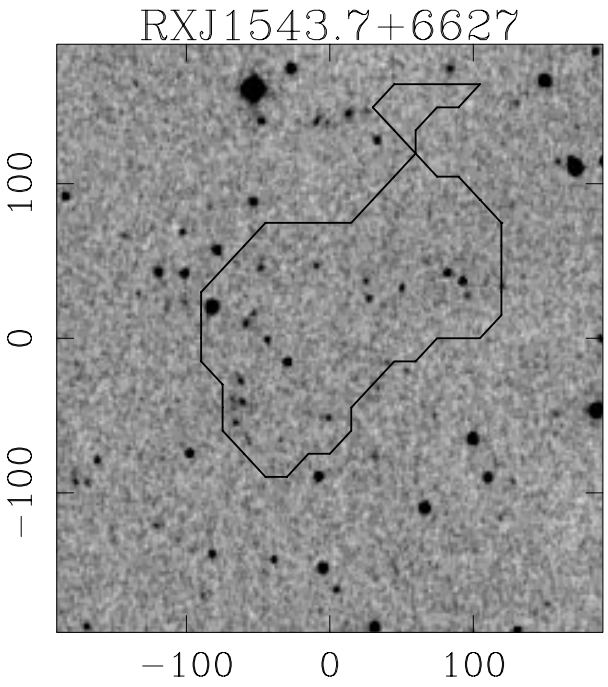

FIG. 78.

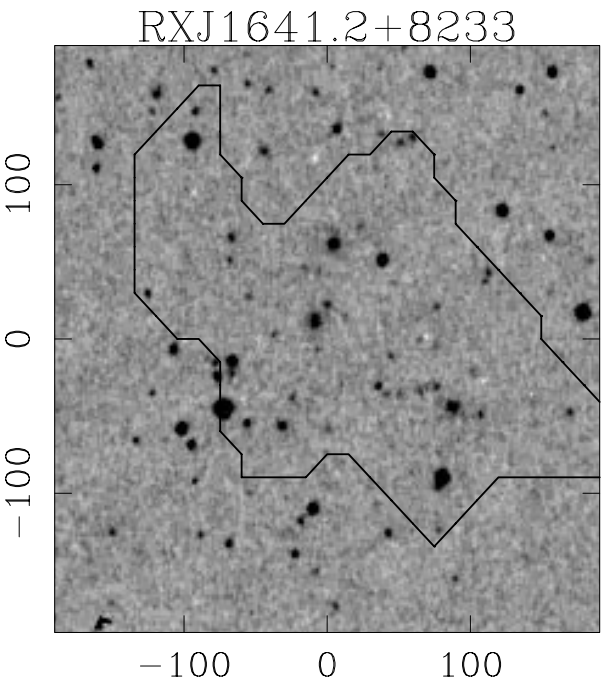

FIG. 79.

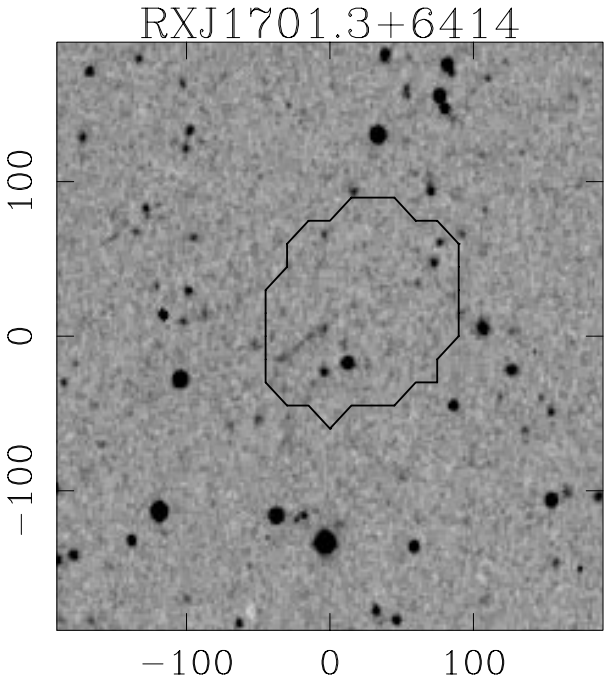

FIG. 80.

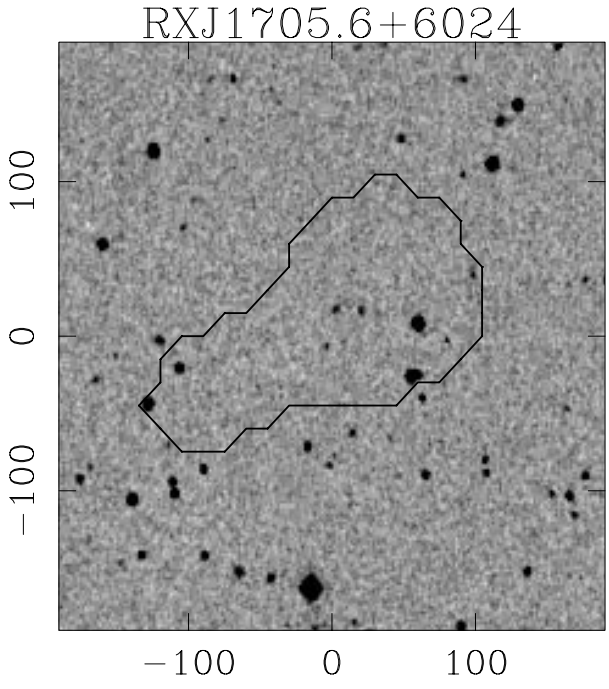

FIG. 81.

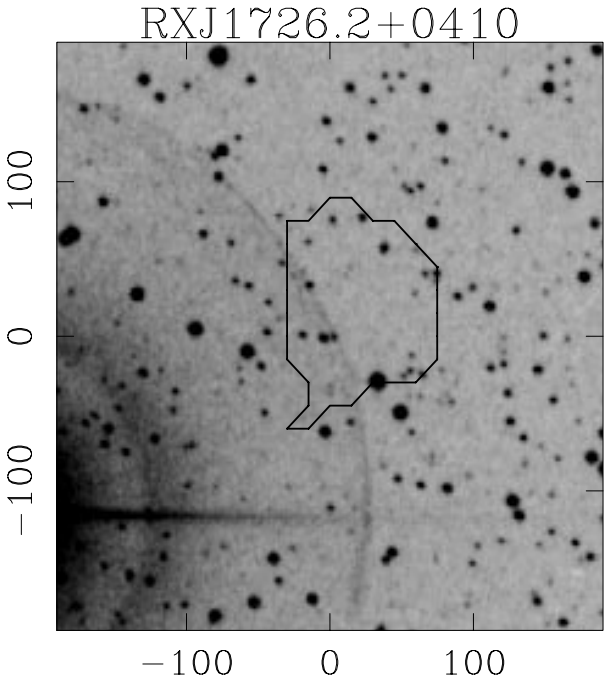

FIG. 82.

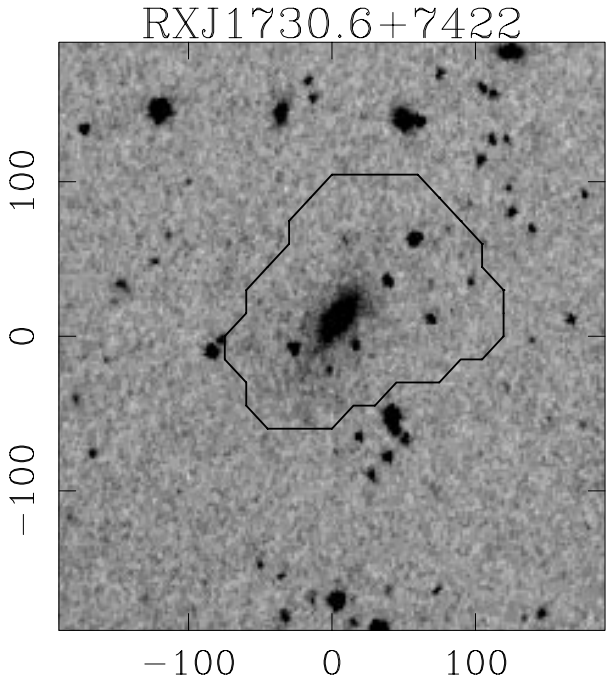

FIG. 83.

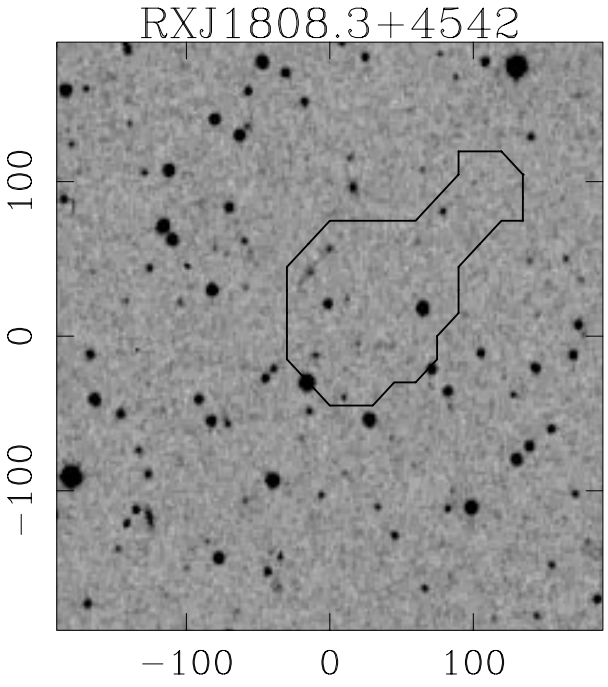

FIG. 84.

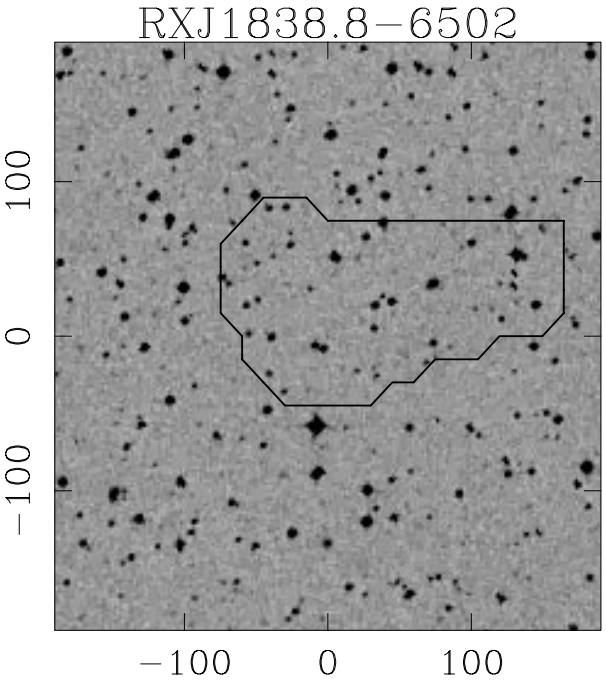

FIG. 85.

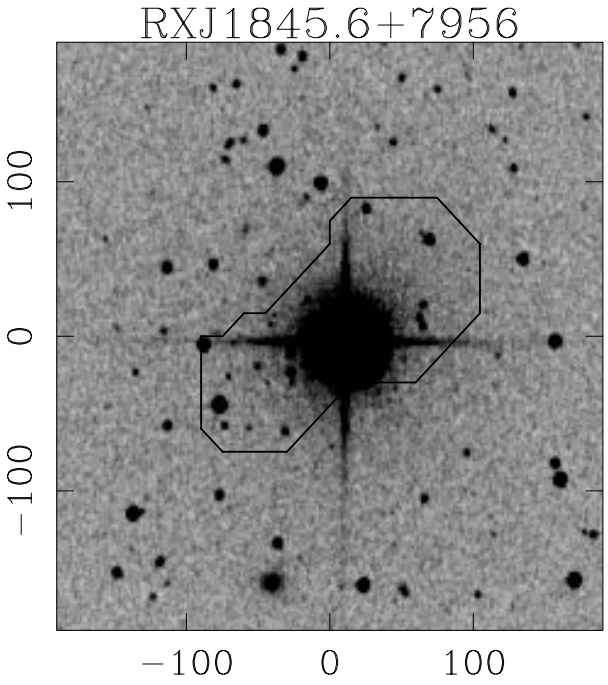

FIG. 86.

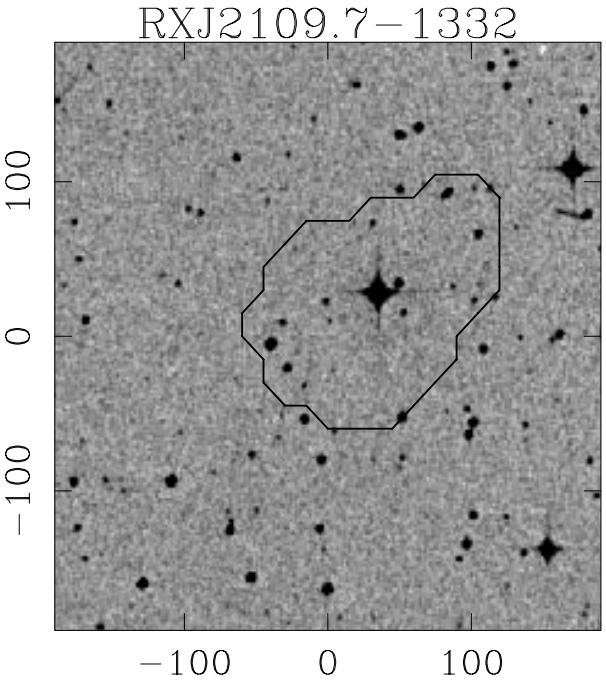

FIG. 87.

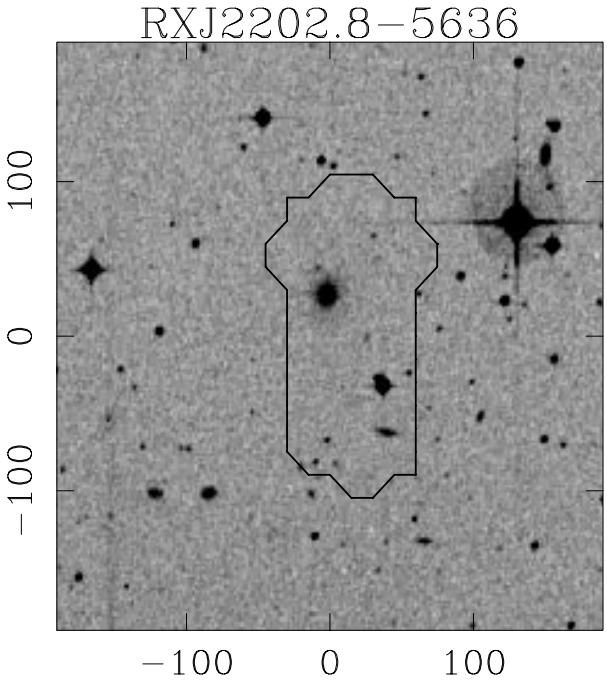

FIG. 88.

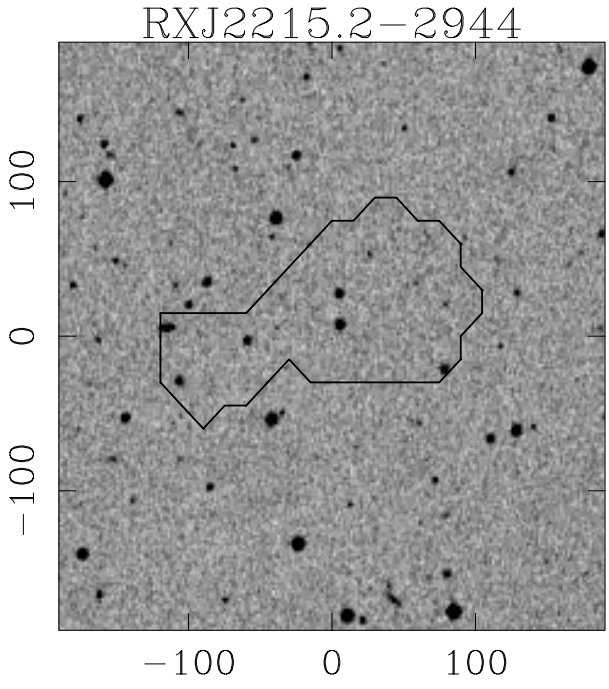

FIG. 89.

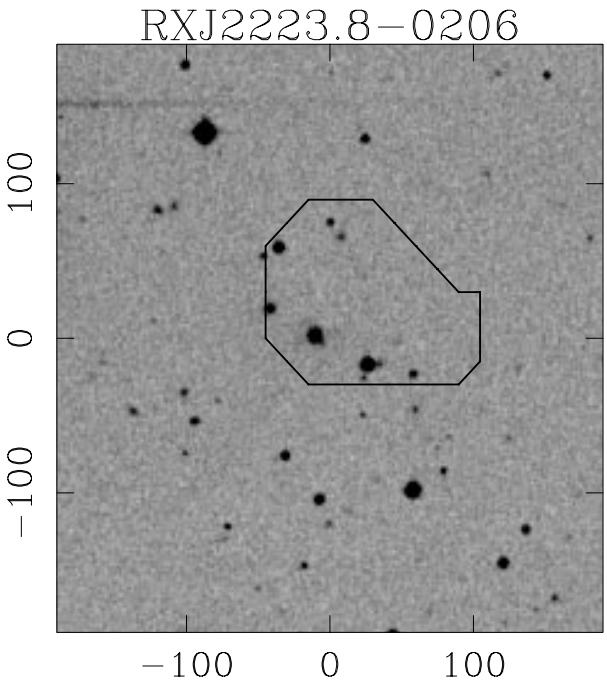

FIG. 90.

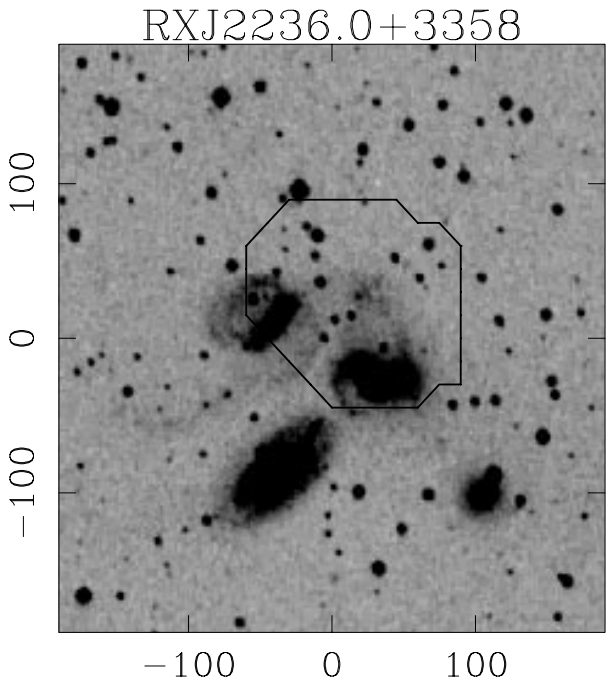

FIG. 91.

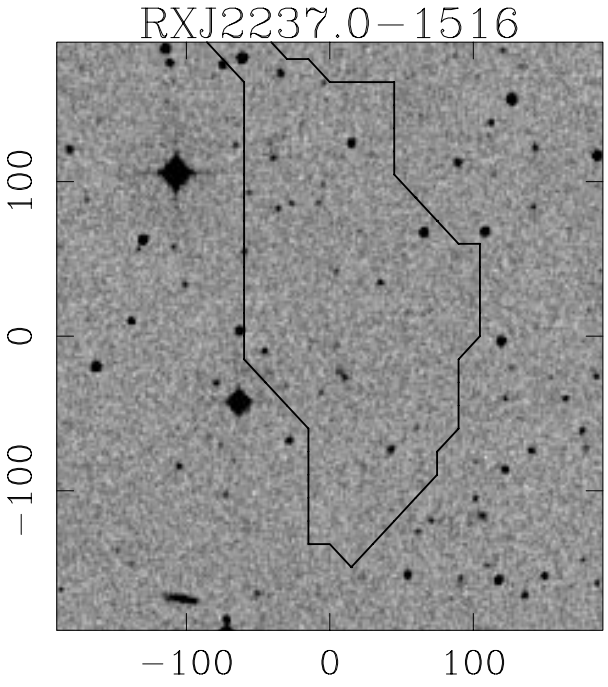

FIG. 92.

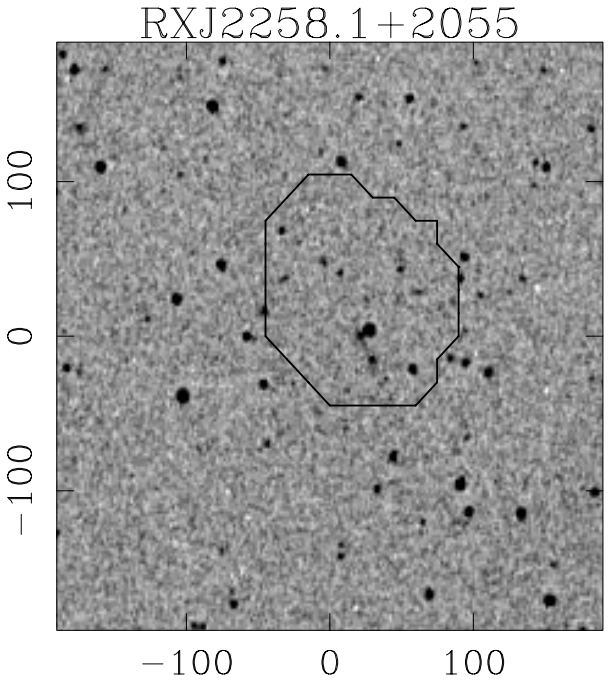

FIG. 93.

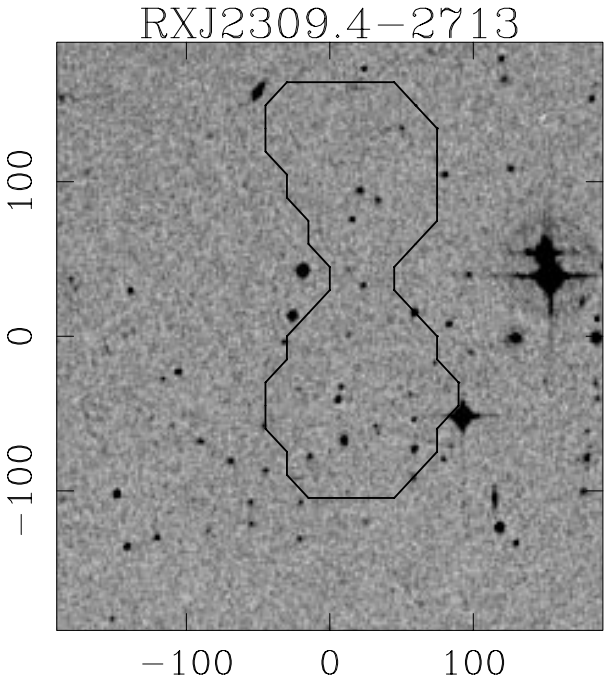

FIG. 94.

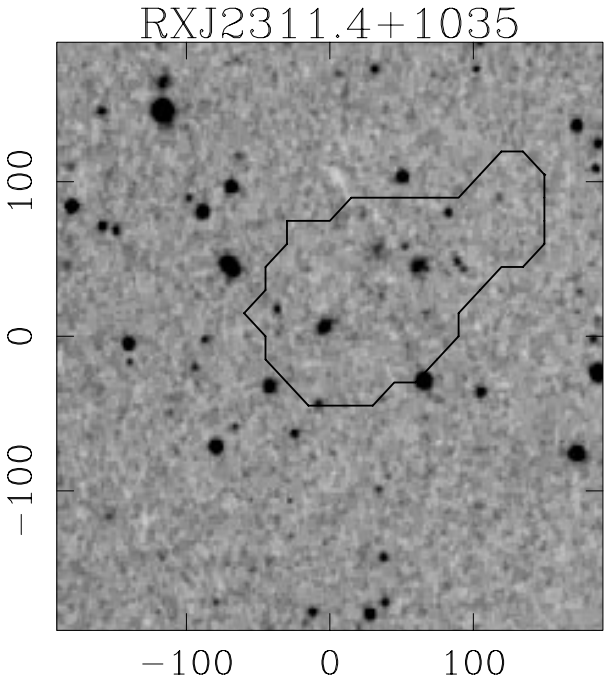

FIG. 95.

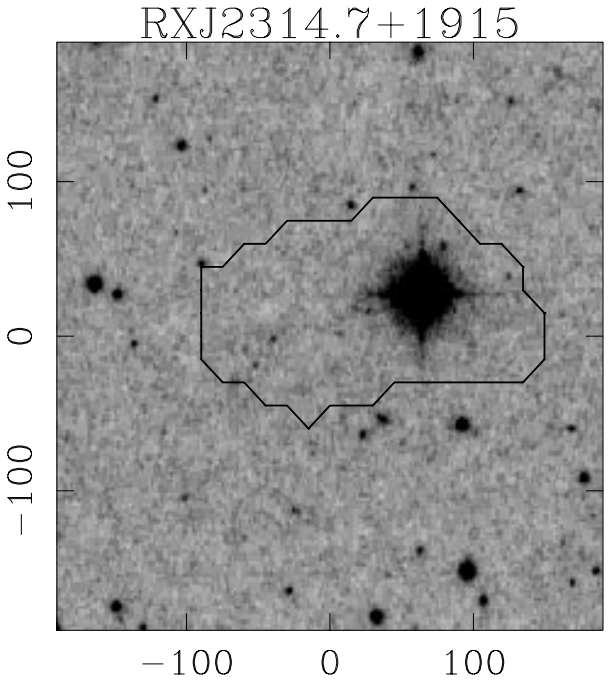

FIG. 96.

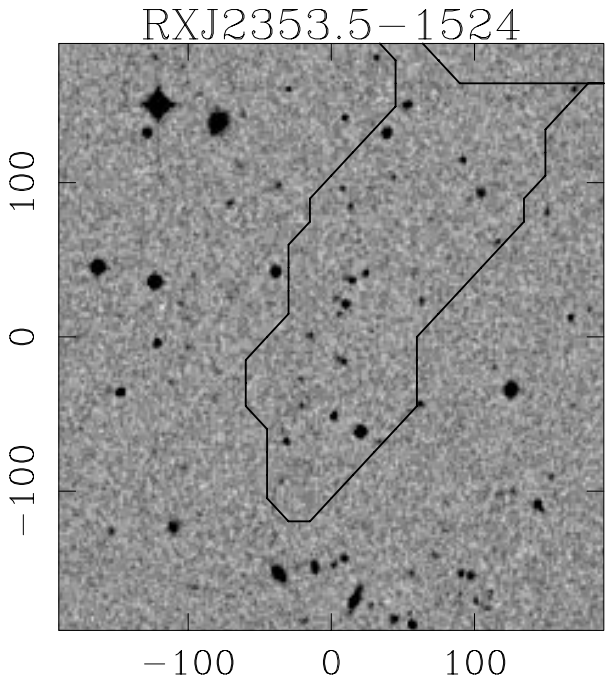

FIG. 97.

APPENDIX D

Figures 98–134 show the source and background apertures used to define total count rates, cr_T, for Bright SHARC clusters. Each image is 120 × 120 pixels, with a pixel scale of 14.″947.

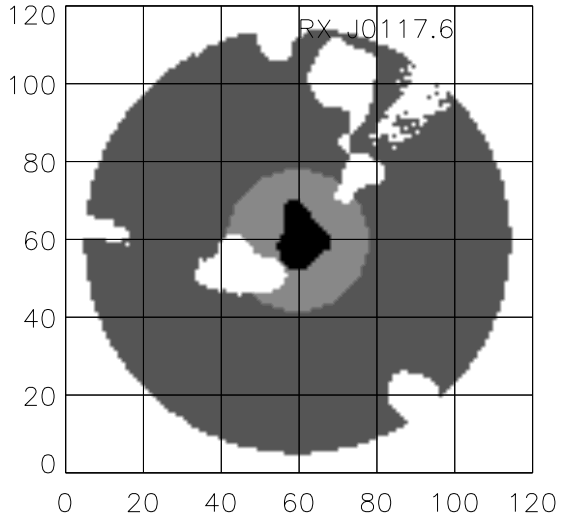

FIG. 98.

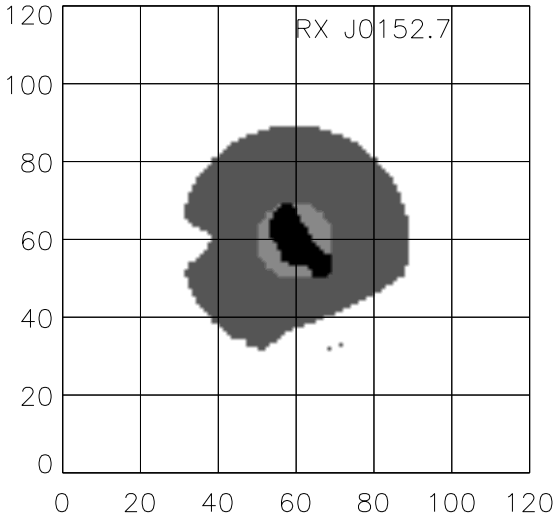

FIG. 99.

Figs. 98–134 show the source (*light gray plus black*) and background (*dark gray*) apertures used to define total count rates, cr_T, for Bright SHARC clusters. Masked out pixels are shown in white. N.B.: The central black region represents the aperture used to define the wavelet count rates, cr_W. Each image is 120 × 120 pixels, with a pixel scale of 14.″947.

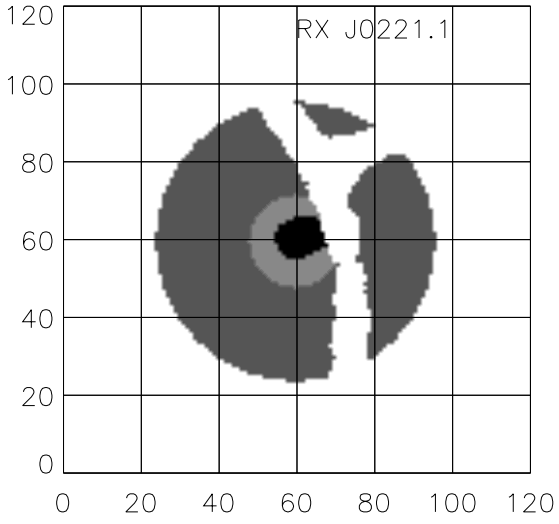

FIG. 100.

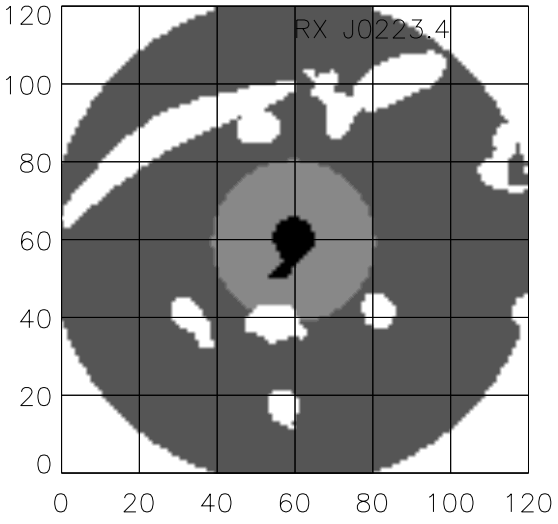

FIG. 101.

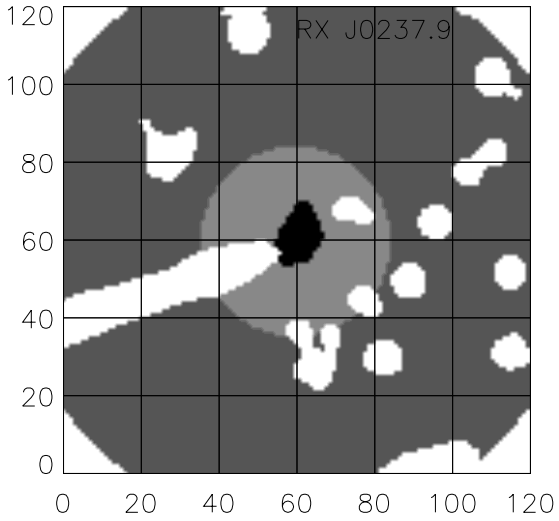

FIG. 102.

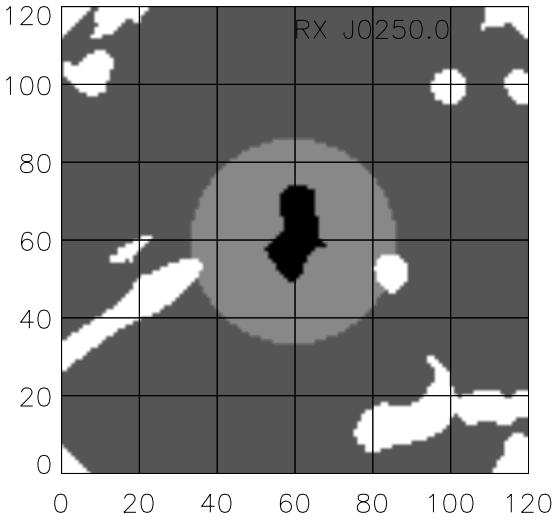

FIG. 103.

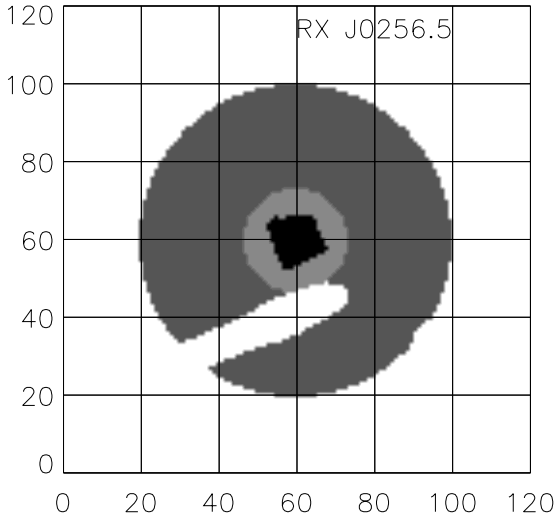

FIG. 104.

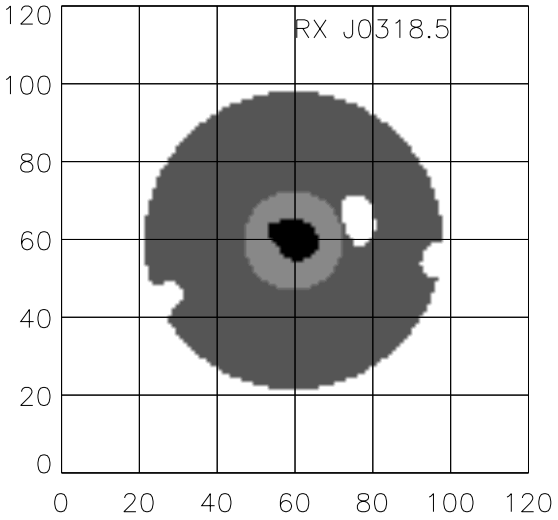

FIG. 105.

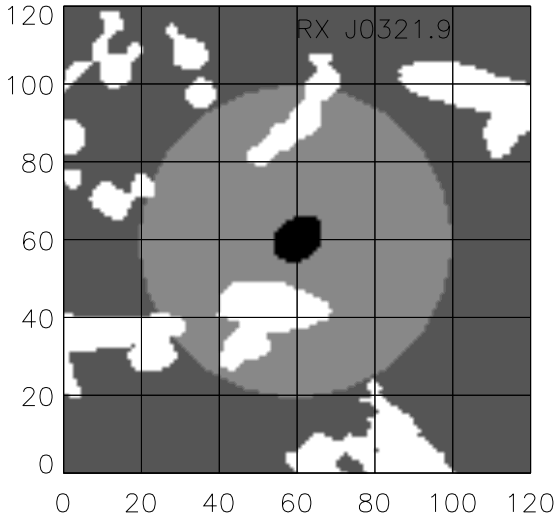

FIG. 106.

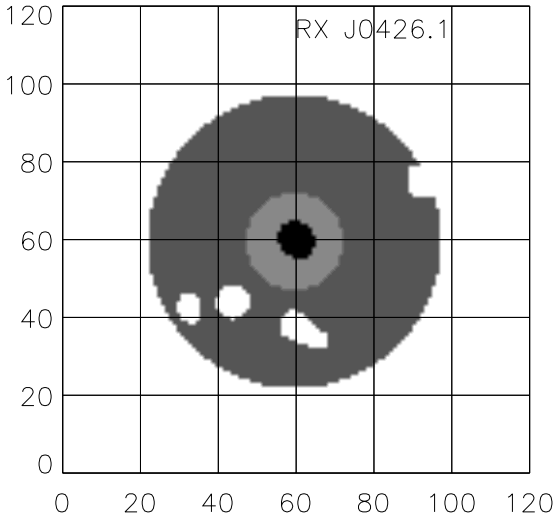

FIG. 107.

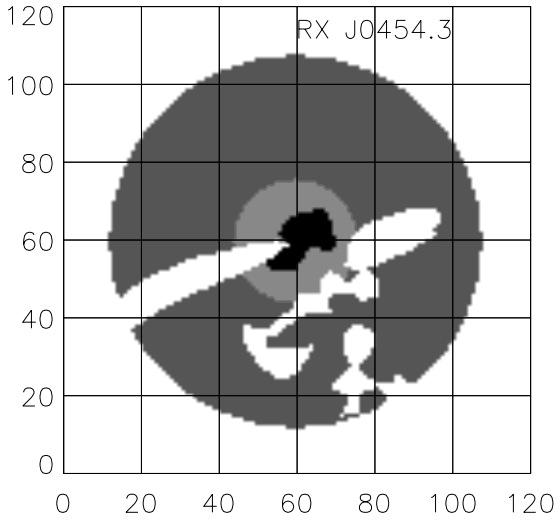

FIG. 108.

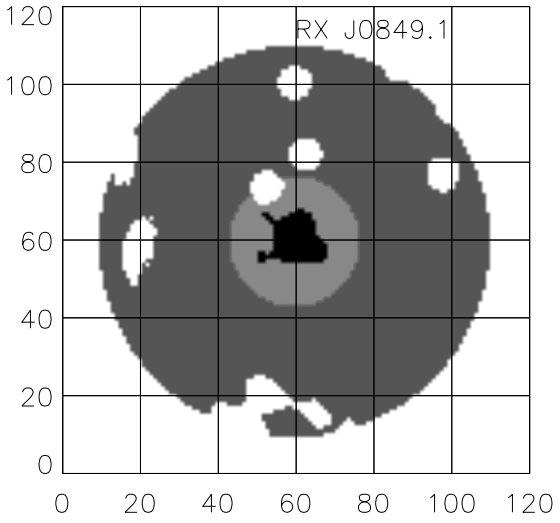

FIG. 109.

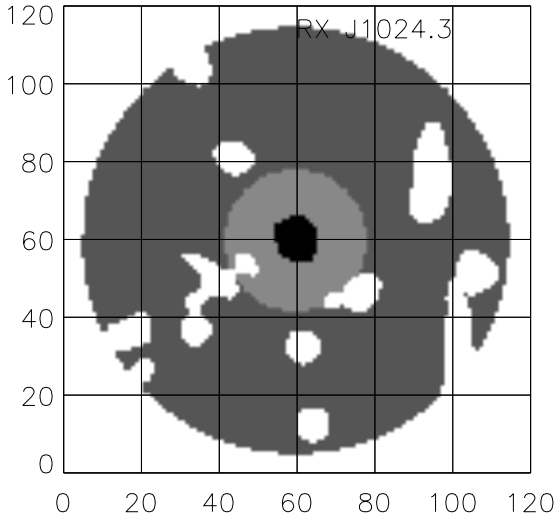

FIG. 110.

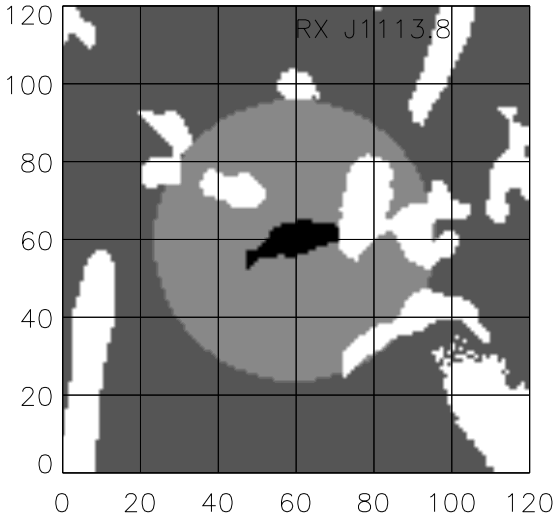

FIG. 111.

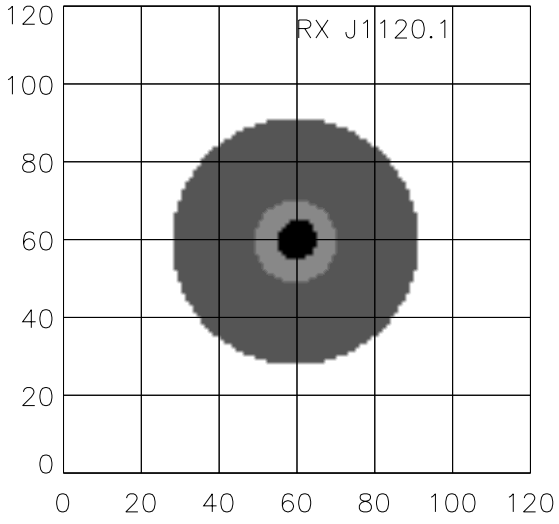

FIG. 112.

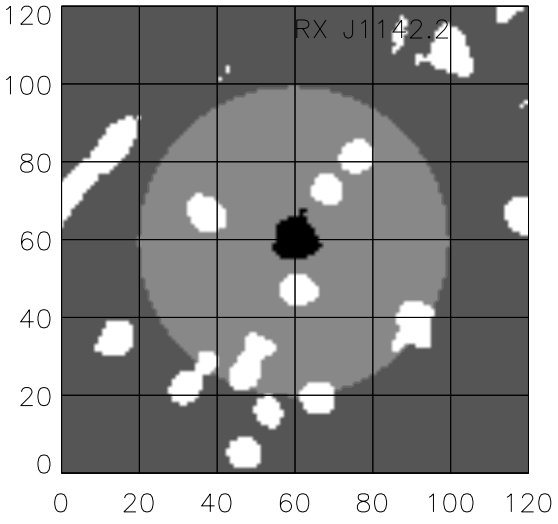

FIG. 113.

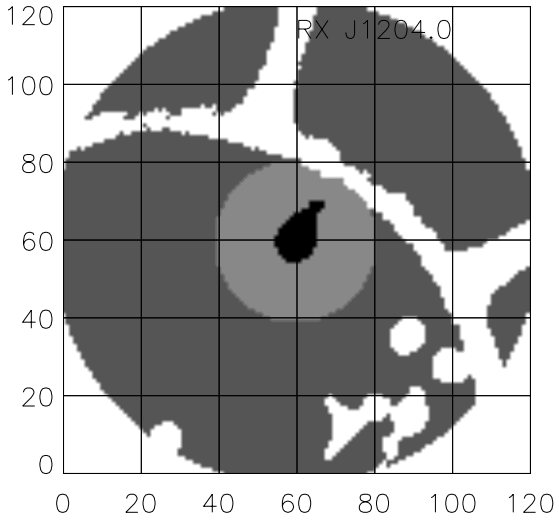

FIG. 114.

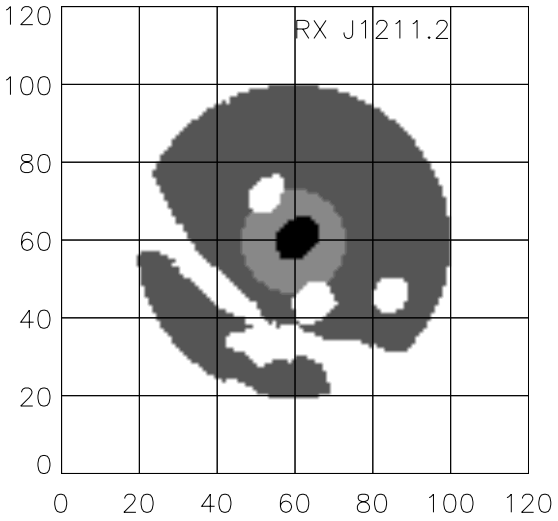

FIG. 115.

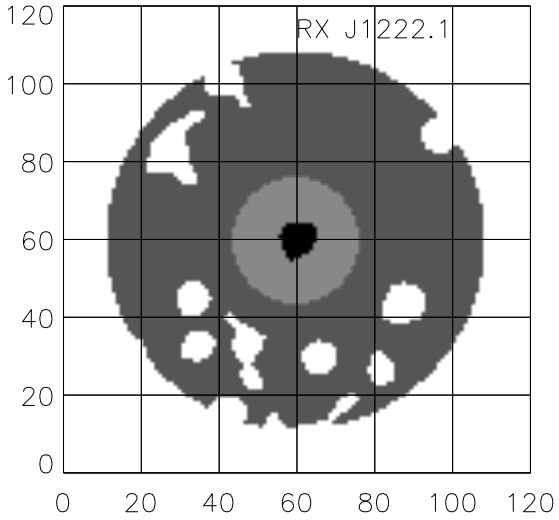

FIG. 116.

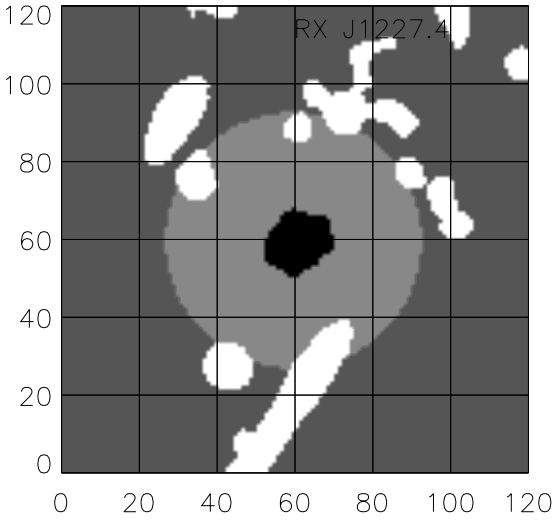

FIG. 117.

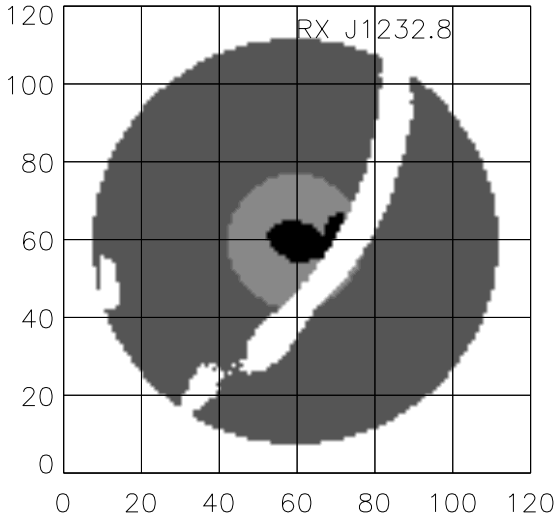

FIG. 118.

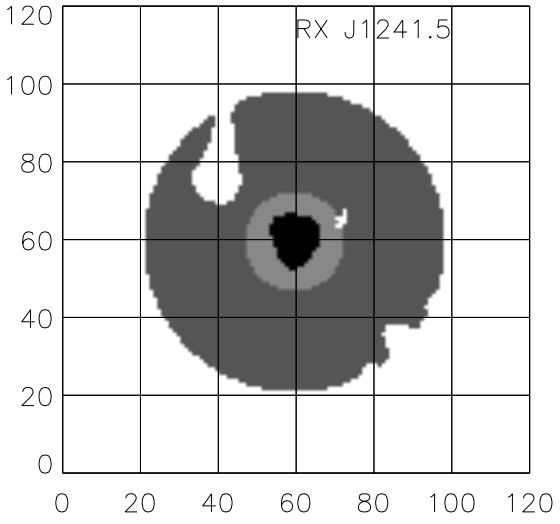

FIG. 119.

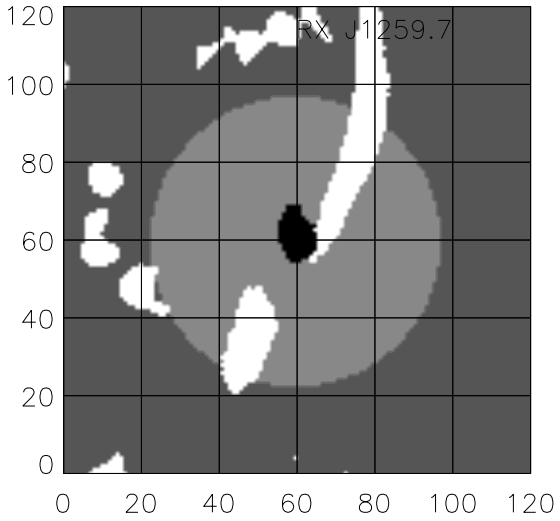

FIG. 120.

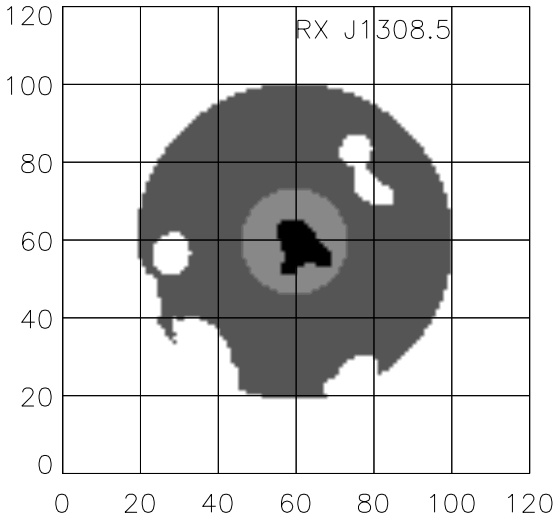

FIG. 121.

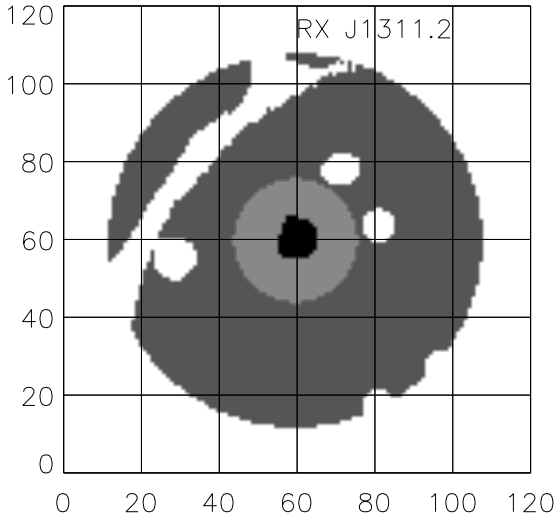

FIG. 122.

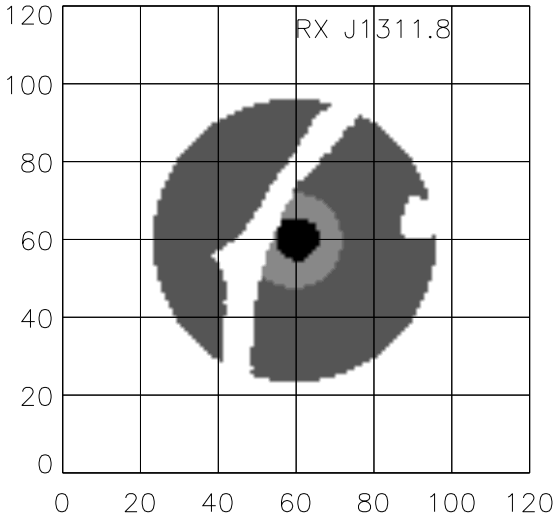

FIG. 123.

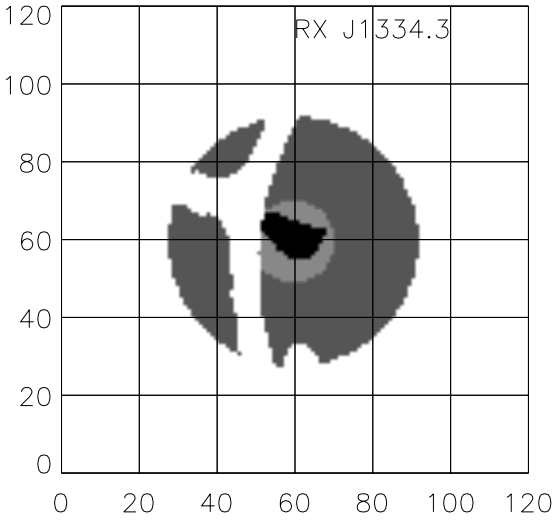

FIG. 124.

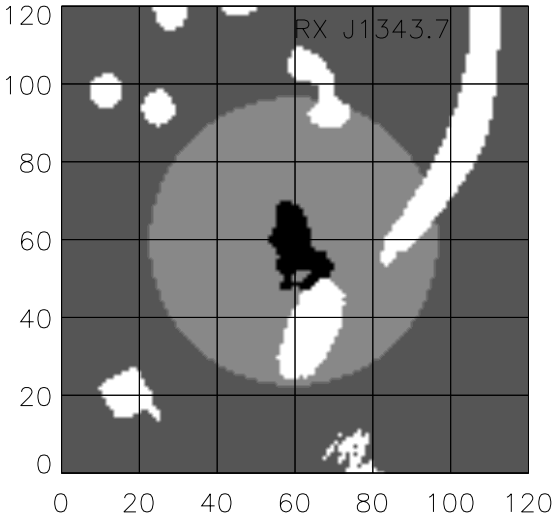

FIG. 125.

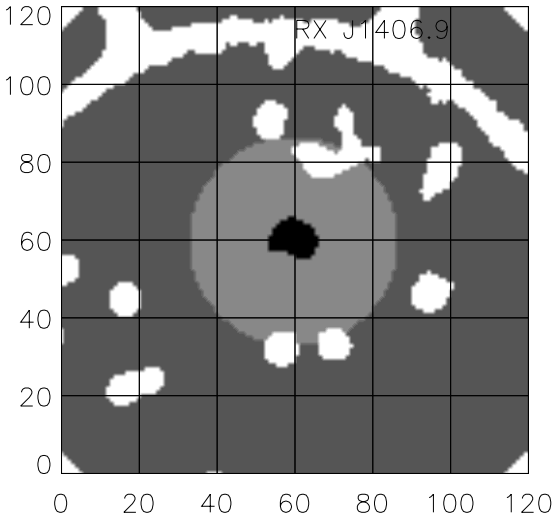

FIG. 126.

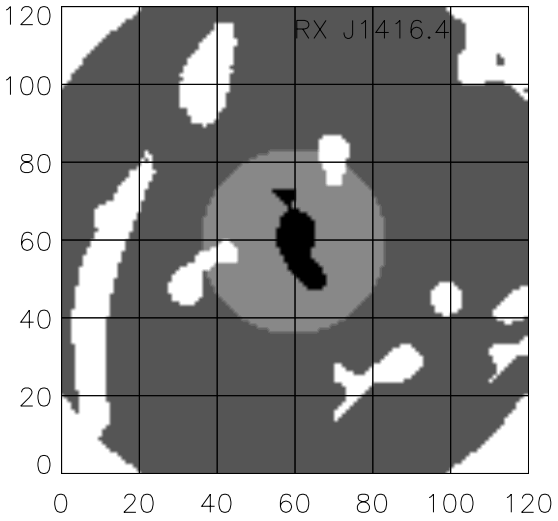

FIG. 127.

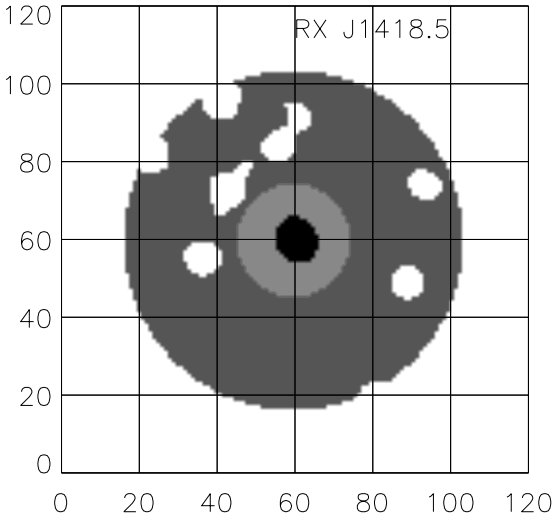

FIG. 128.

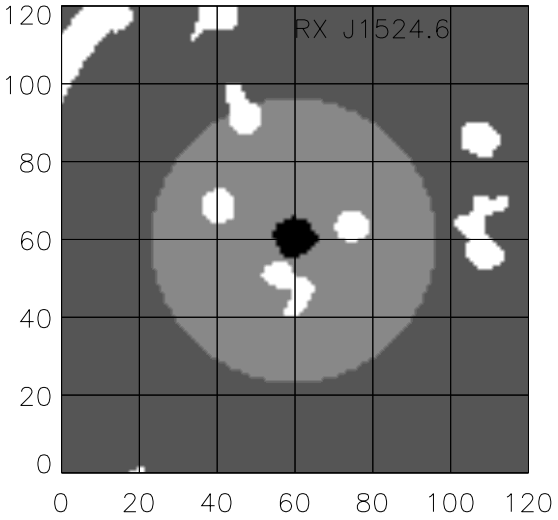

FIG. 129.

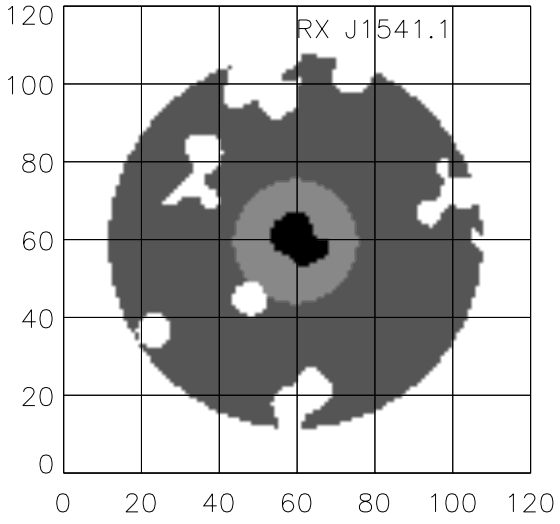

FIG. 130.

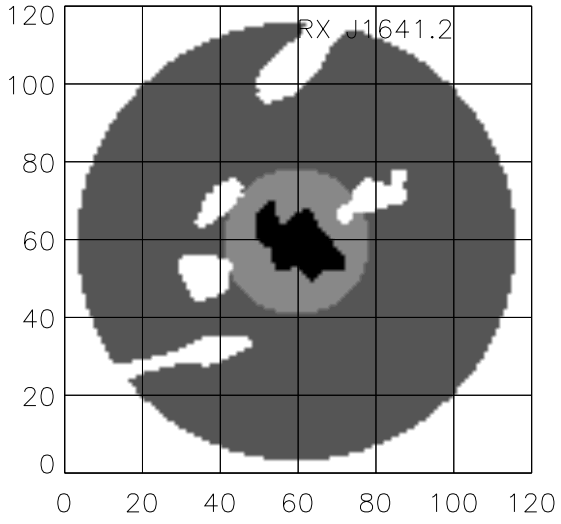

FIG. 131.

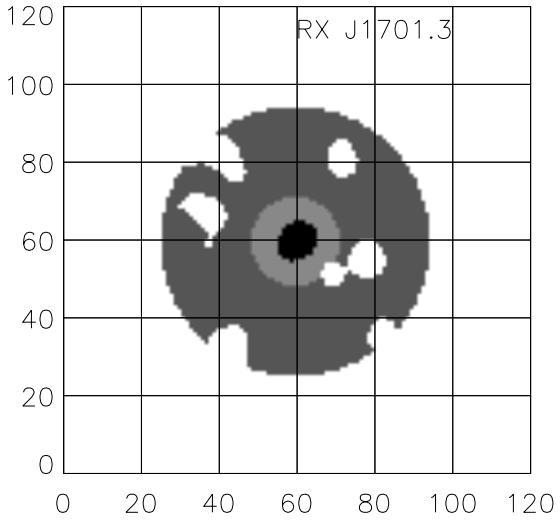

FIG. 132.

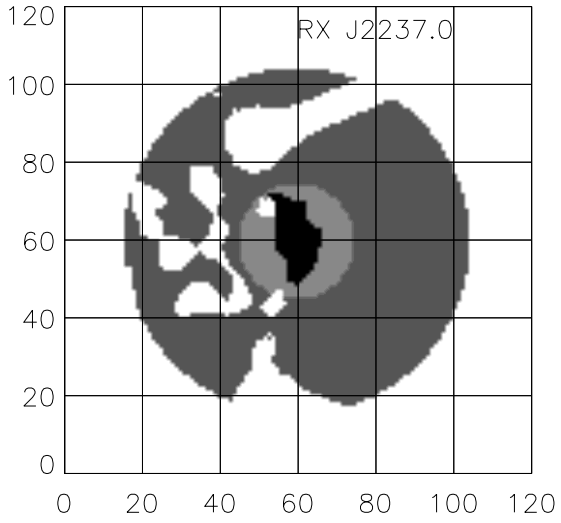

FIG. 133.

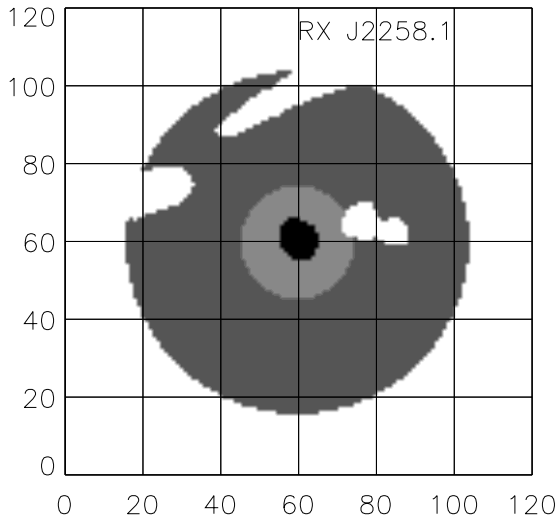

FIG. 134.

APPENDIX E

Table 6 shows the 374 extended sources in the SHARC survey.

TABLE 6

THE 374 EXTENDED SOURCES IN THE SHARC SURVEY

Source (1)	R.A. (J2000) (2)	Decl. (J2000) (3)	cr_W (4)	Pointing (5)
RX J0004.0−2603.....	00 04 5.3	−26 03 36.0	0.308	rp700467n00
RX J0007.3+2042.....	00 07 21.3	+20 42 24.7	0.492	rp700101
RX J0011.7−3612.....	00 11 43.8	−36 12 27.8	0.822	wp800388n00
RX J0018.1+1642.....	00 18 9.4	+16 42 25.8	1.005	rp800253n00
RX J0018.2+1617.....	00 18 17.3	+16 17 44.8	0.692	rp800253n00
RX J0018.6+1620.....	00 18 40.3	+16 20 23.3	0.487	rp800253n00
RX J0019.1+1618.....	00 19 11.8	+16 18 22.6	0.329	rp800253n00
RX J0023.1+0421.....	00 23 6.0	+04 21 15.4	0.467	rp800483n00
RX J0023.6+0416.....	00 23 37.6	+04 16 57.0	0.527	rp800483n00
RX J0030.5+0817.....	00 30 32.4	+08 17 45.9	0.563	rp800486n00
RX J0030.5+2618.....	00 30 33.1	+26 18 14.9	1.034	rp300016
RX J0031.0−3547.....	00 31 3.0	−35 47 21.8	1.263	wp800387n00
RX J0031.3+0828.....	00 31 22.7	+08 28 0.3	0.519	rp800486n00
RX J0031.9−3556.....	00 31 59.5	−35 56 12.1	1.191	wp800387n00
RX J0047.4+3200.....	00 47 28.3	+32 00 3.1	0.576	rp700331
RX J0048.6+3208.....	00 48 36.0	+32 08 54.8	0.501	rp700331
RX J0051.8−2848.....	00 51 53.9	−28 48 44.0	0.841	rp700275n00
RX J0054.6−2831.....	00 54 40.6	−28 31 57.2	0.572	rp900496a01
RX J0056.5−2730.....	00 56 32.4	−27 30 27.6	0.739	wp700528
RX J0056.5−2730.....	00 56 32.4	−27 30 40.7	0.742	rp701223n00
RX J0056.9−2740.....	00 56 56.4	−27 40 22.6	0.663	wp700528
RX J0056.9−2740.....	00 56 57.3	−27 40 30.0	0.586	rp701223n00
RX J0057.4−2731.....	00 57 25.7	−27 31 38.1	0.653	wp700528
RX J0058.0−2721.....	00 58 0.4	−27 21 24.2	1.059	wp700528
RX J0058.0−2721.....	00 58 0.5	−27 21 29.3	1.180	rp701223n00
RX J0058.7−2735.....	00 58 42.1	−27 35 15.2	0.346	rp701223n00
RX J0117.0−2248.....	01 17 5.1	−22 48 32.7	1.053	rp100376n00
RX J0117.6−2238.....	01 17 36.5	−22 38 13.5	1.255	rp100376n00
RX J0118.9−2302.....	01 18 54.0	−23 02 27.5	0.725	rp100376n00
RX J0124.8+0932.....	01 24 48.2	+09 32 30.8	1.920	rp700976
RX J0125.2+0339.....	01 25 14.8	+03 39 12.0	1.057	wp701048
RX J0135.7−1824.....	01 35 47.2	−18 24 31.7	0.755	wp200208
RX J0136.4−1812.....	01 36 25.1	−18 12 2.4	0.429	wp200208
RX J0137.3−1826.....	01 37 21.0	−18 26 22.5	0.468	wp200208
RX J0139.6+0119.....	01 39 38.7	+01 19 23.4	0.829	rp701407n00
RX J0139.9+1810.....	01 39 54.8	+18 10 5.7	1.116	wp701499n00
RX J0152.7−1357.....	01 52 42.0	−13 57 52.9	1.716	rp600005n00
RX J0158.2+3748.....	01 58 15.9	+37 48 30.1	0.698	wp201325
RX J0209.4−1008.....	02 09 24.2	−10 08 4.2	1.340	rp800114n00
RX J0209.9−1003.....	02 09 58.1	−10 03 19.2	1.478	rp800114n00
RX J0217.4−1800.....	02 17 26.1	−18 00 5.7	1.387	rp900352n00
RX J0221.1+1958.....	02 21 8.4	+19 58 25.9	1.545	wp900147
RX J0222.2+1959.....	02 22 17.3	+19 59 49.0	0.507	wp900147
RX J0223.4−0852.....	02 23 28.1	−08 52 14.3	1.202	rp800016n00
RX J0236.6−5214.....	02 36 36.8	−52 14 20.9	0.520	rp701356n00
RX J0236.6−5214.....	02 36 37.7	−52 14 28.5	0.936	rp300201n00
RX J0236.7−5209.....	02 36 47.3	−52 09 15.5	0.446	rp701356n00
RX J0237.9−5224.....	02 37 59.1	−52 24 45.7	2.324	rp300201n00
RX J0238.0−5224.....	02 38 0.2	−52 24 37.0	2.625	rp701356n00
RX J0250.0+1908.....	02 50 2.9	+19 08 29.4	1.426	rp700920
RX J0256.5+0006.....	02 56 32.9	+00 06 11.6	3.614	rp701403n00
RX J0257.8+1944.....	02 57 53.9	+19 44 4.7	1.151	wp900138
RX J0302.1−1533.....	03 02 9.6	−15 33 30.0	1.069	wp800566n00
RX J0317.6−5506.....	03 17 37.0	−55 06 45.6	0.912	rp701036n00
RX J0318.2−0301.....	03 18 17.3	−03 01 21.1	1.337	wp800555n00
RX J0318.5−0302.....	03 18 33.3	−03 02 46.7	2.763	wp800555n00
RX J0319.3−0302.....	03 19 19.1	−03 02 1.8	0.973	wp800555n00

TABLE 6—*Continued*

Source (1)	R.A. (J2000) (2)	Decl. (J2000) (3)	cr_W (4)	Pointing (5)
RX J0319.9−6639.....	03 19 58.4	−66 39 53.5	0.964	rp600504n00
RX J0321.9−5057.....	03 21 55.2	−50 57 4.5	0.588	wp800371n00
RX J0321.9−5119.....	03 21 57.0	−51 19 33.1	6.180	wp800371n00
RX J0322.0−3719.....	03 22 2.0	−37 19 16.4	0.639	rp700437n00
RX J0322.7−3706.....	03 22 43.8	−37 06 14.8	0.686	rp700437n00
RX J0322.8−5329.....	03 22 50.7	−53 29 0.0	0.566	rp800307n00
RX J0323.9−5337.....	03 23 58.3	−53 37 46.8	0.438	rp800307n00
RX J0324.0−5107.....	03 24 5.0	−51 07 15.2	0.702	wp800371n00
RX J0324.6−5103.....	03 24 37.9	−51 03 52.1	1.326	wp800371n00
RX J0327.9+0233.....	03 27 54.3	+02 33 43.2	3.231	rp700099m01
RX J0329.4−5310.....	03 29 29.6	−53 10 59.7	0.815	rp800306n00
RX J0334.0−3905.....	03 34 0.9	−39 05 14.1	1.081	wp800367a01
RX J0337.5−2529.....	03 37 33.5	−25 29 56.3	0.344	wp300079
RX J0337.5−2518.....	03 37 34.2	−25 18 1.5	2.135	wp300079
RX J0337.6−2522.....	03 37 40.2	−25 22 55.6	1.099	wp300079
RX J0338.0−2513.....	03 38 2.5	−25 13 18.8	0.346	wp300079
RX J0338.4−2509.....	03 38 28.0	−25 09 11.4	0.579	wp300079
RX J0338.7−2531.....	03 38 45.6	−25 31 38.8	0.376	wp300079
RX J0340.1−4458.....	03 40 9.0	−44 58 48.2	1.247	rp900495n00
RX J0341.1−4417.....	03 41 9.2	−44 17 47.5	0.281	wp900632n00
RX J0341.3−4449.....	03 41 20.6	−44 49 8.2	0.295	rp900495n00
RX J0341.4−4441.....	03 41 24.8	−44 41 40.2	0.377	rp900495n00
RX J0342.2−4350.....	03 42 14.4	−43 50 20.3	0.481	wp900632n00
RX J0342.2−4350.....	03 42 14.6	−43 50 5.5	0.702	rp150082n00
RX J0342.5−4352.....	03 42 35.3	−43 52 55.0	0.348	wp900632n00
RX J0343.0−4449.....	03 43 5.9	−44 49 31.4	0.293	rp900495n00
RX J0343.1−4454.....	03 43 8.6	−44 54 6.0	0.302	rp900495n00
RX J0343.6−4501.....	03 43 39.1	−45 01 26.9	0.327	rp900495n00
RX J0352.0+1752.....	03 52 1.7	+17 52 58.9	0.737	rp200107m01
RX J0359.1−5300.....	03 59 11.9	−53 00 56.2	1.511	rp800308
RX J0411.7−6547.....	04 11 44.9	−65 47 6.3	0.841	rp800171n00
RX J0413.7−5531.....	04 13 44.3	−55 31 52.4	0.989	wp600623n00
RX J0414.0−1224.....	04 14 5.7	−12 24 24.9	2.508	rp900242n00
RX J0415.7−5535.....	04 15 45.4	−55 35 31.0	1.205	wp600623n00
RX J0416.1−5546.....	04 16 10.3	−55 46 46.3	3.654	wp600623n00
RX J0420.3−5453.....	04 20 22.5	−54 53 59.9	0.645	wp600456n00
RX J0420.9+1444.....	04 20 58.7	+14 44 7.7	2.837	wp200441
RX J0421.2+1340.....	04 21 16.8	+13 40 14.8	1.320	rp200776n00
RX J0421.8−3832.....	04 21 51.2	−38 32 33.7	0.822	rp700026
RX J0426.1+1655.....	04 26 7.3	+16 55 12.1	1.797	rp201369n00
RX J0429.8+1548.....	04 29 51.8	+15 48 47.1	0.906	wp201368
RX J0431.7+1450.....	04 31 45.7	+14 50 42.4	0.880	rp200444n00
RX J0435.4+1523.....	04 35 28.6	+15 23 45.4	0.520	wp201747n00
RX J0439.4−1637.....	04 39 28.8	−16 37 11.1	0.917	rp900017
RX J0440.9−1644.....	04 40 55.9	−16 44 0.0	0.525	rp900017
RX J0452.1−5317.....	04 52 10.7	−53 17 19.0	0.837	wp600436n00
RX J0452.8−5314.....	04 52 53.7	−53 14 32.7	1.133	wp600436n00
RX J0454.3−0239.....	04 54 19.6	−02 39 50.0	1.594	rp800229n00
RX J0454.9−5324.....	04 54 59.7	−53 24 14.9	0.957	wp600436n00
RX J0506.0−2841.....	05 06 3.8	−28 41 44.6	0.813	rp700233n00
RX J0512.8−4823.....	05 12 50.9	−48 23 35.2	0.509	wp800368n00
RX J0514.2−4826.....	05 14 16.7	−48 26 53.4	1.587	wp800368n00
RX J0530.9−4630.....	05 30 56.1	−46 30 59.5	0.488	rp300334n00
RX J0531.2−4639.....	05 31 15.0	−46 39 44.5	0.426	rp300334n00
RX J0531.4−4616.....	05 31 26.0	−46 16 17.4	0.587	rp300334n00
RX J0531.7−4611.....	05 31 42.7	−46 11 28.4	0.395	rp300334n00
RX J0532.1−4610.....	05 32 9.0	−46 10 36.6	0.619	rp300334n00
RX J0609.1−4854.....	06 09 6.5	−48 54 50.4	2.155	rp300111
RX J0639.8+8218.....	06 39 53.1	+82 18 43.7	0.427	wp201603n00
RX J0642.6+8228.....	06 42 37.5	+82 28 28.0	0.463	wp201603n00
RX J0644.5+8226.....	06 44 31.4	+82 26 21.2	0.373	wp201603n00
RX J0719.0+7124.....	07 19 0.3	+71 24 25.1	0.680	rp700210n00
RX J0720.1+7114.....	07 20 6.9	+71 14 58.5	1.057	rp700210n00
RX J0720.2+7132.....	07 20 17.5	+71 32 16.4	0.726	rp700210n00
RX J0741.7+6524.....	07 41 42.1	+65 24 59.8	0.875	rp700112
RX J0750.1+1455.....	07 50 6.0	+14 55 28.1	0.894	wp300388n00

TABLE 6—*Continued*

Source (1)	R.A. (J2000) (2)	Decl. (J2000) (3)	cr_W (4)	Pointing (5)
RX J0750.8+1445.....	07 50 49.4	+14 45 0.6	0.782	wp300388n00
RX J0752.0+1457.....	07 52 0.7	+14 57 50.0	0.536	wp300388n00
RX J0840.1+6419.....	08 40 7.1	+64 19 54.6	0.460	rp200654n00
RX J0848.7+4457.....	08 48 42.6	+44 57 3.3	0.446	rp900009
RX J0849.0+4457.....	08 49 5.5	+44 57 24.3	0.191	rp900009
RX J0849.1+3731.....	08 49 8.9	+37 31 47.9	1.295	rp700546n00
RX J0849.1+4444.....	08 49 11.1	+44 44 57.8	0.175	rp900009
RX J0850.0+4439.....	08 50 5.3	+44 39 18.0	0.247	rp900009
RX J0850.0+4453.....	08 50 5.8	+44 53 55.1	0.235	rp900009
RX J0853.6+1349.....	08 53 41.1	+13 49 29.5	1.173	rp700887n00
RX J0853.9+1335.....	08 53 55.1	+13 35 22.2	0.782	rp700887n00
RX J0857.8+1410.....	08 57 50.1	+14 10 18.9	0.986	rp700436
RX J0858.6+1405.....	08 58 41.8	+14 05 35.6	0.422	rp700436
RX J0858.8+1411.....	08 58 52.1	+14 11 53.8	0.568	rp700436
RX J0906.7+3359.....	09 06 42.7	+33 59 49.4	1.121	rp900327a01
RX J0907.2+3329.....	09 07 15.5	+33 29 34.9	0.583	rp900327a01
RX J0909.3+4236.....	09 09 23.2	+42 36 8.2	0.778	rp700329
RX J0909.3+5414.....	09 09 23.9	+54 14 46.0	0.409	rp201382n00
RX J0922.5+6236.....	09 22 31.0	+62 36 16.1	1.142	wp700211
RX J0937.0+6126.....	09 37 4.4	+61 26 31.9	0.739	rp600207n00
RX J0939.3+3904.....	09 39 22.1	+39 04 32.5	1.034	rp700387
RX J0941.4+3857.....	09 41 25.7	+38 57 14.5	0.580	rp700387
RX J0945.6−1434.....	09 45 40.4	−14 34 5.0	2.304	wp701458n00
RX J0946.6−1408.....	09 46 36.2	−14 08 26.1	0.760	wp701458n00
RX J0947.8+0741.....	09 47 50.5	+07 41 43.0	1.511	wp701587n00
RX J1009.4+5333.....	10 09 29.0	+53 33 47.8	0.878	wp700264
RX J1010.2+5430.....	10 10 12.9	+54 30 9.6	1.418	wp900213
RX J1011.4+5439.....	10 11 25.8	+54 39 29.3	1.023	wp900213
RX J1011.9+5050.....	10 11 54.3	+50 50 55.2	0.878	wp900214
RX J1020.0+3915.....	10 20 2.4	+39 15 50.8	1.185	wp900528n00
RX J1020.2+3926.....	10 20 17.4	+39 26 28.3	0.987	wp900528n00
RX J1020.9+5246.....	10 20 58.5	+52 46 56.6	0.744	wp900400a01
RX J1023.5+4711.....	10 23 31.6	+47 11 23.0	0.774	rp700540n00
RX J1023.6+1931.....	10 23 37.6	+19 31 49.0	1.024	rp700996n00
RX J1024.0+6746.....	10 24 5.6	+67 46 51.5	0.824	wp800641n00
RX J1024.3+6805.....	10 24 20.1	+68 05 5.1	2.602	wp800641n00
RX J1024.3+1952.....	10 24 23.8	+19 52 28.0	0.571	rp700996n00
RX J1031.3−1433.....	10 31 23.3	−14 33 40.6	1.185	rp700461n00
RX J1036.0+0006.....	10 36 4.6	+00 06 22.5	0.895	wp201243n00
RX J1037.6−0026.....	10 37 41.1	+00 26 13.9	0.753	wp201243n00
RX J1046.7−0037.....	10 46 44.9	+00 37 51.2	0.701	wp800366a01
RX J1050.8+5738.....	10 50 48.6	+57 38 8.3	0.360	wp900029a04
RX J1051.8+5733.....	10 51 52.9	+57 33 51.9	0.277	wp900029a04
RX J1053.3+5719.....	10 53 20.0	+57 19 56.0	0.407	wp900029a04
RX J1053.5+5725.....	10 53 33.4	+57 25 16.0	0.725	wp900029a04
RX J1054.1+5712.....	10 54 10.2	+57 12 57.5	0.376	wp900029a04
RX J1102.0+2455.....	11 02 2.7	+24 55 2.2	0.874	wp300291n00
RX J1102.1+6111.....	11 02 7.7	+61 11 55.8	0.846	rp500157n00
RX J1102.3+2505.....	11 02 20.3	+25 05 27.4	0.550	wp300291n00
RX J1103.2+2523.....	11 03 12.1	+25 23 42.0	0.470	wp300291n00
RX J1103.5+2459.....	11 03 35.3	+24 59 18.8	0.411	wp300291n00
RX J1103.7+2453.....	11 03 46.4	+24 53 56.8	0.720	wp300291n00
RX J1104.8+6038.....	11 04 53.2	+60 38 40.3	1.107	rp500157n00
RX J1108.5+7226.....	11 08 35.8	+72 26 9.3	0.950	rp700872n00
RX J1110.8−3726.....	11 10 50.3	−37 26 29.3	0.703	wp600464a01
RX J1111.6−3740.....	11 11 41.8	−37 40 43.3	0.832	wp600464a01
RX J1112.8−2618.....	11 12 51.1	−26 18 59.1	1.034	rp201019n00
RX J1113.8+4017.....	11 13 48.5	+40 17 18.3	1.440	rp700855n00
RX J1116.7+1758.....	11 16 45.6	+17 58 26.8	0.673	rp600263n00
RX J1116.9+1808.....	11 16 58.6	+18 08 54.3	0.988	rp600263n00
RX J1119.3+2113.....	11 19 21.4	+21 13 47.9	0.580	wp700228
RX J1119.4+2106.....	11 19 26.7	+21 06 40.2	0.651	wp700228
RX J1119.4+1302.....	11 19 28.1	+13 02 46.8	0.769	rp600537n00
RX J1120.1+4318.....	11 20 7.5	+43 18 4.9	2.117	rp900383n00
RX J1120.6+1335.....	11 20 37.9	+13 35 17.3	1.054	rp700010
RX J1121.0+3427.....	11 21 4.8	+34 27 27.3	0.571	wp800537n00

TABLE 6—*Continued*

Source (1)	R.A. (J2000) (2)	Decl. (J2000) (3)	cr_W (4)	Pointing (5)
RX J1121.3+3416.....	11 21 23.8	+34 16 52.5	0.498	wp800537n00
RX J1121.7+3421.....	11 21 43.1	+34 21 48.1	0.700	wp800537n00
RX J1136.2+2944.....	11 36 12.4	+29 44 49.4	0.806	rp200091
RX J1137.3−3754.....	11 37 18.3	−37 54 17.8	1.047	rp701357n00
RX J1137.6−3749.....	11 37 36.0	−37 49 44.6	0.893	rp701357n00
RX J1137.8+2947.....	11 37 53.0	+29 47 24.0	0.681	rp200091
RX J1138.9−3801.....	11 38 56.7	−38 01 1.7	0.546	rp701357n00
RX J1141.7+1021.....	11 41 45.4	+10 21 32.1	0.851	wp600420
RX J1142.2+1023.....	11 42 16.1	+10 23 29.6	0.999	wp600420
RX J1142.2+1026.....	11 42 16.7	+10 26 46.9	1.272	wp600420
RX J1142.7+1017.....	11 42 45.1	+10 17 19.3	0.792	wp600420
RX J1143.1+5511.....	11 43 9.1	+55 11 28.9	0.719	rp600236n00
RX J1143.7+5520.....	11 43 46.5	+55 20 13.6	1.980	rp600236n00
RX J1146.6+7237.....	11 46 39.5	+72 37 43.2	1.009	wp300367n00
RX J1156.3+5538.....	11 56 19.6	+55 38 16.3	0.511	rp700055
RX J1200.8−0327.....	12 00 49.0	−03 27 46.3	1.052	wp701202
RX J1202.8−1845.....	12 02 53.8	−18 45 46.3	0.857	wp600468a02
RX J1204.0+2807.....	12 04 3.6	+28 07 3.6	4.492	wp700232
RX J1204.1+2020.....	12 04 9.7	+20 20 40.5	2.041	rp800039
RX J1204.2−0318.....	12 04 12.7	−03 18 8.8	0.414	rp201367m01
RX J1204.3−0351.....	12 04 23.4	−03 51 0.2	0.408	rp201367m01
RX J1204.4−0342.....	12 04 24.1	−03 42 45.8	0.251	rp201367m01
RX J1204.8+2751.....	12 04 49.1	+27 51 3.3	0.928	wp700232
RX J1205.0−0332.....	12 05 2.5	−03 32 44.4	0.282	rp201367m01
RX J1205.8+4429.....	12 05 52.3	+44 29 22.0	0.486	wp700557m01
RX J1210.4+3929.....	12 10 25.9	+39 29 7.6	14.30	wp700277
RX J1211.1+3907.....	12 11 9.5	+39 07 44.4	2.145	rp600625n00
RX J1211.2+3911.....	12 11 14.5	+39 11 41.1	1.525	wp700277
RX J1211.2+3911.....	12 11 15.6	+39 11 45.8	1.750	rp600625n00
RX J1211.4+3914.....	12 11 25.0	+39 14 25.7	0.544	wp700277
RX J1213.8+1310.....	12 13 52.2	+13 10 40.8	1.039	wp800421n00
RX J1214.4+3313.....	12 14 27.1	+33 13 38.5	0.565	rp600130
RX J1218.2+0551.....	12 18 12.3	+05 51 17.6	0.663	rp700425n00
RX J1218.6+3015.....	12 18 36.4	+30 15 16.6	0.813	rp700970n00
RX J1219.4+0348.....	12 19 29.5	+03 48 52.8	1.020	wp600166
RX J1219.8+0545.....	12 19 48.8	+05 45 40.2	0.745	rp700425n00
RX J1220.3+7522.....	12 20 18.0	+75 22 10.2	4.652	rp700434
RX J1221.3+3015.....	12 21 18.7	+30 15 31.2	0.905	wp701056
RX J1222.1+7526.....	12 22 6.9	+75 26 16.8	1.175	rp700434
RX J1222.5+2550.....	12 22 30.8	+25 50 26.7	36.93	wp200307
RX J1227.1+0906.....	12 27 11.3	+09 06 57.5	0.565	wp600587n00
RX J1227.4+0849.....	12 27 27.6	+08 49 53.1	5.872	wp600587n00
RX J1232.8+2605.....	12 32 48.3	+26 05 39.0	1.828	rp600162
RX J1234.5+0745.....	12 34 35.0	+07 45 11.5	0.753	rp600518n00
RX J1241.5+3250.....	12 41 33.1	+32 50 22.9	2.386	rp600129a00
RX J1242.9+1136.....	12 42 59.0	+11 36 13.1	1.020	rp600017
RX J1244.1+1134.....	12 44 8.2	+11 34 16.8	1.167	rp600017
RX J1247.7−0548.....	12 47 42.9	−05 48 49.0	0.516	rp600262a02
RX J1250.4+2530.....	12 50 26.1	+25 30 17.6	1.717	wp900212
RX J1252.1+2522.....	12 52 11.1	+25 22 24.5	1.075	wp900212
RX J1253.2+1556.....	12 53 12.9	+15 56 6.7	0.973	wp800393a01
RX J1254.9+5649.....	12 54 58.1	+56 49 38.2	1.099	wp700208
RX J1255.5+4711.....	12 55 35.2	+47 11 5.7	0.909	rp700073
RX J1257.0+4738.....	12 57 5.7	+47 38 4.4	0.685	rp700073
RX J1257.6+4736.....	12 57 37.6	+47 36 44.8	0.637	rp700073
RX J1257.8+4706.....	12 57 48.5	+47 06 33.9	0.572	rp700073
RX J1259.7−3236.....	12 59 45.4	−32 36 59.9	1.198	rp800384n00
RX J1308.5+5342.....	13 08 32.6	+53 42 19.3	1.254	wp300394n00
RX J1311.2+3228.....	13 11 12.3	+32 28 53.2	2.539	wp700216
RX J1311.8+3227.....	13 11 49.8	+32 27 40.4	1.472	wp700216
RX J1313.6−3250.....	13 13 41.0	−32 50 45.9	1.281	wp300219
RX J1316.8+2924.....	13 16 51.8	+29 24 24.6	0.876	rp100308n00
RX J1317.2+4204.....	13 17 12.4	+42 04 30.0	0.944	wp600191
RX J1325.0−3814.....	13 25 3.0	−38 14 12.9	0.695	wp600419
RX J1325.6−3825.....	13 25 36.1	−38 25 49.4	0.610	wp600419
RX J1330.9+5815.....	13 30 58.5	+58 15 0.6	0.736	wp600458n00

TABLE 6—*Continued*

Source (1)	R.A. (J2000) (2)	Decl. (J2000) (3)	cr_W (4)	Pointing (5)
RX J1333.9+3753.....	13 33 59.0	+37 53 26.9	0.273	wp700283
RX J1334.2+3757.....	13 34 16.7	+37 57 10.2	0.221	wp700283
RX J1334.3+5030.....	13 34 20.0	+50 30 54.2	1.366	rp800047
RX J1334.4+3736.....	13 34 27.1	+37 36 13.4	0.523	wp700283
RX J1334.4+3808.....	13 34 28.0	+38 08 50.5	0.281	wp700283
RX J1334.7+3759.....	13 34 42.3	+37 59 43.0	0.575	wp700283
RX J1335.1+3810.....	13 35 9.4	+38 10 48.6	0.269	wp700283
RX J1335.4+3804.....	13 35 27.0	+38 04 44.9	0.238	wp700283
RX J1335.5+3756.....	13 35 35.0	+37 56 55.0	0.356	wp700283
RX J1340.4+5146.....	13 40 28.0	+51 46 5.6	0.873	rp300285n00
RX J1342.0+5200.....	13 42 5.5	+52 00 34.0	0.915	rp300285n00
RX J1343.0−0013.....	13 43 2.5	+00 13 3.3	0.811	rp701000a01
RX J1343.5+0002.....	13 43 30.6	+00 02 15.8	0.637	rp800369a01
RX J1343.7+5538.....	13 43 45.2	+55 38 20.3	1.808	rp700922n00
RX J1348.9+0819.....	13 48 55.3	+08 19 59.6	1.006	rp300028
RX J1349.0+0750.....	13 49 1.3	+07 50 9.6	0.510	rp300028
RX J1349.2−0712.....	13 49 12.3	−07 12 41.2	1.515	rp800637n00
RX J1406.2+2830.....	14 06 15.8	+28 30 46.1	0.570	rp700061
RX J1406.9+2834.....	14 06 55.1	+28 34 15.7	1.304	rp700061
RX J1407.7+2824.....	14 07 43.4	+28 24 43.5	0.565	rp700061
RX J1408.1+2819.....	14 08 10.7	+28 19 6.8	0.653	rp700061
RX J1412.4+4355.....	14 12 29.8	+43 55 31.2	2.327	wp700248
RX J1413.3+4405.....	14 13 20.2	+44 05 23.0	0.467	wp700248
RX J1413.7+5904.....	14 13 47.8	+59 04 36.7	0.725	wp400134n00
RX J1415.1+3611.....	14 15 10.7	+36 11 57.8	0.673	wp600462
RX J1416.2+1146.....	14 16 15.3	+11 46 30.4	1.049	rp700122
RX J1416.4+2315.....	14 16 26.6	+23 15 32.8	4.804	rp800401a01
RX J1417.3+2513.....	14 17 23.3	+25 13 43.0	0.770	wp150071
RX J1417.9+5417.....	14 17 57.5	+54 17 51.3	1.260	wp150046
RX J1418.5+2510.....	14 18 31.4	+25 10 45.8	3.788	wp150071
RX J1427.6+3312.....	14 27 41.1	+33 12 30.4	0.447	wp200329
RX J1500.8+6623.....	15 00 48.7	+66 23 29.0	0.800	rp170001n00
RX J1501.9+4010.....	15 01 58.2	+40 10 5.0	0.960	wp201536n00
RX J1504.5+6613.....	15 04 33.9	+66 13 18.4	0.773	rp170001n00
RX J1508.4+5537.....	15 08 24.6	+55 37 5.3	1.168	rp600119n00
RX J1515.6+4411.....	15 15 39.3	+44 11 24.8	1.137	rp200965n00
RX J1517.1+3140.....	15 17 8.4	+31 40 58.4	1.296	rp201018
RX J1524.6+0957.....	15 24 39.6	+09 57 44.8	1.646	rp701001n00
RX J1525.3+4201.....	15 25 23.3	+42 01 0.0	1.263	rp701405n00
RX J1541.1+6626.....	15 41 10.3	+66 26 25.0	1.517	rp800511n00
RX J1543.3+6621.....	15 43 21.6	+66 21 53.9	0.647	rp800511n00
RX J1543.7+6627.....	15 43 42.7	+66 27 42.3	1.258	rp800511n00
RX J1552.2+2013.....	15 52 14.9	+20 13 26.0	0.822	wp701213
RX J1556.5+6353.....	15 56 35.1	+63 53 44.4	0.934	wp701526n00
RX J1558.6+3316.....	15 58 39.0	+33 16 35.2	0.398	rp800003
RX J1559.3+3323.....	15 59 22.6	+33 23 42.9	0.485	rp800003
RX J1603.3+4300.....	16 03 21.2	+43 00 56.1	0.678	rp800239
RX J1604.4+2046.....	16 04 25.1	+20 46 6.2	1.078	wp600588n00
RX J1604.5+4303.....	16 04 31.8	+43 03 34.7	0.550	rp800239
RX J1605.0+4320.....	16 05 1.2	+43 20 32.9	0.389	rp800239
RX J1626.3+7816.....	16 26 21.0	+78 16 56.7	0.748	wp170154
RX J1629.8+7811.....	16 29 48.2	+78 11 36.7	0.710	wp170154
RX J1631.7+7812.....	16 31 43.2	+78 12 36.3	0.664	wp170154
RX J1634.4+4152.....	16 34 25.7	+41 52 16.8	0.908	wp701552n00
RX J1641.2+8233.....	16 41 13.9	+82 33 1.7	3.550	rp700098
RX J1650.2+6010.....	16 50 15.7	+60 10 29.0	0.736	rp900166n00
RX J1651.4+6112.....	16 51 29.4	+61 12 55.3	0.975	wp900207
RX J1655.7+6236.....	16 55 46.1	+62 36 28.1	0.619	rp900169n00
RX J1658.0+5254.....	16 58 4.5	+52 54 1.3	0.701	wp900591n00
RX J1658.6+6236.....	16 58 41.3	+62 36 21.9	0.686	rp900169n00
RX J1659.8+6421.....	16 59 50.8	+64 21 47.9	0.834	wp701457n00
RX J1659.9+6422.....	16 59 59.8	+64 22 5.5	0.827	wp701457n00
RX J1701.3+6414.....	17 01 22.5	+64 14 8.3	1.986	wp701457n00
RX J1704.4+5948.....	17 04 28.7	+59 48 31.9	0.767	wp900211
RX J1705.6+6024.....	17 05 37.5	+60 24 11.0	1.469	rp701439n00
RX J1705.9+5312.....	17 05 54.6	+53 12 56.8	0.530	rp900493n00

TABLE 6—*Continued*

Source (1)	R.A. (J2000) (2)	Decl. (J2000) (3)	cr_W (4)	Pointing (5)
RX J1717.6+4954.....	17 17 40.7	+49 54 40.9	0.672	rp800017
RX J1717.9+4957.....	17 17 59.2	+49 57 3.8	0.445	rp800017
RX J1720.2+4758.....	17 20 17.2	+47 58 45.4	0.792	rp701080n00
RX J1720.4+4958.....	17 20 26.1	+49 58 12.2	1.095	rp800017
RX J1726.2+0410.....	17 26 14.4	+04 10 23.8	1.981	rp200522n00
RX J1730.6+7422.....	17 30 37.6	+74 22 23.8	3.204	wp701200
RX J1749.8+6823.....	17 49 49.8	+68 23 10.5	0.928	wp701523n00
RX J1756.0+6615.....	17 56 2.2	+66 15 2.8	1.129	wp170075
RX J1756.7+6612.....	17 56 45.5	+66 12 29.8	0.570	wp170075
RX J1759.7+6629.....	17 59 47.1	+66 29 7.7	0.251	rp100378n00
RX J1808.3+4555.....	18 08 20.5	+45 55 12.4	0.958	rp300103
RX J1808.3+4542.....	18 08 20.9	+45 42 35.2	2.371	rp300103
RX J1838.8−6502.....	18 38 48.8	−65 02 9.9	1.608	rp701020n00
RX J1841.4+5545.....	18 41 29.8	+55 45 42.7	0.527	rp201505n00
RX J1843.4+5527.....	18 43 26.3	+55 27 35.3	0.449	rp201505n00
RX J1844.1+7939.....	18 44 6.3	+79 39 43.3	1.025	rp700058
RX J1845.6+7956.....	18 45 41.3	+79 56 34.6	2.237	rp700058
RX J1942.4+7701.....	19 42 25.8	+77 01 46.7	0.712	rp701410n00
RX J2035.9−2512.....	20 35 55.2	−25 12 33.0	0.689	wp800536n00
RX J2047.6−3631.....	20 47 37.4	−36 31 14.9	0.366	wp201374a02
RX J2047.9−3645.....	20 47 56.1	−36 45 36.5	0.383	wp201374a02
RX J2048.6−3641.....	20 48 39.4	−36 41 1.6	0.514	wp201374a02
RX J2051.6−5704.....	20 51 37.5	−57 04 29.1	0.677	wp700538
RX J2052.7−5717.....	20 52 42.1	−57 17 11.8	0.571	wp700538
RX J2109.7−1332.....	21 09 47.8	−13 32 24.2	1.386	rp201007n00
RX J2114.8−6748.....	21 14 50.7	−67 48 53.2	0.618	rp900133n00
RX J2117.1−6746.....	21 17 11.4	−67 46 31.0	0.695	rp900133n00
RX J2139.5−4303.....	21 39 30.0	−43 03 4.2	0.833	wp800336a01
RX J2146.0+0423.....	21 46 5.7	+04 23 17.2	0.884	rp800150a01
RX J2146.7+0404.....	21 46 44.8	+04 04 28.8	0.988	rp800150a01
RX J2151.4−4817.....	21 51 29.5	−48 17 55.8	0.533	rp600512n00
RX J2152.3−4830.....	21 52 20.9	−48 30 25.0	0.856	rp600512n00
RX J2202.8−5636.....	22 02 52.9	−56 36 8.3	1.634	rp200559n00
RX J2215.2−2944.....	22 15 16.4	−29 44 29.2	1.957	rp701390n00
RX J2223.8−0206.....	22 23 48.8	−02 06 13.0	2.197	rp701018n00
RX J2235.0+3412.....	22 35 0.1	+34 12 2.1	1.099	wp800066
RX J2236.0+3358.....	22 36 0.3	+33 58 24.0	3.187	wp800066
RX J2236.0+3412.....	22 36 4.4	+34 12 13.8	0.868	wp800066
RX J2237.0−1516.....	22 37 0.5	−15 16 8.0	1.683	wp201723n00
RX J2237.2−2554.....	22 37 14.3	−25 54 40.9	0.739	rp700873n00
RX J2250.3+2431.....	22 50 23.0	+24 31 13.5	0.803	wp201552n00
RX J2257.7−3632.....	22 57 46.2	−36 32 0.8	0.408	rp600266n00
RX J2258.1+2055.....	22 58 8.4	+20 55 15.0	2.262	rp201282n00
RX J2302.7+0844.....	23 02 46.9	+08 44 42.5	1.012	rp700423
RX J2303.5−0829.....	23 03 34.4	−08 29 43.0	1.102	wp701250n00
RX J2305.4−3545.....	23 05 25.1	−35 45 32.3	1.156	wp201339n00
RX J2309.4−2713.....	23 09 27.9	−27 13 20.1	1.194	rp900323n00
RX J2311.4+1035.....	23 11 25.9	+10 35 6.7	3.521	rp100578n00
RX J2313.1−4950.....	23 13 6.5	−49 50 34.1	0.903	rp400144n00
RX J2314.7+1915.....	23 14 44.0	+19 15 23.3	1.392	rp800488n00
RX J2353.5−1524.....	23 53 31.5	−15 24 51.2	1.188	wp701501n00
RX J2359.2−3227.....	23 59 13.6	−32 27 2.4	0.760	wp800372a01
RX J2359.5−3211.....	23 59 35.7	−32 11 6.9	0.732	wp800372a01

NOTES.—Units of right ascension are hours, minutes, and seconds, and units of declination are degrees, arcminutes, and arcseconds. Count rates are quoted in units of 10^{-2} counts s^{-1}.

REFERENCES

Abell, G. O. 1958, ApJS, 3, 211
Abell, G. O., Corwin, H. G., & Olowin, R. P. 1989, ApJS, 70, 1
Adami, C. Ulmer, M. P., Holden, B. P., Romer, A. K., Nichol, R. C., & Pildis, R. A. 2000, ApJS, submitted
Allen, S. W., Edge, A. C., Fabian, A. C., Böhringer, H., Crawford, C. S., Ebeling, H., Johnstone, R. M., Naylor, T., & Schwarz, R. A. 1992, MNRAS, 259, 67
Allen, S. W., & Fabian, A. C. 1998, MNRAS, 297, 57
Arnaud, K. A. 1996, in ASP Conf. Proc. 101, Astronomical Data Analysis Software and Systems V, ed. G. H. Jacoby & J. Barnes (San Francisco: ASP), 17
Arnaud, M., & Evrard, A. E. 1999, MNRAS, 305, 631
Bahcall, N. A., & Fan, X. 1998, ApJ, 504, 1
Böhringer, H., et al. 1998, in Wide Field Surveys in Cosmology, ed. S. Colombi, Y. Mellier, & B. Raban (Gif-sur-Yvette: Editions Frontières), 261
Borgani, S., Rosati, P., Tozzi, P., & Norman, C. 1999, ApJ, 515, 40
Boyle, B. J., McMahon, R. G., Wilkes, B. J., & Elvis, M. 1995, MmRAS, 272, 462
Burke, D. 1998, Ph.D. thesis, Univ. Durham
Burke, D. J., Collins, C. A., Romer, A. K., Holden, B. P., & Nichol, R. C. 1997, ApJ, 488, L83
Carballo, R., Warwick, R. S., Barcons, X., Gonzalez-Serrano, J. I., Barber, C. R., Martinez-Gonzalez, E., Perez-Fournon, I., & Burgos, J. 1995, MNRAS, 277, 1312
Carlberg, R. G., Morris, S. L., Yee, H. K. C., & Ellingson, E. 1997, ApJ, 479, L19
Castander, F. J., et al. 1995, Nature, 281, 59
Collins, C. A., Burke, D. J., Romer, A. K., Sharples, R. M., & Nichol, R. C. 1997, ApJ, 479, L117
Couch, W. J., Ellis, R. S., Malin, D. F., & MacLaren, I. 1991, MNRAS, 249, 606
Crawford, C. S., Allen, S. W., Ebeling, H., Edge, A. C., & Fabian, A. C. 1999, MNRAS, 306, 857
Dalton, G. B., Efstathiou, G., Maddox, S. J., & Sutherland, W. J. 1994, MNRAS, 269, 151
De Grandi, S., et al. 1999a, ApJ, 513, L17
———. 1999b, ApJ, 514, 148
De Vaucouleurs, G., De Vaucouleurs, A., Corwin, H. G., Jr., Buta, R. J., Paturel, G., & Fouque, P. 1991, Third Reference Catalogue of Bright Galaxies (New York: Springer) (D91)
Dickey, J. M., & Lockman, F. J. 1990, ARA&A, 28, 215
Ebeling, H., Edge, A. C., Böhringer, H., Allen, S. W., Crawford, C. S., Fabian, A. C., Voges, W., & Huchra, J. P. 1998, MNRAS, 301, 881
Ebeling, H., Edge, A. C., Fabian, A. C., Allen, S. W., Crawford, C. S., & Böhringer, H. 1997, ApJ, 479, L101
Ebeling, H., et al. 2000, ApJ, submitted
Ebeling, H., Voges, W., Böhringer, H., Edge, A. C., Huchra, J. P., & Briel, U. G. 1996, MNRAS, 281, 799
Fairall, A. P., et al. 1992, AJ, 103, 11
Gioia, I. M., Henry, J. P., Maccacaro, T., Morris, S. L., Stocke, J. T., & Wolter, A. 1990, ApJ, 356, L35
Gioia, I. M., & Luppino, G. A. 1994, ApJS, 94, 583
Gioia, I. M., Henry, J. P., Mullis, C. R., Ebeling, H., & Wolter, A. 1999, AJ, 117, 2608
Hasinger, G., Turner, T. J., George, I. M., & Boese, G. 1992, Legacy, 2, 77
Hattori, M., et al. 1997, Nature, 388, 146
Henry, J. P. 1997, ApJ, 489, L1
Henry, J. P., Gioia, I. M., Maccacaro, T., Morris, S. L., Stocke, J. T., & Wolter, A. 1992, ApJ, 386, 408
Henry, J. P., Gioia, I. M., Mullis, C. R., Clowe, D. I., Luppino, G. A., Böhringer, H., Briel, U. G., Voges, W., & Huchra, J. P. 1997, AJ, 114, 1293
Hewitt, A., & Burbidge, G. 1993, ApJS, 87, 451
Hickson, P. 1982, ApJ, 255, 382
Hickson, P., De Oliveira, C. M., Huchra, J. P., & Palumbo, G. G. G. 1992, ApJ, 339, 353
Holden, B. P., Romer, A. K., Nichol, R. C., & Ulmer, M. P. 1997, AJ, 115, 1701
Huchra, J. P., Henry, J. P., Postman, M., & Geller, M. J. 1990, ApJ, 365, 66
Jones, C., & Forman, W. 1992, in Clusters and Superclusters of Galaxies, ed. A. C. Fabian (Dordrecht: Kluwer), 49
Jones, L. R., Scharf, C., Ebeling, H., Perlman, E., Wegner, G., Malkan, M., & Horner, D. 1998, ApJ, 495, 100
Lobo, C., Lazzati, D., Iovino, A., Guzzo, K., & Chincarini, G. 1998, in Wide Field Surveys in Cosmology, ed. S. Colombi, Y. Mellier, & B. Raban (Gif-sur-Yvette: Editions Frontières), 239
Longhetti, M., Rampazzo, R., Bressan, A., & Chiosi, C. 1998, A&AS, 130, 367
Lumsden, S. L., Nichol, R. C., Collins, C. A., & Guzzo, L. 1992, MNRAS, 258, 1
Morrison, R., & McCammon, D. 1983, ApJ, 270, 119
Mulchaey, J. S., & Zabludoff, A. I. 1998, ApJ, 514, 133
Nichol, R. C., Briel, O. G., & Henry, J. P. 1994a, MNRAS, 267, 771
Nichol, R. C., Holden, B. P., Romer, A. K., Ulmer, M. P., Burke, D. J., & Collins, C. A. 1997, ApJ, 481, 644 (N97)
Nichol, R. C., Ulmer, M. P., Kron, R. G., Wirth, G., & Koo, D. C. 1994b, ApJ, 432, 464
Nichol, R. C., et al. 1999, ApJ, 521, L21 (N99)
Oukbir, J., & Blanchard, A. 1992, A&A, 262, L21
Perlman, E. S., Padovani, P., Giommi, P., Sambruna, R., Jones, L. R., Tzioumis, A., & Reynolds, J. 1998, AJ, 115, 1253
Ponman, T. J., Allan, D. J., Jones, L. R., Merrifield, M., McHardy, I. M., Lehto, H. J., & Luppino, G. A. 1994, Nature, 369, 462
Postman, M., Lubin, L. M., Gunn, J. E., Oke, J. B., Hoessel, J. M., Schneider, D. P., & Christensen, J. A. 1996, AJ, 111, 615
Raymond, J. C., & Smith, B. W. 1977, ApJS, 35, 419
Reichart, D. E., Nichol, R. C., Castander, F. J., Burke, D. J., Romer, A. K., Holden, B. P., Collins, C. A., & Ulmer, M. P. 1999, ApJ, 518, 521
Reimers, D., Toussaint, F., Hagen, H.-J., Hippelein, H., & Meisenheimer, K. 1997, A&A, 326, 489
Romer, A. K. 1995, Ph.D. thesis, Univ. Edinburgh
Romer, A. K., Collins, C. A., Böhringer, H., Cruddace, R. G., Ebeling, H., MacGillivray, H. G., & Voges, W. 1994, Nature, 372, 75
Romer, A. K., Viana, P. T. P., Liddle, A. R., & Mann, R. G. 2000, ApJ, submitted (astro-ph/9911499)
Rosati, P., Della Ceca, R., Norman, C., & Giacconi, R. 1998, ApJ, 492, 21
Sadat, R., Blanchard, A., & Oukbir, J. 1998, A&A, 329, 21
Slezak, E., Bijaoui, A., & Mars, G. 1990, A&A, 227, 301
Slinglend, K., Batuski, D., Miller, C., Haase, S., Michaud, K., & Hill, J. M. 1998, ApJS, 115, 1
Snowden, S. L., McCammon, D., Burrows, D. N., & Mendenhall, J. A. 1994, ApJ, 424, 714
Stark, A. A., Gammie, C. F., Wilson, R. W., Balley, J., Linke, R. A., Heiles, C., & Hurwitz, M. 1992, ApJS, 79, 77
Stocke, J. T., Morris, S. L., Gioia, I. M., Maccacaro, T., Schild, R., Wolter, A., Fleming, T. A., & Henry, J. P. 1991, ApJS, 76, 813 (S91)
Struble, M. F., & Rood, H. J. 1987, ApJ, 63, 543
Trümper, J. 1993, Science, 260, 1769
Tucker, W. H., Tananbaum, H., & Remillard, R. A. 1995, ApJ, 444, 532
Viana, P. T. P., & Liddle, A. R. 1999, MNRAS, 303, 535
Vikhlinin, A., McNamara, B. R., Forman, W., Jones, C., Quintana, H., & Hornstrup, A. 1998a, ApJ, 502, 558 (V98)
———. 1998b, ApJ, 498, L21
Vikhlinin, A., McNamara, B. R., Hornstrup, A., Quintana, H., Forman, W., Jones, C., & Way, M. 1999, ApJ, 520, L1
Zabludoff, A. I., Geller, M. J., Huchra, J. P., & Vogeley, M. S. 1993, AJ, 106, 1273
Zwicky, F., Herzog, E., & Wild, P. 1968, Catalogue of Galaxies and of Clusters of Galaxies (Pasadena: Caltech)